SEISMIC DESIGN METHODOLOGY FOR CIRCULAR STEEL BRIDGE PIERS SUBJECTED TO MULTI-DIRECTIONAL EARTHQUAKE MOTIONS

Kulkarni Nishigandha Gajanan

SEISMIC DESIGN METHODOLOGY FOR CIRCULAR STEEL BRIDGE PIERS SUBJECTED TO MULTI-DIRECTIONAL EARTHQUAKE MOTIONS

Submitted in Partial Fulfillment of the Requirements
for the Degree of
Doctor of Engineering

By

Kulkarni Nishigandha Gajanan

MAY 2012

Department of Civil Engineering,
NAGOYA UNIVERSITY
JAPAN

ACKNOWLEDGEMENTS

I wish to take this opportunity to express my gratitude towards my research supervisor, Prof. Yoshito Itoh and co-advisor Associate Prof. Akira Kasai (Kumamoto University), for their guidance and valuable suggestions in my research work. Prof. Itoh is very strict in research but very kind and friendly in nature. I am very pleased that I got a chance to work with Prof. Itoh. Prof. Kasai who was my former supervisor, guided me in initial stage of my research and encouraged whenever I found myself in difficulties. I really want to express my thanks to him.

I would like to deliver my gratitude towards the members of my doctoral defense examination committee, Prof. Yoshiaki Goto (Nagoya Institute of Technology), Prof. Hikaru Nakamura, Prof. Yoshito Itoh and Associate Prof. Akira Kasai (Kumamoto University) for their important comments and suggestions.

I must convey my appreciation to Associate Prof. Yasuo Kitane and Dr. Mikihito Hirohata who have helped me in various kinds of academic work by understanding me as a foreign student. My special thanks to Prof. Hanbin Ge (Meijo University), for his valuable advice.

I am very thankful to all members of our laboratory for their warm friendship and helping nature, especially Dr. Xi Chen (China) and Dr. Paramashanti (Indonesia) with whom I discussed both technical and nontechnical subjects freely. I would also like to mention the other members and they are; Japanese: Ms. Junko Torii, Mr. Hisayuki Tsuboi, Dr. Kazuo Furunishi, Dr. Naohito Watanabe, Mr. Syuichi Inaba, Mr. Keisuke Kaneko, Mr. Masashi Takayanagi, Mr. Saeshiro Inagaki, Mr. Takaki Sugiura, Mr. Yuuki Sugiura, Mr. Koji Itoh, Mr. Masataka Fukimoto, Mr. Akihiro Hosoi, Mr. Seiji Itoh, Mr. Tatsuya Mori, Mr. Atsushi Kurama, Mr. Jyunya Takemi, Mr. Yuta Nishijima, Mr. Akihiro Yoshino, Mr. Kohei Hashimoto (Kumamoto University) and Ms. Makoto Iwanaga (Secretary); Chinese: Dr. Zhirong Lin, Dr. Xiao Chen, Ms. Wen Liu, Mr. Shen Wang; Korean: Dr. Haeyong Kim; Combodian: Mr. Ung Seiha and Veitnamese: Mr. Thanh Huu Le.

My sincere thanks to Department of Civil Engineering, Nagoya University for allowing me to do research and giving me opportunities to participate in various conferences held in Japan and overseas. I would like to give special thanks to Ms. Hiroko Kawahara (Foreign student office member), Ms. Misumi Hirota (Civil Engineering office

member) and Ms. Aiko Ohara (Private apartment owner), who helped me a lot during my stay in Nagoya University.

I am greatly indebted to ‘Mombukagakusho’ (Ministry of Education, Science, Sports, and Culture of the Japanese Government) for providing financial support through my doctor course.

Finally but not the least, I wish to express my deepest appreciation to my husband, Dr. Sandip Talwalkar, who encouraged me for higher education and giving me continuous support and confidence at each and every stage of my life during this research work. I also feel great respect towards my parents for preparing me mentally strong and giving me lots of blessings. My daughter also deserves many thanks and lots of love; because of her I experienced pleasant motherhood during this research period.

Kulkarni Nishigandha Gajanan

ABSTRACT

Thin-walled steel tubular columns are often used for elevated highway bridge piers in Japan due to their good earthquake resistance. However, in 1995 Kobe earthquake, damages are observed in terms of local buckling near the base, cracking, fatigue etc. in the steel bridge piers. The lessons learned from this catastrophe are considered to revise the Japanese seismic design codes. Accordingly, revisions were issued in 1996 and 2002. The latest revision of specification has adopted a new design concept Performance-based design, which controls the damages in the bridge piers by confirming their seismic performance under the input earthquake waves within allowable values. Therefore, it is very essential to observe demand of steel columns during earthquake motions applied in such a way that causes coupling of its components and hence severe than effect of a single component. Further, this implies to investigate the capacity of the steel columns under critical loading conditions.

The research up to the present, was limited to capacity prediction of steel columns under monotonic loadings or cyclic uni-directional loading patterns and which might overestimated the capacity values owing to lack of most critical loading pattern. Therefore, in the present work, the capacity formulas are proposed by applying cyclic bi-directional loading as one of the critical loading pattern on circular steel columns used in bridge piers.

Chapters 1 and 2 are about introduction and progress in ductility formulation respectively. As the ductility capacities can be expressed in terms of displacement of top of the column and strain within the effective failure region at the base of columns; in chapter 3 displacement-based ductility formulas are evaluated along with the seismic design procedure to explain the application of proposed formulas in bi-directional seismic design of steel bridge piers. In addition to this study, the effects of change in design parameters such as, radius-thickness ratio, slenderness ratio and axial force ratio on the strength and ductility reduction are observed including two distinct loading conditions i.e. cyclic uni-directional and circular bi-directional.

Similar to this study in chapter 4, strain-based ductility formulas and seismic design method are proposed. Effect of change in cyclic loading patterns on the behavior of ultimate strains in steel columns having different slenderness ratio is investigated and it is

observed that slenderness ratio has significant impact on ultimate strains and hence it is inevitably appeared in ultimate strain formulation. The dynamic analysis of steel bridge piers are carried out and their responses are checked against displacement-based and strain-based seismic design method. It is observed that strain-based design method provides minimum allowable limit value than the displacement-based method and hence it endorsed that the derived ultimate strain formulas are satisfactorily useful in seismic design process.

In chapter 5, the comparative study is performed between response of bridge piers under two horizontal components and two horizontal including vertical components of actual strong earthquake motions. In addition to this study, scaling effect of earthquake components is also investigated. It is observed that inclusion of vertical component has great impact on the axial force response in the steel column whereas, displacement and strain responses are found to be dependent on horizontal components of earthquake. Hence, these observations further implied to examine the varying axial force effect on the capacity of steel columns which was kept constant during ductility prediction process explained in chapters 3 and 4.

In chapter 6, proportional varying axial force patterns along with bi-directional displacement loading are applied on steel columns and their hysteretic behavior, envelop curves, energy dissipation and local buckling are compared. It is verified from energy dissipation curves that equal amount of energy get dissipated in either varying axial force pattern or constant axial force corresponding to mean value of varying pattern. Moreover, the observed ultimate strain values due to variation in axial force are compared with the equation line of ultimate strain developed in chapter 4 and found that these values are laid on safer side of the equation line. This indicated that the proposed ultimate strain formulas by keeping constant axial force are equally applicable in seismic design when three-directional earthquake motions are applied simultaneously. . Finally, summary and concluding remarks on the present research work are presented in chapter 7 followed by some future work topics at the end.

TABLE OF CONTENTS

LIST OF TABLES

LIST OF FIGURES

Chapter 1

INTRODUCTION

1.1 Developments in the Seismic Design Methodology

Seismic design methods for highway bridges in Japan have been developed and improved based on the lessons learned from the various past bitter experiences after the Kanto (Tokyo) Earthquake (M 7.9) in 1923. The first Japanese design document that prescribed seismic resistant design requirements appeared in 1926. It was specified that, earthquake lateral forces of 15-40% of bridge self-weight (depending on location and ground conditions) be considered during design, introducing the concept of 'seismic coefficient', *k*. Hence from then onward, although the magnitude of the seismic coefficient fluctuated somewhat over time (between 20% and 35% for Kobe area), seismic related lateral strength requirements for bridges have been apparently existed for more than 70 years in Japan. Moreover, these earthquake design requirements were changed time to time after major earthquakes (M > 7) to take account for soil-liquefaction, bridge foundation problems, span failures etc. However, on 17 January, 1995 great Hyogo-ken Nanbu earthquake, many civil structures including highway steel bridges as well as reinforced concrete bridges suffered by severe damage or complete collapse (see **Fig. 1.1**). The partial reason why a number of steel piers behaved poorly during this earthquake is that the earthquake-resistant design requirements for bridges in Japan prior to the 1995 Hyogo-ken Nanbu earthquake, did not included any requirements to ensure ductile response of steel piers although it was believed that steel has sufficient inherent ductile property (Bruneau, 1998).

After this Hyogo-ken Nanbu earthquake, the 'Committee for Investigation on Damage of Highway Bridges Caused by Hyogo-ken Nanbu Earthquake' was established to survey the damage and to clarify the factors which affected the damage. The 'Guide Specifications for Reconstruction and Repair of Highway Bridges which suffered damage due to Hyogo-ken Nanbu Earthquake' was reported by this committee on 25 May, 1995 and enforced to use in all sections of Japan as emergency measures for seismic design of new highway bridges and seismic strengthening of existing highway bridges until the Design Specifications of Highway Bridges were

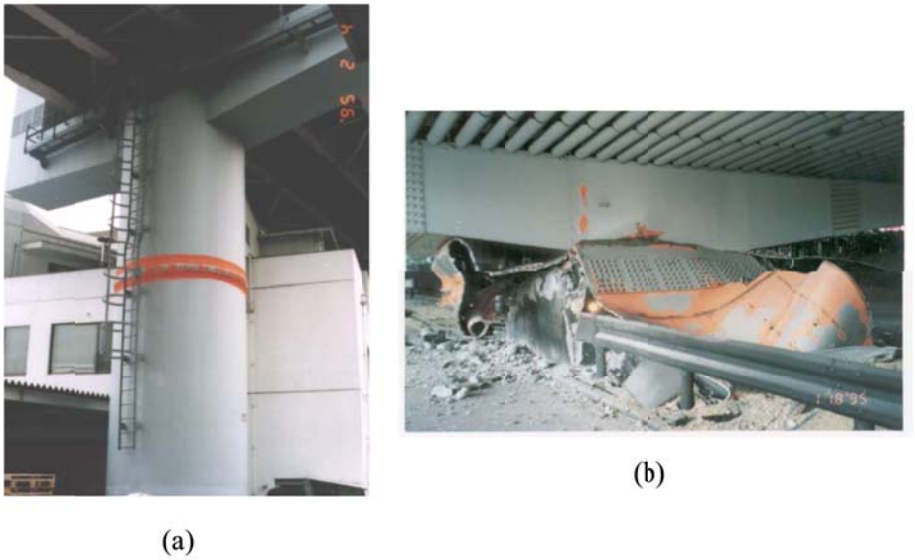

(a) (b)

Fig. 1.1 (a) Local Buckling and (b) Complete Collapse of Steel Bridge Pier

revised.

According to the various investigations of damage due to Hyogo-ken Nanbu earthquake, the specifications for highway bridges were significantly revised in 1996 (Japan Road Association, 1996; Kawashima and Unjoh, 1997). As a result, the intensive earthquake motion with a short distance from the inland earthquakes like Hyogo-ken Nanbu earthquake has been considered in the design process.

After that, revision of design specifications of highway bridges has been continuously made. The target point of the revision was Performance-based design concept and enhancement of the durability of bridge structures for a long-term use, as well as the inclusion of the improved knowledge on the bridge and construction methods after the 1996 specifications. The 2002 design specifications for highway bridges were issued by Ministry of Land, Infrastructure and Transport on December 27, 2001 (Japan Road Association, 2002; Kawashima and Unjoh, 2004).

The Japanese Specifications for Highway Bridges is composed of the following five parts;

- Part I: Common design principles
- Part II: Steel bridges
- Part III: Concrete bridges
- Part IV: Substructures
- Part V: Seismic design

Out of these, Part V: Seismic design, prescribes seismic design philosophies, earthquake effects including seismic loads, seismic instabilities of soils such as

liquefaction-induced lateral spreading, and unseating prevention. The following paragraphs give brief introduction to the Performance-based design concept employed in 2002 specifications.

Performance Matrix for Highway Bridges

Two-level design method is used in the 2002 specifications as it was mentioned in 1996 specifications. First level is the seismic design against small-to-medium earthquakes, which have been traditionally implemented. The second level is the seismic design against large earthquakes such as 1995 Hyogo-ken Nanbu earthquake.

Table 1.1 Seismic Performance Matrix

<table>
<tr><td colspan="2">Type of design ground motion

(1)</td><td>Standard bridges
(Type-A)
(2)</td><td>Important bridges
(Type-B)
(3)</td></tr>
<tr><td colspan="2">Level 1 Earthquake: High probability ground motion</td><td colspan="2">SPL 1: Prevent damage</td></tr>
<tr><td rowspan="2">Level 2 Earthquake: Low-probability ground motions</td><td>Inter-plate earthquake (Type I)</td><td rowspan="2">SPL 3: Prevent critical damage</td><td rowspan="2">SPL 2: Limited damage for function recovery</td></tr>
<tr><td>Inland earthquake (Type II)</td></tr>
</table>

Table 1.1 shows the basic principles in seismic design mentioned in the specifications through a performance matrix of design earthquake ground motion and Seismic Performance Level (SPL). This performance matrix illustrates combinations of two levels of earthquake motions and corresponding requirements of structural performance level defined by the specifications.

Typical Design Ground Motions

Level 1 earthquake is of small to medium magnitude and their acceleration response spectrum amplitudes are around 0.2g to 0.3g for usual characteristic periods of highway bridges.

Level 2 earthquakes are extremely strong, but they are very unlikely to strike the structure during its service period. The characteristics of inelastic behavior of both

soils and structural members during such earthquake are greatly affected by the intensity and the duration of the earthquake. Accordingly, the Level 2 earthquakes involve two types of ground motion, i.e., Type I and Type II Earthquake motions. The ground motion in Tokyo during the 1923 Kanto earthquake is typical of Type I earthquake motions which is associated with the inter-plate earthquake generated at the plate boundaries in the ocean. The peak amplitudes related to Type I earthquake are smaller than those for Type II earthquake, but Type I earthquake motions have longer duration.

The Grate Hyogo-ken Nanbu earthquake in 1995 is typical example of Type II earthquake, which is inland-strike type motions and caused by faults movement located at very short distance from bridge site. Type II earthquakes have high intensity but short durations. The return period of Type II earthquake motions may be longer than that of the Type I earthquake motions.

Performance Levels of Bridges

The Seismic Performance Level (SPL) depends on the importance of the bridge. The bridge importance is classified into two groups: standard bridges (Type-A) and important bridges (Type-B). Both Type-A and Type-B bridges must resist Level 1 earthquakes to achieve SPL 1, where SPL 2 prescribes that the bridge performs elastically during an earthquake with minimal and no damage. While in case of minor damage, bridges shall be repaired easily. Type-A bridges must resist Level 2 earthquakes to achieve SPL 3, where SPL 3 prescribes that the bridge resists ‘critical failure’ that would lead to collapse of bridge during an earthquake. Type-B bridges must resist Level 2 earthquakes to satisfy SPL 2, where SPL 2 prescribes that the bridge is functional especially for ‘rescue operation’ even after sustaining a limited degree of damage.

Like the Japanese seismic design specifications, the Performance-based seismic design (PBSD) concept is more or less similarly adopted by the countries like U.S.A., New Zealand, Canada and Europe. Hence, it can be said that PBSD concept has attained international harmonization of design codes.

Verification Methods of Seismic Performance

It is the fundamental policy of the verification of seismic performance that the response of bridge structures against design earthquake ground motions does not

Table 1.2 Verification Methods of Seismic Performance Depending on Earthquake Response Characteristics of Bridge Structure

Dynamic characteristics →	Simple bridges	Bridges with multiple plastic hinges and cannot apply Energy Constant rule	Bridges with limited application of static analysis	
SPL to be verified			With multimode response	With complicated behavior
(1)	(2)	(3)	(4)	(5)
SPL 1	Static verification	Static verification	Dynamic verification	Dynamic verification
SPL 2/SPL 3		Dynamic verification		
Examples of bridges	Other bridges	* Bridges with Rubber bearings * Seismically isolated bridges * Rigid frame bridges * Bridges with steel columns	* Bridges with long natural period * Bridges with high piers	* Cable stayed bridges, suspension bridges * Arch bridges * Curved bridges

exceed the determined limit states.

Table 1.2 shows the applicable verification methods of seismic performance of bridge structures. In the seismic design of highway bridges, it is important to increase the strength and ductility capacity to appropriately resist the intensive earthquake. The verification methods are based on the ‘static analysis’ and ‘dynamic analysis’. In 1996 specifications, the seismic coefficient methods with ‘elastic design’, ‘ductility design methods’ and ‘dynamic analysis’ were specified and these design methods had to be selected based on the structural conditions of bridges. The basic concept is same as employed in 1996 but in 2002 revision, the verification methods are rearranged based on static and dynamic analyses. However, in these verification methods, the allowable limit states i.e. strength and ductility capacity of bridge members are placed as the acceptable solutions, which can be modified by the designers with the necessary verifications.

1.2 Evolution in Capacity Prediction of Steel Bridge Piers

As mentioned in the previous paragraphs that since 1996 Specifications, ductility design has been introduced for bridge piers and their foundations and also continued into 2002 revision. The salient point of this ductility design is to consider relationship between possible damage states and the stability of the structure from the viewpoint of deformation capacity. For example, the steel bridge piers should be designed in such a way that, when they are subjected to strong earthquake motion, their maximum deformation must remain within the limit of ultimate deformation i.e. the capacity of particular pier. Therefore, number of researchers has been contributed in the evolution of capacity of bridge piers considering that the pier is the main component in the bridge system which has potential of inelastic behavior. And hence it can become a key controlling member in the seismic designing of bridges.

Generally speaking, the steel columns modeling as bridge piers can be classified into two categories: (1) Hollow steel columns, and (2) Concrete filled steel columns. At the beginning when concrete filled steel piers were built, the concrete was placed into the steel piers up to a certain height only to provide extra protection if a vehicle collides on them. Later, it was noticed that use of partially in-filled concrete piers could enhance the seismic performance, and then after research was initiated in this topic.

For hollow steel columns of cantilever type, extensive experimental and numerical studies have been conducted. In examining seismic performance of steel columns modeling bridge piers, the following parameters must be taken into account: (1) cross section shape, (2) steel grade, (3) structural configuration, (4) width to thickness ratio, (5) column slenderness ratio, (6) axial load, (7) lateral loading history and so on (Usami et al., 1992). Initially, the effect of these geometric parameters on the ultimate strength and ductility were investigated by using monotonic stress-strain model for material and combined compressive and bending load on the steel cylinders (Gao et al., 1998a; Zheng et al., 2000). In the next stage of research it was realized that, merely considering compressive and bending load effect on the steel short cylinders is inadequate to understand the behavior of whole column. Hence, full length steel column models with uni-directional cyclic loading and constant axial force due to superstructure were started to be instigated. Nakagawa (1996) analyzed the box section column subjected to a constant axial load and cyclic loads using the

isotropic hardening material model. However, it was found that, the isotropic hardening model unable to capture the inelastic behavior of the thick-walled columns observed in experiment. Hence, to incorporate the cyclic behavior of material in the numerical analysis, the user defined material constitutive laws were developed based on the experimental results of various structural steel grades. Goto et al., (1997) analyzed the steel box and pipe columns under cyclic loading using the three-surface model to consider material nonlinearity and concluded that when compared with isotropic hardening and kinematic hardening models; 'three-surface model' is able to predict the test results with good accuracy. Similarly, Gao et al., (1998b) and Usami et al., (1998) have also studied the cyclic loading effect on the strength and ductility of steel columns using their 'modified two-surface model' (M2SM).

When the earthquake generated loading effect on the structures was noticed carefully, it was realized that seismic response is complex and multi-directional and differing to the conventionally assumed uni-directional approach (Okazaki et al., 2003). Hence, number of experimental and analytical studies was initiated to investigate the effect of cyclic multi-directional loading on the behavior of steel columns. The main conclusion drawn from experimental work is that in comparison with uni-directional loading bi-directional loading cause extensive degradation of column stiffness, strength and ductility and hence it should be incorporated in seismic design process (Watanabe et al., 2000; Oyawa et al., 2004; Onishi et al., 2005; Goto et al. 2006). This literature review reveals that the focus of research up to the present deals to observe the effect of bi-directional loading on steel columns and evaluation of their ultimate capacity. With the rapid development of computer techniques and advantages of Finite Element method, it is now possible to observe multi-directional dynamic response of complex bridge structures; however, application methodology of the available ultimate limit values in the seismic design process is not clearly established. Therefore, the main objective of the present work is to propose seismic design method for the circular steel bridge piers when subjected to multi-directional earthquake by using the ultimate ductility values i.e. capacity, calculated from numerical static analysis with different loading conditions.

1.3 Objectives and Contents of Present Study

This research is projected to extend the basic knowledge of uni-directional cyclic

loading effect on the strength and ductility of steel columns which has been developed in past few decades; to that of using bi-directional cyclic loading. As the previous research work by Gao et al., (1998b) and Usami et al., (1998) had verified the accuracy of the in-house developed material constitutive law-'modified two-surface model' (M2SM) for predicting the cyclic hysteretic behavior of steel structures under uni-directional cyclic loading, hence it is assumed that same constitutive law is suitable for bi-directional cyclic loading also.

In the present work, an inelastic large displacement finite element analyses are carried out considering material and geometrical nonlinearity. The material nonlinearity is obtained by M2SM and geometrical nonlinearity is considered through the finite element program ABAQUS. The effect of local buckling in the steel columns is captured by employing the shell type elements and to neglect this effect, beam type elements are used. The parametric study is carried out to investigate the influence of the important parameters such as radius-thickness ratio, slenderness ratio and axial force ratio. As a result, strength and ductility formulas taking into account the effect of such parameters are proposed to check the seismic performance of steel circular columns.

This dissertation consists of seven chapters. Following paragraphs give brief description of each chapter. The present chapter explains about the need of this research and general introduction of this topic. **Fig. 1.2** shows the organization of chapters in short.

Chapter 2 is concerned with the historical review of various ductility prediction formulas developed since last few decades. The step by step improvement in FE modeling and various loading conditions on the circular steel columns are summarized. Finally, current requirement in evaluation of ductility for circular steel columns is explained.

Chapter 3 deals with displacement-based ductility prediction using bi-directional cyclic loading with constant vertical load. The effect of design parameters on the strength and ductility are observed by carrying out parametric study. Based on these parametric results, ultimate displacement formulas are developed and depending on them a seismic design procedure is proposed. The bi-directional dynamic analyses are carried out to confirm the proposed method.

Chapter 4 is related to strain-based ductility evaluation for circular steel columns keeping the loading condition same as used in Chapter 3. The effect of bi-directional

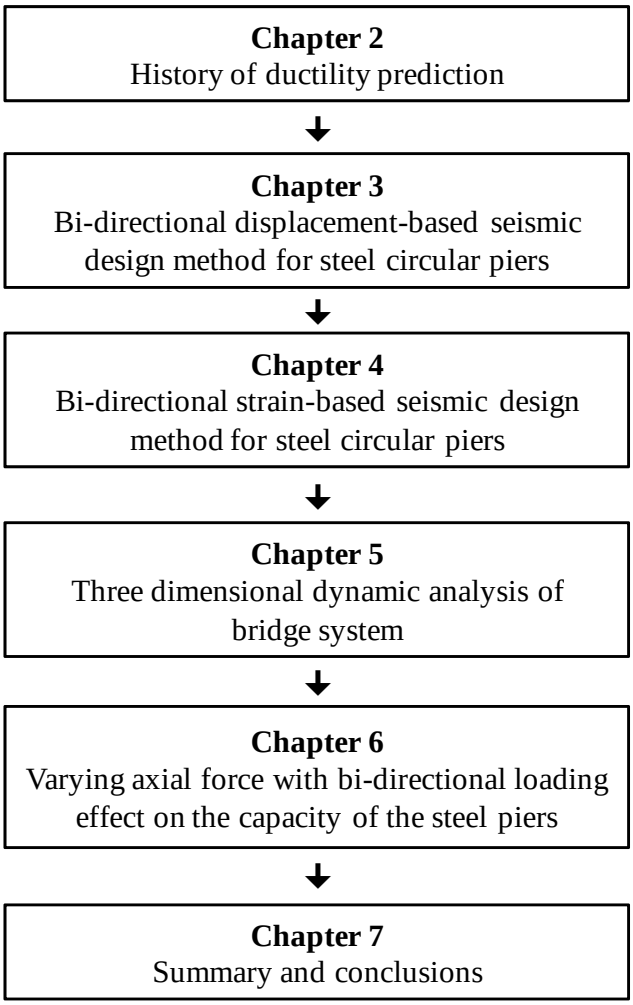

Fig 1.2 Organization of Chapters and In-Short Content

loading patterns on the behavior of ultimate strains is explained. From the parametric study, the ultimate strain formulas are predicted and a seismic design procedure is defined. To confirm this proposed method, some bi-directional dynamic analyses are conducted and compared with former displacement-based method.

In Chapter 5, dynamic analyses are carried out on simple bridge systems by applying two horizontal and one vertical component of earthquakes. The influence of vertical component over two horizontal components of the earthquake on bridge pier behavior is investigated.

The work carried out in Chapter 6 is based on the conclusions of Chapter 5. Accordingly, it was found in Chapter 5 that 3D earthquake has caused large variations in the axial force response. Hence, the static nonlinear analyses are conducted by applying various patterns of varying axial force along with the bi-directional

displacement loadings and their influences on strength, ductility, dissipated energy and local buckling of the pier are compared. Finally, Chapter 7 includes summary and concluding remarks drawn from present research work.

Chapter 2

HISTORY OF DUCTILITY PREDICTION FOR STEEL BRIDGE PIERS

2.1 Introduction

As introduced in Chapter 1, seismic design of steel bridge piers is very important for the urban transportation network, which became much clear after the 1995 Hyogo-ken Nanbu earthquake. The ability of such structures to survive in severe earthquakes depends on both the strength and ductility of the structures. Hence, from last few decades, great efforts aimed at investigating inelastic cyclic behavior of thin-walled steel bridge piers and at providing fundamental data for coding of seismic design rules have been contributed by many researchers. Of which, most of the research activities are mainly concerned with experimental investigations which is very important to perform, but at the same time precise numerical methods are also necessary to establish procedures for seismic design of the structures. And this has been the objective of past research work.

Up to the present, various stress-strain relationships, such as elastic-perfectly plastic, bilinear with hardening, and tri-linear with both strain hardening and Bauschinger effect, have been proposed and used to simulate the material behavior (Nakashima and Wakabayashi, 1992). Tree-surface plasticity model (Goto et al., 1997) and modified two-surface plasticity model (Shen et al., 1992, 1995; Mamaghani et al., 1995) based on the material model proposed by Dafalias and Popov (1975), are also developed to predict the cyclic behavior of the structures. These models can treat the cyclic behavior of structural steel even within the yield plateau. Hence, progress in both the numerical technique and constitutive law have brought into a possibility of simulating the cyclic behavior of steel structures with certain guarantee.

The present chapter deals with the historical review of ductility predictions mainly for circular steel bridge piers. The empirical formulas proposed by the past studies for steel cylinders, steel circular pipe sections, under various loading conditions are summarized here.

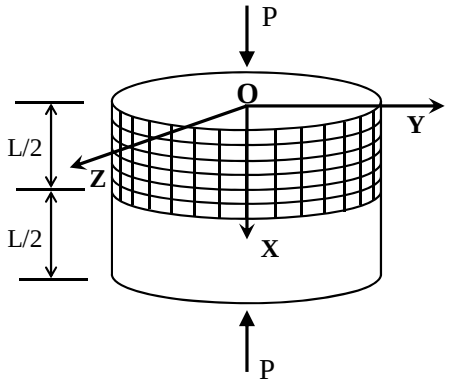

Fig. 2.1 Steel Short Cylinder under Pure Compression

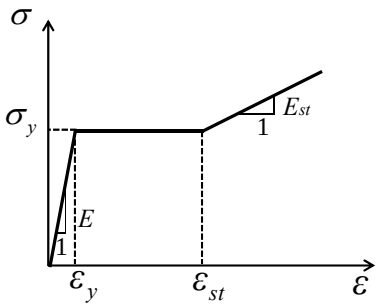

Fig. 2.2 Stress-Strain Relationship of Material

2.2 Ductility of Steel Short Cylinders

As observed in the Hyogo-ken Nanbu earthquake, damages were not happened only to steel box-section piers, but also to the steel pipe-section piers as shown in **Fig. 1.1**. Different from columns usually used in the buildings, these bridge piers are characterized by lower axial load ratio and are designed with relatively large radius-thickness ratios of component plates. This makes them susceptible to damage by local buckling during severe earthquake events. To control the damage of such columns, it was believed to investigate the ductility capacity of steel short cylinders. In the following sub-sections, ductility formulations in different loading cases are discussed.

2.2.1 Pure Compression

The shell element models were developed for a portion between two diaphragms which would show local buckling in compression loading as illustrated in **Fig. 2.1**. The monotonic stress-strain relationship which considers yield plateau and strain hardening as given in **Fig. 2.2** is used. Both the initial geometric deflections and residual stress due to welding were taken into consideration. The ultimate strength formula and ultimate strain corresponding to 95% of ultimate strength after peak load were proposed as given by **Eqs. (2.1)** and **(2.2)** respectively (Gao et al., 1998a).

$$\frac{\sigma_m}{\sigma_y} = 1 - 0.43\sqrt{R_t - 0.03} \qquad (0.03 \le R_t \le 0.50) \tag{2.1}$$

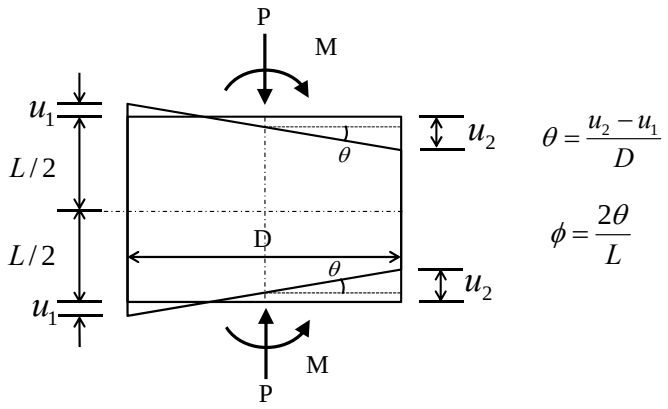

Fig. 2.3 Steel Short Cylinder under Combined Compression and Bending

$$\frac{\varepsilon_u}{\varepsilon_y} = \frac{0.445}{(R_t - 0.03)} + 1.0 \qquad (0.03 \le R_t \le 0.50) \tag{2.2}$$

where, R_t is the radius-thickness ratio parameter and can be obtained by **Eq. (2.3)**,

$$R_t = \left(\frac{\sigma_y}{E}\right)\left(\frac{D}{2t}\right)\sqrt{3(1-\nu^2)} \tag{2.3}$$

in which, σ_y = yield stress; E = Young's modulus; ν = Poisson's ratio; and D and t are diameter and plate thickness of the cylinder respectively.

2.2.2 Combined Compression and Bending

Fig. 2.3 shows pipe-section stub-column subjected to combined compression and bending. Besides the parameter R_t, axial force P is also taken as a dependent variable. The ultimate bending moment normalized by plastic moment M_p, is given by **Eq. (2.4)** and normalized failure curvature, ϕ_u / ϕ_y and normalized failure strain, $\varepsilon_u / \varepsilon_y$ are given by **Eqs. (2.5)** and **(2.6)** respectively (Gao et al., 1998a).

$$\frac{M_u}{M_p} = 1 - 0.43\sqrt{R_t - 0.030}\left(1 + \frac{P}{P_y}\right)^{2.90} \tag{2.4}$$

$$\frac{\phi_u}{\phi_y} = \frac{0.12}{(R_t - 0.03)^{1.5}(1 + P/P_y)^5} + 2.2(1 - P/P_y) \tag{2.5}$$

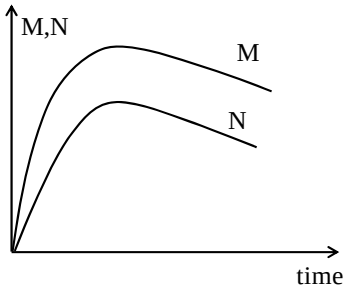

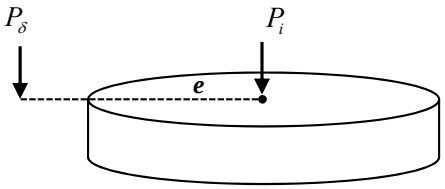

Fig. 2.4 Monotonic Loading for Moment and Axial Force

Fig. 2.5 Loading Method for Axial Fluctuation

$$\frac{\varepsilon_u}{\varepsilon_y} = \frac{0.12(1+4(P/P_y))}{(R_t-0.03)^{1.45}(1+P/P_y)^5} + 3.6(1-P/P_y) \tag{2.6}$$

where, $0.03 \le R_t \le 0.50$； $P/P_y \le 0.3$.

Above mentioned ultimate strain formula was modified again by Ge et al., (2004) with similar condition of loading and wider range of axial force ratio and which is as following **Eq. (2.7)**;

$$\frac{\varepsilon_u}{\varepsilon_y} = \frac{0.14(1-P/P_y)^{1.8}}{(R_t-0.03)^{1.4}} + \frac{3}{(1+P/P_y)^{0.7}} \le 20.0 \tag{2.7}$$

where, $0.03 \le R_t \le 0.50$； $0 \le P/P_y \le 1.0$.

The maximum limit is set on the ultimate strain as 20.0. The explanation to this assumption is given in the subsequent chapter.

2.2.3 Combined Bending and Axial Force Fluctuations

In many structures the axial force fluctuates considerably along with bending moment during earthquake. These fluctuations are significant and may have influence on capacity, especially in portal frame bridge piers and arch bridges. Cetinkaya et al., (2008), have carried out analytical study on the steel short cylinders, taking into account fluctuation of axial force. They considered the axial force fluctuation parameter α, as a ratio of final axial force P_f to initial axial force P_i. The monotonic loading as shown in **Fig 2.4** was adopted as an idealization of this kind of

cyclic fluctuation in which the axial force and bending moment increase together in linear manner. In order to simulate the axial force fluctuation, an eccentric displacement load P_δ that results in linear axial force and bending moment was applied at the top of the cylinder as shown in **Fig. 2.5**.

Instead of generating new formula for ductility, the influence of axial force fluctuation on existing constant axial force formula (i.e. **Eq. (2.7)**) was captured by defining appropriate correction function (Cetinkaya et al., 2008) as follows;

$$f(R_t, P_f / P_y, \alpha) = \frac{(0.095\alpha + 0.024)P_f / P_y + 1.001}{R_t^{[(0.017\alpha+0.007)P_f / P_y - 0.006\alpha - 0.003]}} \geq 1 \tag{2.8}$$

The final failure strain can be obtained by multiplying correction value from **Eq. (2.8)** with the ultimate strain value from **Eq. (2.7)**.

2.3 Ductility of Cantilever Column under Cyclic Loading

Similar to the aforementioned ultimate strain formulas for steel short cylinders under various loadings, the ductility of steel bridge piers can be measured in terms of deformation. For this purpose, it is important to choose critical loading pattern. In early research, the uni-directional cyclic loading pattern was considered to observe hysteretic behavior and to propose the ductility and strength of the bridge piers. Later the bi-directional cyclic loading was found to be more destructive than uni-directional cyclic pattern. Some ultimate strength and ductility formulas developed for the circular pipe sections under both types of cyclic loading are given in following paragraphs.

2.3.1 Uni-directional Cyclic Loading

The numerical analyses were carried out for finite element models with material and geometrical nonlinearity by applying constant axial force and horizontal cyclic displacement at the top as shown in **Fig. 2.6**. The modified two-surface model was adopted for material cyclic behavior. The peak strength is considered as limiting value for strength. However, for the ultimate displacement definition, the value corresponding to 95% of peak strength was selected and formulas are proposed as follows (Gao et al., 1998b);

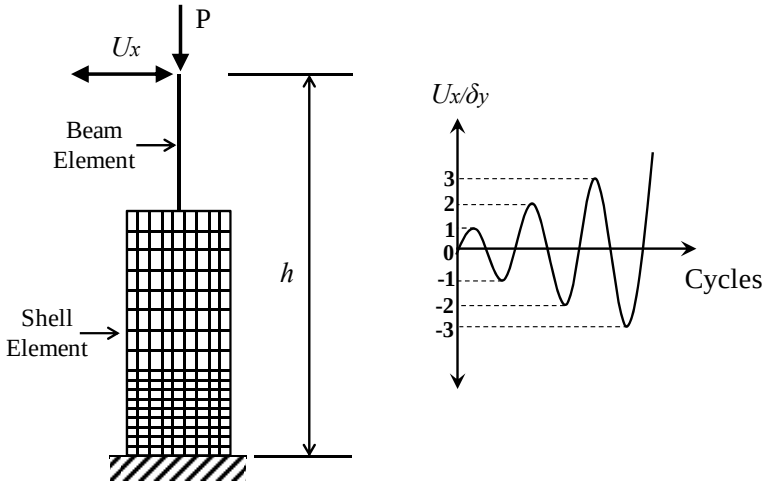

(a) Analytical FE Model (b) Uni-directional Loading

Fig. 2.6 FE Model and Uni-directional Loading (Gao et al., 1998b)

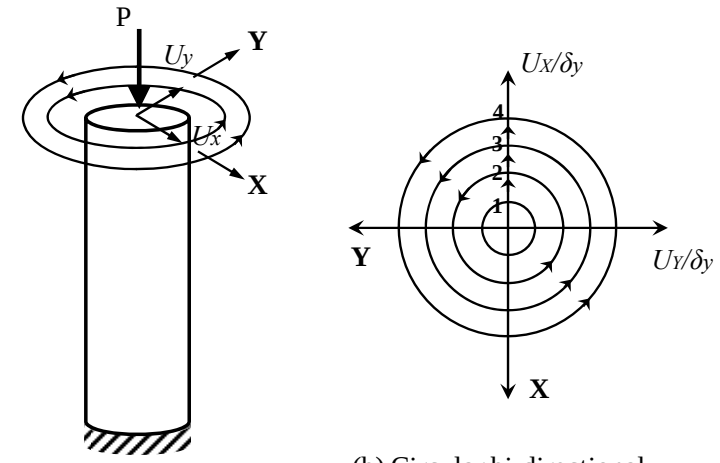

(a) Analytical FE Model (b) Circular bi-directional Loading

Fig. 2.7 FE Model and Bi-directional Loading (Goto et al., 2006)

$$\frac{H_{\max}}{H_y} = \frac{0.02}{(R_t\bar{\lambda})^{0.8}} + 1.10 \tag{2.9}$$

$$\frac{\delta_m}{\delta_y} = \frac{1}{3(R_t\bar{\lambda}^{0.5})^{0.8}} - \frac{2}{3} \tag{2.10}$$

$$\frac{\delta_{95}}{\delta_y} = \frac{0.24}{(1+P/P_y)^{2/3}\bar{\lambda}^{1/3}R_t} \tag{2.11}$$

Along with the radius-thickness ratio parameter R_t and axial force ratio P/P_y, these formulas are dependent on the slenderness ratio parameter $\bar{\lambda}$. Moreover, in the

maximum strength and ductility formulas (i.e. **Eqs. (2.9)** and **(2.10)**), the term P/P_y is ignored because of its small influence.

2.3.2 Bi-directional Cyclic Loading

Effect of various bi-directional patterns on the strength reduction of steel bridge piers has been studied experimentally and analytically (Watanabe et al., 2000; Oyawa et al., 2004). However, in the case of steel circular columns, circular bi-directional loading is apparently considered as more destructive than any other bi-directional loading such as; diagonal, rectangular or diamond. Goto et al., (2006) carried out analytical study on circular steel columns with the bi-directional loading pattern as shown in **Fig. 2.7**. The three-surface model was used to consider cyclic behavior of material. The strength and ductility formulas were proposed on the bases of formerly developed uni-directional strength and ductility formulas (Gao et al., 1998b).

$$\frac{H_{\max}}{H_y} = \frac{0.063}{R_t^{3/4}\bar{\lambda}^{1/4}} + 0.90 \tag{2.12}$$

$$\frac{\delta_m}{\delta_y} = \frac{0.27}{R_t^{3/4}\bar{\lambda}^{1/4}} + 0.18 \tag{2.13}$$

$$\frac{\delta_{95}}{\delta_y} = \frac{0.6}{R_t^{3/4}\bar{\lambda}^{1/4}(1+P/P_y)^{1/2}} \tag{2.14}$$

2.4 Ultimate State of Cantilever Column Subjected to Bi-directional Earthquakes

Even if the ultimate strength and ductility formulas were proposed for the steel circular columns subjected to bi-directional loading (Goto et al., 2006); their application in bi-directional seismic design process was not explained so far. Hence, based on the so-called pushover analysis under monotonically increasing unidirectional horizontal displacement, two types of circular ultimate interaction curves for columns are derived in terms of two horizontal restoring force components and two sway displacement components (Goto et al., 2009). The nonlinear dynamic analysis has shown that the ultimate horizontal restoring force interaction curves give good prediction of ultimate states of the column than that of the displacement curves. Therefore, a formula was derived to provide the ultimate interaction curves for

arbitrary thin-walled circular columns as follows for SM490 steel grade;

$$\frac{H_u^p}{H_y} = \left(\frac{0.123}{R_t^{0.575} \bar{\lambda}^{0.339} (1 + P/P_y)^{3.090}} + 0.814 \right) (1 - P/P_y)^{-1} \tag{2.15}$$

2.5 Summary

The present chapter dealt with the historical review of ultimate strength and ductility formulation derived from last few decades and particularly for the thin-walled steel circular bridge piers. For confirming the safe performance of steel columns under earthquake excitations, the above mentioned ultimate formulas calculate allowable limit within which the displacement and strain responses should be laid. Therefore, it is necessary to have such an ultimate formulation which can predict the critical strength or ductility carrying capacity of the steel columns and this implies to discover severe loading pattern. The similar development can be seen in past research such as; for short cylinder initially only compression loading was considered then modified to combine compression and bending and further to combined bending and fluctuating axial force. And in the case of cantilever columns, initially uni-directional loading was considered and after that the bi-directional circular loading.

The research has been continued to define the critical loading patterns and development of ductility formulas. Furthermore, attention has also been paid for applicability of derived ultimate formulas for seismic design of steel bridge piers under one or more dimensional earthquake motions. One of the ways for bi-directional seismic design for circular steel columns was introduced in this chapter, which is based on the ultimate interaction curve for restoring strength (Goto et al., 2009). And hence in progress of this theme, ultimate states of steel bridge piers in terms of displacement and strain ductility considering bi-directional loading and based on that seismic design methods are proposed by author in following Chapters 3 and 4.

Chapter 3

DISPLACEMENT-BASED BI-DIRECTIONAL SEISMIC DESIGN FOR STEEL CIRCULAR PIERS

3.1 Introduction

The construction of steel bridge piers in urban area and concrete bridge piers in country side area is a common practice in Japan. The steel bridge piers have advantage of smaller cross section and rapid erection and hence ideal for urban areas where the land prices are high. Moreover, when compared with concrete bridges, the seismic performance of steel highway bridges was found better during Hyogo-ken Nanbu earthquake because, new constructions were based on revised code in 1990. However, many older and few new steel bridges suffered remarkable damages and numerous types of bridge failures which were observed for the first time, such as severe to fatal buckling of steel columns, brittle column failures and new types of bearing failure (Bruneau, 1998). This implies that seismic design of the steel bridge piers is very important for urban transportation after the strong earthquake events and the ability of bridge piers to perform well in the severe earthquakes depends on both its energy dissipation and ductility capacity.

As mentioned in Chapter 2, various strength and ductility formulas are defined for steel circular bridge piers using various types of loading conditions so far. The recent past studies have proved that earthquake waves consists of three-directional components and act simultaneously in the seismic event (Anderson and Mahin, 2004; Okazaki et al., 2003). Therefore, it is necessary to predict accurately the ultimate behavior of steel bridge piers during severe earthquakes. Particularly, the coupling of two horizontal components is expected to have an adverse effect on the ultimate behavior of these steel columns. However, the past research on this topic was mainly concerned with reinforced concrete columns (Takizawa et al., 1976; Saatcioglu et al., 1989; Zahn et al., 1989; Wong et al., 1993; Bousias et al., 1995; Qiu et al., 2002). Related to the steel columns, few numbers of cyclic bi-directional loading experiments were carried out by Watanabe et al., (2000), Fujimoto et al., (2000) and Goto et al., (2006). From which, Goto et al., (2006) proposed ultimate strength and ductility formulas for circular steel columns (given in Chapter 2), but, implementation

of these ultimate ductility formulas in bi-directional seismic design method was not clarified anywhere. For this purpose, the present work is aimed at developing such a seismic design method which incorporates uni- as well as bi-directional earthquake effects on steel circular columns and verify their performance.

Present study deals with bi-directional cyclic behavior of steel circular columns by using modified two-surface model which accounts cyclic nonlinearity of material and development of ductility formulas. In which first, a description of numerical analytical method is presented, then the local buckling of column in uni- and bi-directional loading is illustrated by contour plots. The parametric study is conducted to investigate the effect of important parameters such as; radius-thickness ratio, slenderness ratio and magnitude of axial force. Empirical formulas are proposed for strength and ductility and based on these formulas; a bi-directional seismic design method is developed. To check the applicability of this method, nonlinear dynamic analyses are carried out on some piers.

3.2 Analytical Method

To solve the problem of uniform steel circular bridge piers subjected to constant axial force and cyclic lateral loading, Finite Element (FE) method is considered as an ideal method, which accounts large deformations in the model and gives fairly acceptable results. The construction of FE model, types of cyclic lateral loading and analytical method used to solve this problem is briefly explained in the following paragraphs.

3.2.1 Finite Element Model

For thin-walled steel columns of uniform circular sections subjected to constant axial force and cyclic lateral loading, local bucking always occurs near the base of the columns which is also called as ‘an elephant foot bulge’. Hence, shell elements are used for lower part of the FE model. The height of this lower part is assumed as three times of diameter of the column *D*. Compared to the lower part of the column, bending moments are insignificant in upper part; therefore beam elements are employed in this portion of the FE model. Ring type diaphragms with inner radius of *0.8R* and plate thickness of *9 mm* are placed along the column height at an interval of *D* as shown in **Fig. 3.1**. Section-I of shell element portion is divided into 30 segments

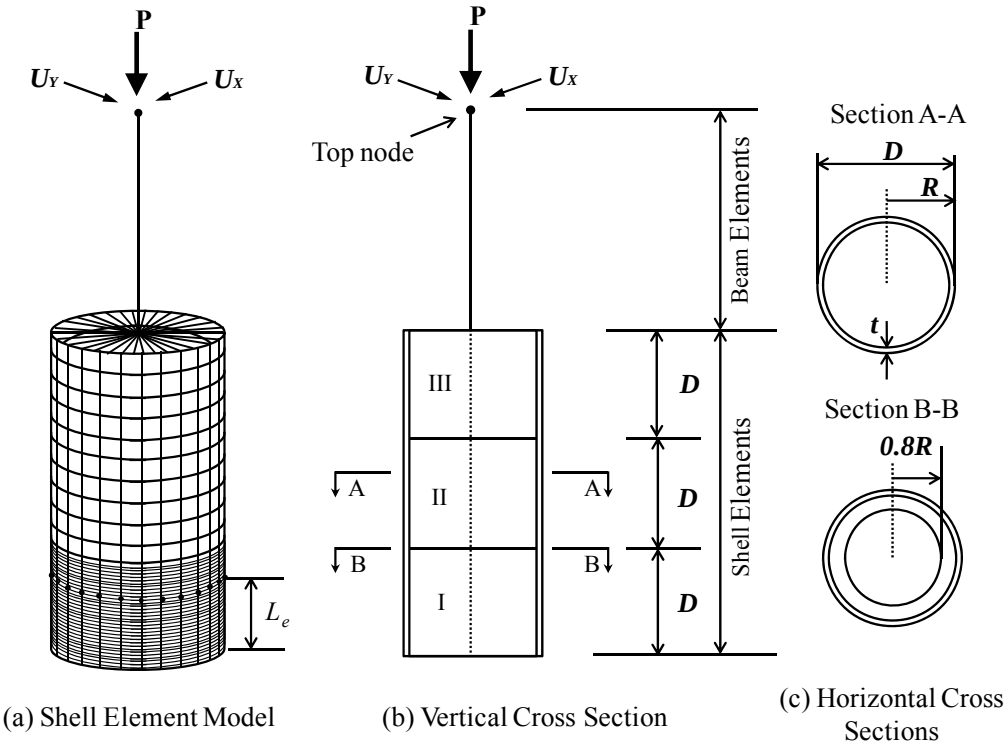

Fig. 3.1 Details of Shell Element Model

and sections-II and III into 5 segments along the height of the column. And all these three sections are divided into 30 segments circumferentially. The upper beam element portion is made up of 10 segments. This meshing pattern is based on the reference of past study carried out by Gao et al., (1998b). Rigid elements are used in between interface of shell and beam element parts, to maintain plane boundary condition and connectivity between two different types of element. For modeling and analyzing this FE model, standard ABAQUS nonlinear FE software (Dussault System Simulia Corp., 2007) is used.

For beam elements, Timoshenko PIPE31 beam elements included in ABAQUS element library are employed. The spread of plasticity in these elements is considered in both through the cross section and along the member length. The incremental stress-strain relationship for each integration point of beam element is defined by uniaxial formulation of modified two-surface model (Shen, 1993).

For shell elements, reduced integration four-node general elements S4R are used and spread of plasticity is assumed in both through the thickness and plane of the element. Hence, the multiaxial formulation of M2SM is applied for stress-strain relationship (Shen, 1993). Theoretical explanation about uniaxial and multiaxial

M2SM is given in **Appendix A** along with accuracy check of 2SM with experimental data. Cyclic behavior of the structural steel grade SM490 ($\sigma_y = 315$ MPa) is adopted in FE analysis through M2SM defined in the subroutine UMAT. The properties of SM490 grade steel are also presented in **Appendix A**.

3.2.2 Loading Patterns

In the past few studies, bi-directional loading patterns such as biaxial square, circular, diamond, plus were proposed and their effect on the hysteretic behavior of steel columns were examined by conducting experiments (Bousias et al., 1995; Watanabe et al., 2000 and Qiu el al., 2002). Among them bi-directional circular pattern was found to be apparently severe for circular steel columns (Goto et al., 2006). Hence, in the present study similar bi-directional loading pattern is used so that it can be easily compared with conventional uni-directional loading. **Fig 3.2 (a)** shows the development of circular loading pattern from two mutually perpendicular uni-directional patterns. When the circular loading trajectory crosses the X axis; it completes one cycle of rotation as shown in **Fig. 3.2 (b)**. Following **Eqs. (3.1)** and **(3.2)** give the magnitude of displacements in positive and negative X directions;

(a) Progressing in positive X direction

$$\left.\begin{aligned} \frac{U_X}{\delta_y} &= \frac{1}{2} - \left(n - \frac{1}{2}\right)\cos(\pi s) \\ \frac{U_Y}{\delta_y} &= -\frac{b}{a}\left(n - \frac{1}{2}\right)\sin(\pi s) \end{aligned}\right\} \qquad (3.1)$$

(b) Progressing in negative X direction

$$\left.\begin{aligned} \frac{U_X}{\delta_y} &= n\cos(\pi s) \\ \frac{U_Y}{\delta_y} &= \frac{b}{a} n \sin(\pi s) \end{aligned}\right\} \qquad (3.2)$$

where, n = number of cycles ($n \geq 1$); s = time dependent variable; b/a = ratio of displacement amplitudes in Y to X directions in which a = major axis length and b = minor axis length of elliptical path as defined in **Fig. 3.2 (b)**. When $b/a = 0$, the loading becomes uni-directional and when $b/a = 1$ the loading changes to circular as

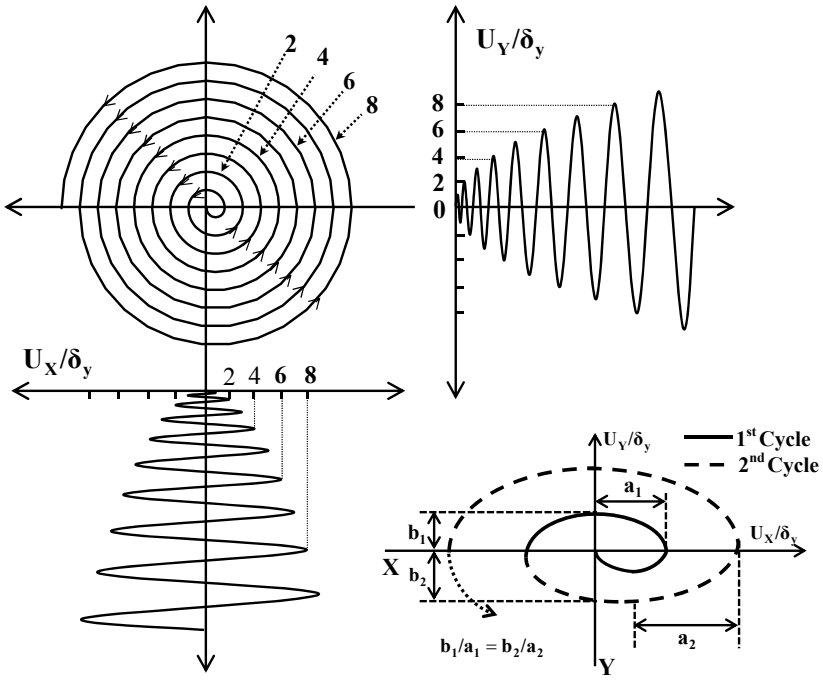

(a) Development of Bi-directional Loading

(b) Definition of One Cycle

Fig. 3.2 Details of Uni- and Bi-directional Loading

shown in **Fig. 3.2 (a)**. The displacement amplitude applied in each cycle is in multiplication of yield displacement, δ_y which is given by **Eq. (3.3)**;

$$\delta_y = \frac{H_y h^3}{3EI} + \frac{H_y h}{\kappa GA} \tag{3.3}$$

where, H_y = yield strength; which is obtained from the smaller value of following **Eqs. (3.4)** and **(3.5)**.

$$H_y = \frac{M_y}{0.85h}\left(1-\frac{P}{P_E}\right)\left(1-\frac{P}{P_u}\right) \tag{3.4}$$

$$H_y = \frac{M_y}{h}\left(1-\frac{P}{P_y}\right) \tag{3.5}$$

in which, M_y = yield moment; h = height of the column; P = axial compressive load; P_E = Euler's buckling load ($P_y/\bar{\lambda}^2$); P_u = ultimate load ($(1.109-0.545\bar{\lambda})P_y$); P/P_y = axial force ratio; P_y = squash load ($\sigma_y A$).

3.2.3 Analysis Technique

FE model of steel circular columns are analyzed by applying constant axial downward force and lateral cyclic displacement loadings as shown in **Fig. 3.1** using the ABAQUS program. The material and geometric nonlinearities are also considered. The modified Newton iteration technique coupled with the displacement control method is used for analysis. The details of solution procedure can be found in the ABAQUS theory manual (2007). The displacement convergence criterion is adopted in the analysis and the convergence tolerance is taken as 10^{-5}. The initial geometrical deflections and residual stresses are not taken into consideration, as it has negligible effect in cyclic behavior of steel columns.

3.2.4 Parameters of Analytical Models

For the thin-walled steel circular columns, the important design parameters are; radius-thickness ratio parameter (R_t), slenderness ratio parameter ($\bar{\lambda}$), and axial force ratio (P/P_y). The definition of R_t is given in **Eq. (2.3)** of Chapter 2 and slenderness ratio parameter is defined as follows;

$$\bar{\lambda} = \frac{2h}{r}\frac{1}{\pi}\sqrt{\frac{\sigma_y}{E}} \tag{3.6}$$

where, r = radius of gyration of the column section; σ_y = yield stress and E = modulus of elasticity.

The ranges of these parameters assumed in the present study are given in **Table 3.1**. The column names are designated by their R_t and $\bar{\lambda}$ values. For example, P75-40 means the column having $R_t = 0.075$ and $\bar{\lambda} = 0.4$. **Table 3.1** gives effective failure length (L_e) values for each column. The effective failure length is also known as critical wavelength, the term used by Timoshenko and Gere (1996). Based on this critical wavelength concept, Gao et al., (1998a) had carried out study on effect of L_e / D on ultimate strength of steel cylinders for different R_t values and derived the equation for L_e (see **Eq. (3.7)**) defining minimum height of cylinder within which local buckling occurs as illustrated in **Fig. 3.1.**

$$L_e = 1.2D\left(\frac{1}{R_t^{0.08}} - 1\right) \tag{3.7}$$

Table 3.1 Properties of Circular Steel Columns

Columns (1)	R_t (2)	$\bar{\lambda}$ (3)	D (mm) (4)	h(mm) (5)	t (mm) (6)	L_e (mm) (7)
P50-20	0.050	0.20	789	2152	20	256
P50-40	0.050	0.40	789	4303	20	256
P50-60	0.050	0.60	789	6455	20	256
P60-20	0.060	0.20	942	2582	20	285
P60-40	0.060	0.40	942	5164	20	285
P60-60	0.060	0.60	942	7745	20	285
P75-20	0.075	0.20	1173	3227	20	324
P75-40	0.075	0.40	1173	6454	20	324
P75-60	0.075	0.60	1173	9681	20	324
P90-20	0.090	0.20	1403	3872	20	358
P90-40	0.090	0.40	1403	7744	20	358
P90-60	0.090	0.60	1403	11620	20	358

Note: Axial force ratio (P/P_y) values: 0.0, 0.05, 0.10, 0.15, 0.20.

3.3 Effect of Loading Pattern on Local Buckling

As mentioned before local buckling appears near the base of the steel columns when subjected to cyclic loading. Hence, the effect of uni- and bi-directional cyclic loading patterns at the base part of columns is observed in the form of contour plots. The nodal deformations from the initial position are measured as illustrated in **Fig. 3.3 (a)**. The i^{th} node on the surface of the column, is supposed to be at the point A $(x(0)_i, y(0)_i)$ as an initial position. After $\bar{t}$ seconds of loading the point A shifts to new position point B $(x(\bar{t})_i, y(\bar{t})_i)$. The amount of deformation outside the surface of the column is observed as $\delta_d(\bar{t})_i$. By using simplified formulation, the deformation of the i^{th} node outside the surface of the column can be calculated as follows,

$$\delta_d(\bar{t})_i = \sqrt{x(\bar{t})_i^{\,2} + y(\bar{t})_i^{\,2}} - R \tag{3.8}$$

where, R = radius of the column.

In this way the deformation of each node on the surface of the column are calculated and normalized by thickness t of the plate i.e. δ_d / t. These deformation

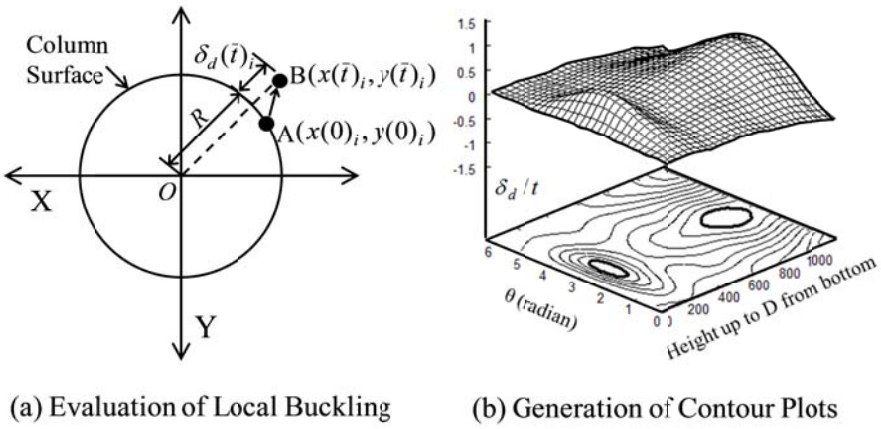

(a) Evaluation of Local Buckling (b) Generation of Contour Plots

Fig. 3.3 Concept of Local Buckling

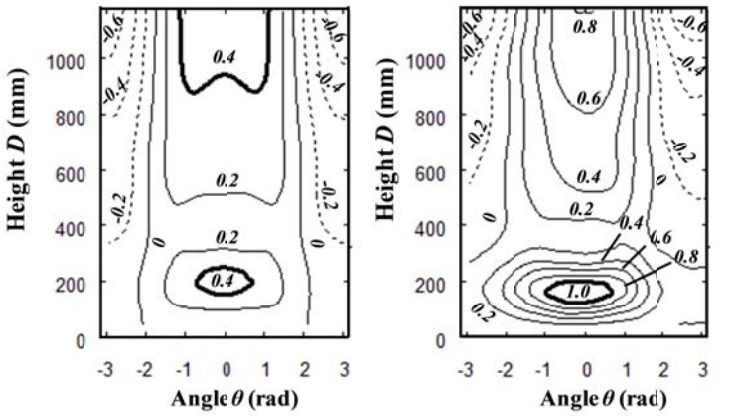

(a) Uni-directional Loading (b) Bi-directional Loading

Fig. 3.4 Contour Plots for Column P75-40

quantities are further plotted against angular distance θ radians of each node along the circumference of the column as shown in **Fig. 3.3 (b)**. Further, the contour lines are drawn at an interval of $\delta_d / t = 0.2$ in which, dashed lines are for inward buckling and solid lines are for outward buckling. The solid thick line indicates the maximum outward buckling.

Fig. 3.4 shows contour plots for the column P75-40 with $P / P_y = 0.15$ when subjected to uni- and circular bi-directional loading and plotted at the time interval of their respective ultimate states. **Figs. 3.4 (a)** and **(b)**, clearly show that, circular cyclic bi-directional loading generates large maximum buckling of about $1.0\,\delta_d / t$ in comparison with $0.4\,\delta_d / t$ for cyclic uni-directional loading. In other words, in bi-directional loading each point of the column cross section passes through tension-

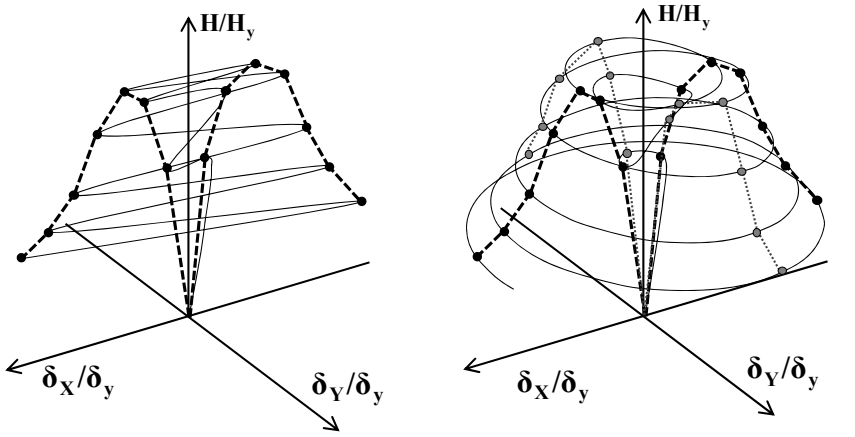

(a) Cyclic Uni-directional Strength and Ductility Relationship

(b) Cyclic Bi-directional Strength and Ductility Relationship

Fig. 3.5 3D Strength and Ductility Relationship

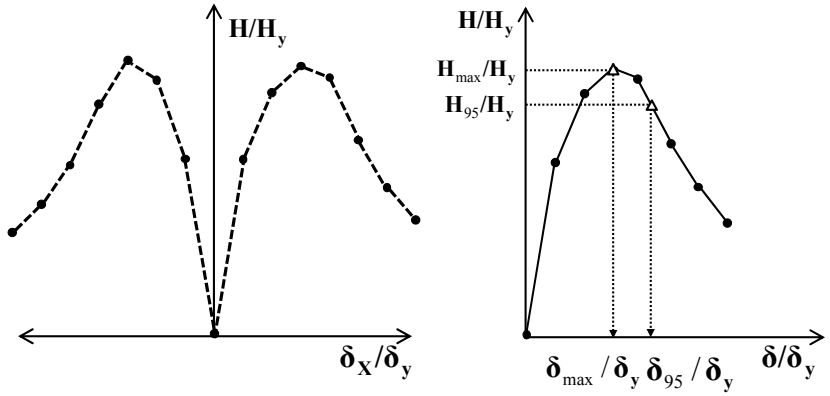

(a) Strength Envelop Curves in Both Sides of X axis

(b) Strength Envelop Curve and Definition of Ultimate State

Fig. 3.6 Strength Envelop Curves

compression cycles and hence plasticity spreads evenly through the cross section. However, in uni-directional loading, two opposite points of column cross section experience extreme tension-compression cycles and plasticity initiates from these points and then propagates to the points in near vicinity along the cross section. This phenomenon is responsible for rapid loss of column strength and ductility in bi-directional loading in comparison with uni-directional loading.

3.4 Parametric Study

In all 12 columns (see **Table 3.1**) are analyzed to investigate the influence of main parameters (i.e. R_t, $\bar{\lambda}$ and P/P_y) and loading patterns on the strength and

ductility of steel circular columns.

Before going to observe the effect of these parameters, it is necessary to understand the concept of generation of envelop curves for strength versus ductility under cyclic loading. In monotonic lateral loading, the strength and ductility relationship is quite easy to imagine. However, in case of cyclic loadings the strength and ductility profile oscillates between two opposite sides of the axis. Moreover, in bi-directional cyclic loading one more axis is get added in this swing of strength and ductility. Hence, for strengths in two mutually perpendicular axes X and Y, the concept of unique restoring strength i.e. $H = \sqrt{H_X^2 + H_Y^2}$ is employed based on past study (Goto et al., (2006)). **Figs. 3.5 (a)** and **(b)** show three-dimensional view of normalized strength H/H_y and normalized ductility δ_X/δ_y, δ_Y/δ_y in X and Y axes for uni- and circular bi-directional loadings respectively. The dashed lines are drawn by connecting the crossing points of solid trajectories to X and/or Y axis which is called as strength envelop curve. For uni-directional case (**Fig. 3.5 (a)**), two envelops can be plotted, whereas for bi-directional case (**Fig. 3.5 (b)**), four envelops are possible to draw. As the cyclic loading patterns used in this study has equal amplitudes on both sides of axis in each cycle, ductility only along X axis are considered for plotting envelop curves as shown in **Fig. 3.6 (a)**. Positive X axis side envelop curve is selected for further study of comparison as illustrated in **Fig. 3.6 (b)**.

3.4.1 Effect of Radius-thickness Ratio Parameter

Fig. 3.7 shows the strength-ductility envelop curves plotted for constant $P/P_y =$ 0.10. The major observation indicates that as R_t increases the maximum strength decreases. Concerned to uni-directional loading (abbreviated as UNI hereafter), it is found that as $\bar{\lambda}$ increases the post peak curves become steeper. Whereas, in the case of circular bi-directional loading (abbreviated as CIR hereafter), with $\bar{\lambda} = 0.2$ shows rapid decrease in strength after peak than the cases of $\bar{\lambda} = 0.4$ and 0.6. When compared with UNI and CIR effect, CIR loading lowers down maximum strength carrying capacity of columns irrespective of R_t and $\bar{\lambda}$.

While designing the steel bridge piers, for example $R_t = 0.06$ and $\bar{\lambda} = 0.2$, the displacement corresponding to maximum strength is 5δ if loading is UNI; which implies that column P60-20 has large energy absorption capacity and high ductility. On the other hand, if the loading pattern changes to CIR, the same column shows poor maximum strength and 2δ will be the corresponding displacement. Therefore, setting

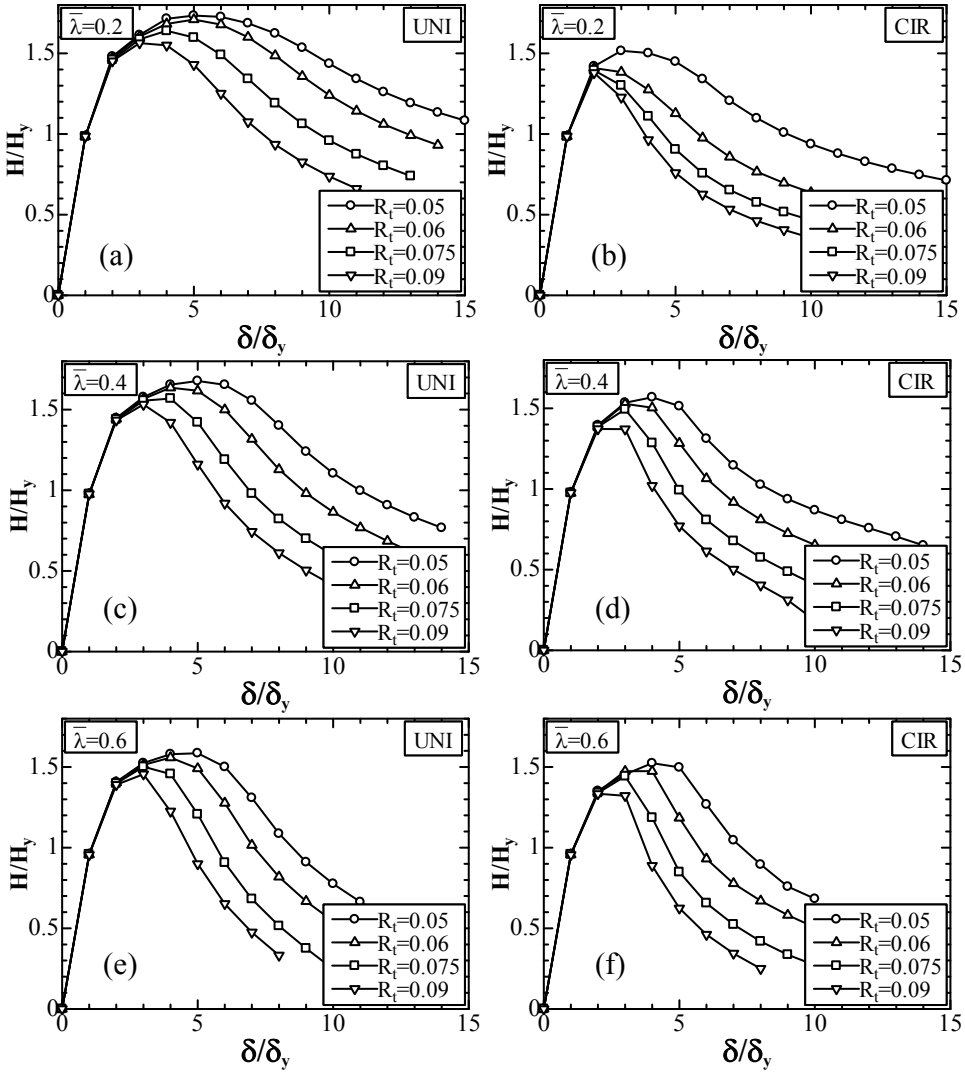

Fig. 3.7 Effect of R_t on Strength and Ductility Capacity

the value of $\bar{\lambda}$ is equally important as R_t in the designing of steel columns subjected to bi-directional earthquake motions.

3.4.2 Effect of Slenderness Ratio Parameter

To study the effect of column slenderness ratio; the strength-ductility envelop curves are plotted as shown in **Fig. 3.8** considering unique case of $P/P_y = 0.10$. Concerned with UNI loading, it is observed that as $\bar{\lambda}$ increases the maximum strength decreases independent of R_t values. Moreover, as R_t increases, the post peak curves become steeper. Whereas, in case of CIR loading the columns with $\bar{\lambda} = 0.4$ has shown large maximum strength than other two cases (i.e. $\bar{\lambda} = 0.2$ and 0.6). And columns with $\bar{\lambda} = 0.2$ have indicated significant strength reduction after the peak

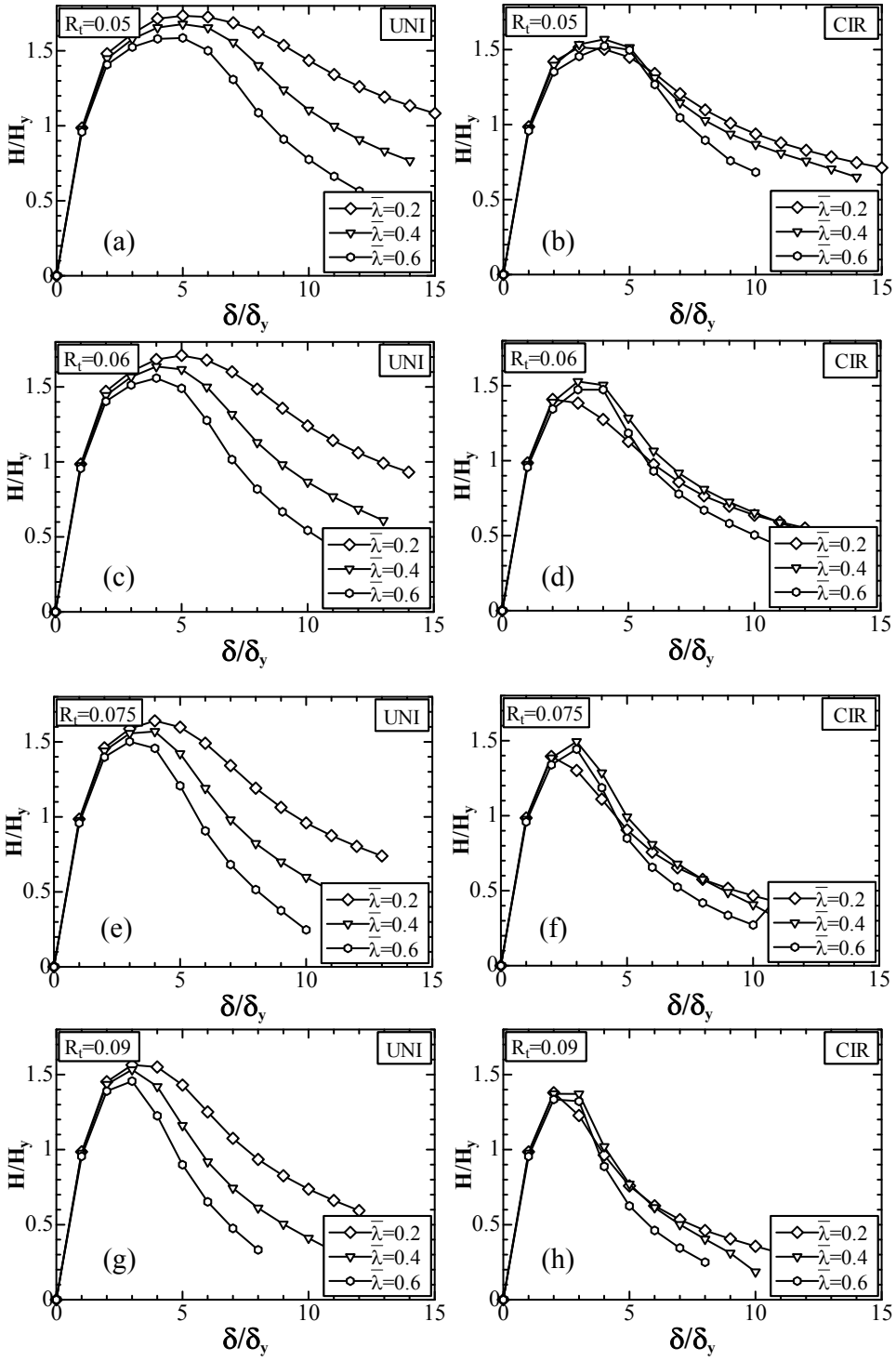

Fig. 3.8 Effect of $\bar{\lambda}$ on Strength and Ductility Capacity

excluding for the case $R_t = 0.05$. Similar to UNI loading cases, in CIR loading the post peak curves become more slanting as R_t increases.

As mentioned before, the effect of slenderness ratio is significant when it is less than 0.4 and R_t ranges from 0.06 to 0.09. This range covers large number of

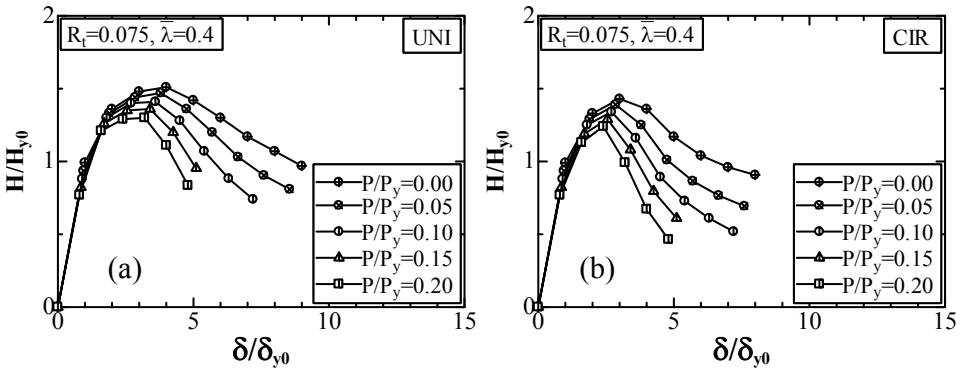

Fig. 3.9 Effect of Axial Force

practical steel bridge pier dimensions. Hence, it is very important to consider $\bar{\lambda}$ along with R_t in design of steel piers when subjected to bi-directional components.

3.4.3 Effect of Axial Force

To understand the influence of axial force on a sample steel column P75-40, five cases of axial forces are considered such as; P/P_y = 0.0, 0.05, 0.10, 0.15 and 0.20. **Fig. 3.9** shows the normalized horizontal strength (H/H_{y0}) versus horizontal displacement (δ/δ_{y0}) curves for this column. It should be noted that H_{y0} and δ_{y0} are denoted for the horizontal yield force and yield displacement corresponding to zero axial load and used in nondimesionalizing the curves to highlight the effect of axial force. In both cases of loadings UNI and CIR, it is observed that as the axial force increases, the maximum strength decreases. The possible reason lies in the significant P-Δ effect for large axial load. Moreover, **Fig. 3.9** indicates that as the axial force increases the post peak curves become steeper. Especially for the CIR loading, the ductility capacity of the column reduces significantly. An average percentage decrease in ductility corresponding to the maximum strength is 25% when loading changes from UNI to CIR.

3.5 Strength and Ductility Formulation for Steel Circular Columns

In the conventional seismic design of columns under uni-directional seismic horizontal load (Japan Road Association, 2002), it is assumed that the column reaches to its ultimate state when restoring strength approaches to peak on the strength-displacement envelop curve as shown in **Fig. 3.6 (b)**. Therefore $H_{\max}/H_y$

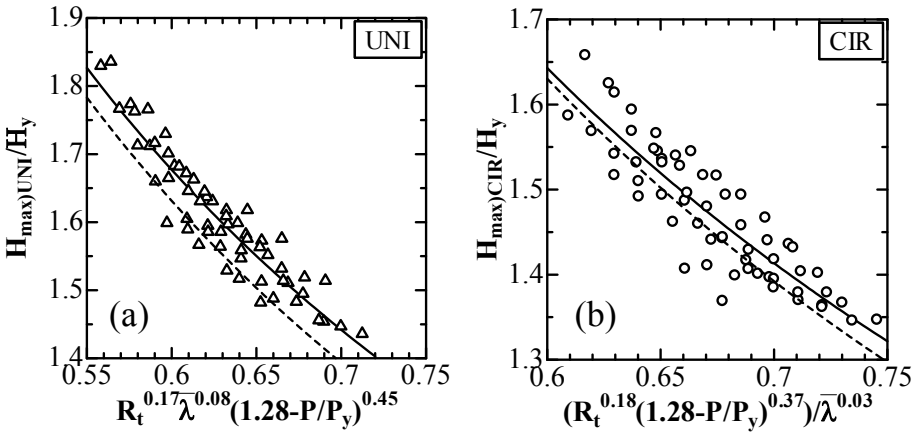

Fig. 3.10 Ultimate Strength Formulation

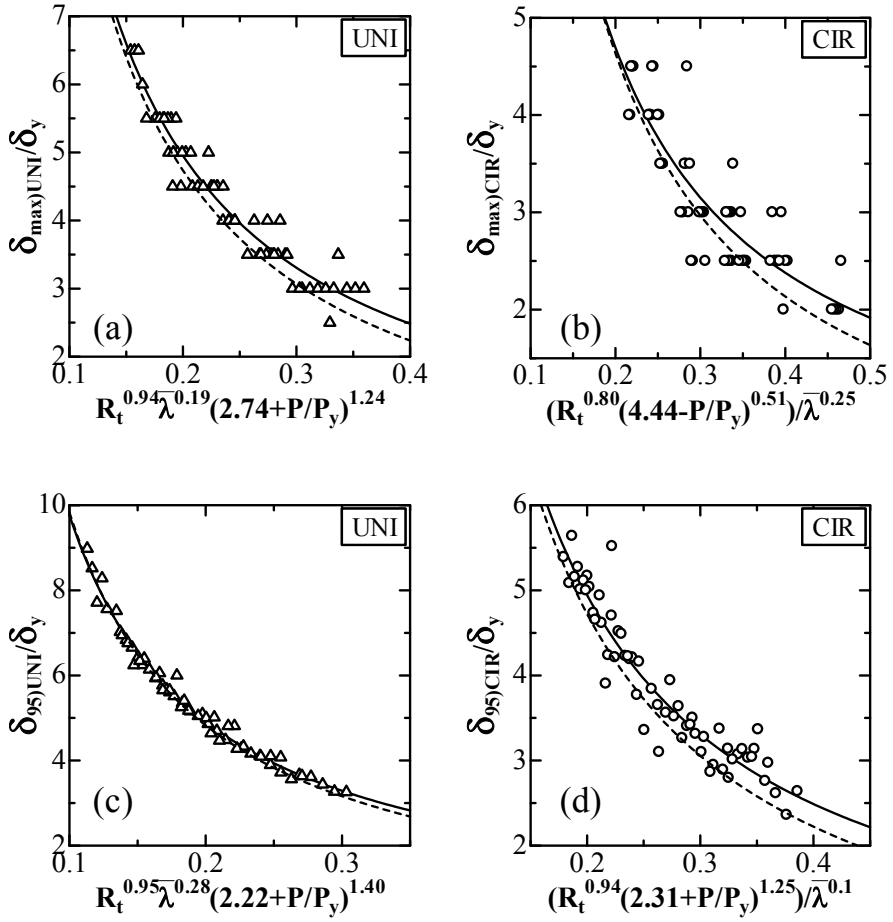

Fig. 3.11 Ductility Formulation

parameter is selected to define ultimate state of column in terms of strength. However, to describe ductility capacity, two ductility parameters $\delta_{\max}/\delta_y$ and δ_{95}/δ_y are selected. Here, $\delta_{\max}$ is the displacement corresponding to the maximum strength and δ_{95} is the displacement at the point where the strength reduces to 95% of ultimate strength on post peak curve (see **Fig. 3.6 (b)**). Even though ductility factor $\delta_{\max}/\delta_y$ is physically clear, it does not incorporate the cyclic loading characteristics fully. Therefore, it seems more reasonable to use the definition δ_{95}/δ_y to evaluate ductility formulas (Gao et al., 1998b).

The values of $H_{\max}/H_y$, $\delta_{\max}/\delta_y$ and δ_{95}/δ_y are plotted against integrated factor of R_t, $\bar{\lambda}$ and P/P_y in **Figs. 3.10** and **3.11** separately for UNI and CIR loadings. Constants and powers of these integrated factors are determined by nonlinear regression analysis to fit the discrete data. Following are the equations predicted from the fitted curves for ultimate strengths and ductility;

(a) For cyclic uni-directional loading;

$$\frac{H_{\max)UNI}}{H_y} = \frac{1}{R_t^{0.17}\bar{\lambda}^{0.08}(1.28 - P/P_y)^{0.45}} - 0.04 \tag{3.9}$$

$$\frac{\delta_{\max)UNI}}{\delta_y} = \frac{1}{R_t^{0.94}\bar{\lambda}^{0.19}(2.74 + P/P_y)^{1.24}} - 0.26 \tag{3.10}$$

$$\frac{\delta_{95)UNI}}{\delta_y} = \frac{1}{R_t^{0.95}\bar{\lambda}^{0.28}(2.22 + P/P_y)^{1.40}} - 0.17 \tag{3.11}$$

(b) For cyclic circular bi-directional loading;

$$\frac{H_{\max)CIR}}{H_y} = \frac{\bar{\lambda}^{0.03}}{R_t^{0.17}(1.28 - P/P_y)^{0.37}} - 0.04 \tag{3.12}$$

$$\frac{\delta_{\max)CIR}}{\delta_y} = \frac{\bar{\lambda}^{0.25}}{R_t^{0.80}(4.44 - P/P_y)^{0.51}} - 0.37 \tag{3.13}$$

$$\frac{\delta_{95)CIR}}{\delta_y} = \frac{\bar{\lambda}^{0.10}}{R_t^{0.94}(2.31 + P/P_y)^{1.25}} - 0.28 \tag{3.14}$$

Valid for the ranges, $0.05 \le R_t \le 0.09$, $0.2 \le \bar{\lambda} \le 0.6$ and $0.0 \le P/P_y \le 0.2$

To validate these proposed equations, it is necessary to judge them against some existing equations or experimental data. Hence, the equations fitted for strength and ductility considering only one case of $P/P_y = 0.15$ are compared with the equations from past study (Goto et al., 2006) and given in **Appendix B**. **Eqs. (3.10)**, **(3.11)** and **(3.13)**, **(3.14)** indicate that for a given ductility demand, the critical value of R_t and $\bar{\lambda}$ can be obtained when either of them is known. **Table 3.2** contains the limit values of R_t for various required ductility using δ_{95}/δ_y as the ductility evaluation index. The axial load is assumed as $0.15P_y$. It is found that for UNI loading, the column with $\bar{\lambda} = 0.3$ and $R_t < 0.089$, the value of $\delta_{95)UNI}/\delta_y$ can be guaranteed to exceed 4.0 and in the case of $\bar{\lambda} = 0.5$, for same ductility demand, the value of R_t should be less than 0.076. On the other hand, when loading is CIR, the column with $\bar{\lambda} = 0.3$ and $R_t = 0.056$ has maximum ductility capacity 4.0; but when $\bar{\lambda}$ of the column increases to 0.5 and to achieve the same ductility $R_t = 0.060$ should be the minimum value. This apparently means, while designing for bi-directional loading, as the column height increases the columns become thinner. This is exactly opposite to the concept of designing for uni-directional loading. The probable reason for this phenomenon will be explained in the following chapter.

Table 3.2 Limit Values of R_t for Required Ductility

UNI						
$\delta_{95)UNI}/\delta_y$	$\bar{\lambda}$	R_t	$\bar{\lambda}$	R_t	$\bar{\lambda}$	R_t
(1)	(2)	(3)	(4)	(5)	(6)	(7)
3.0	0.3	0.118	0.4	0.109	0.5	0.102
4.0	0.3	0.089	0.4	0.082	0.5	0.076
5.0	0.3	0.071	0.4	0.065	0.5	0.061
6.0	0.3	0.059	0.4	0.054	0.5	0.051
CIR						
$\delta_{95)CIR}/\delta_y$	$\bar{\lambda}$	R_t	$\bar{\lambda}$	R_t	$\bar{\lambda}$	R_t
(1)	(2)	(3)	(4)	(5)	(6)	(7)
3.0	0.3	0.075	0.4	0.077	0.5	0.079
4.0	0.3	0.056	0.4	0.058	0.5	0.060
5.0	0.3	0.045	0.4	0.046	0.5	0.047
6.0	0.3	0.037	0.4	0.039	0.5	0.040

The ductility formulas derived here for seismic designing of steel bridge piers when subjected to uni-directional earthquake excitation, can be used directly to evaluate the deformation capacity. However, when bi-directional earthquake excitations are applied to bridge pier, the pier top displaces randomly in two perpendicular directions. Therefore, even if the ductility formulas proposed here for CIR loading, they cannot be used directly in the seismic designing process. Hence, it is needed to develop such a seismic design method which can take into account the deformation response of steel bridge piers when subjected to simultaneous two horizontal earthquake components.

3.6 Displacement-based Bi-directional Seismic Design Method

It is well accepted that when the structure is subjected to a single component of earthquake it vibrates in corresponding single degree of freedom only if the structure has no irregularity. On the other hand, when two orthogonal components of the earthquake are subjected to the structure or even under single earthquake component is applied to the asymmetry structure; the resulting displacement response history spreads between two perpendicular directions and shows complex nature. The verification of such two-dimensional displacement response against the allowable ductility is not explained anywhere so far. Therefore, in the present study a new concept of displacement-based bi-directional seismic design method is proposed.

The ductility formulas developed earlier (**Eqs. (3.11)** and **(3.14)**) are presented in new relationship between the ratio $\delta_{95)CIR} / \delta_{95)UNI}$ and a combined factor including R_t, $\bar{\lambda}$ and P / P_y parameters and shown in **Fig. 3.12**. This relationship can be formulated as follows;

$$\frac{\delta_{95)CIR}}{\delta_{95)UNI}} = R_t^{0.04} \bar{\lambda}^{0.37} (2.07 + P / P_y)^{0.2} - 0.06 \tag{3.15}$$

Although in the bi-directional dynamic study, the earthquake components are applied in two mutually perpendicular directions, the outer profile of displacement response of the piers has shown various shapes ranging from elliptical to circular which is different from the CIR loading pattern assumed while deriving ductility formulas. Therefore, it is necessary to correlate **Eq. (3.15)** with the shape factor (*b/a*)

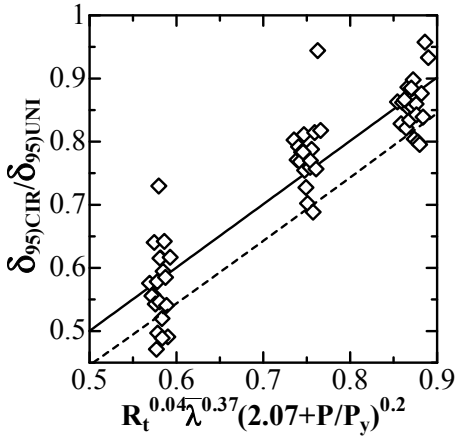

Fig. 3.12 Relationship between Ductility of CIR and UNI Loading

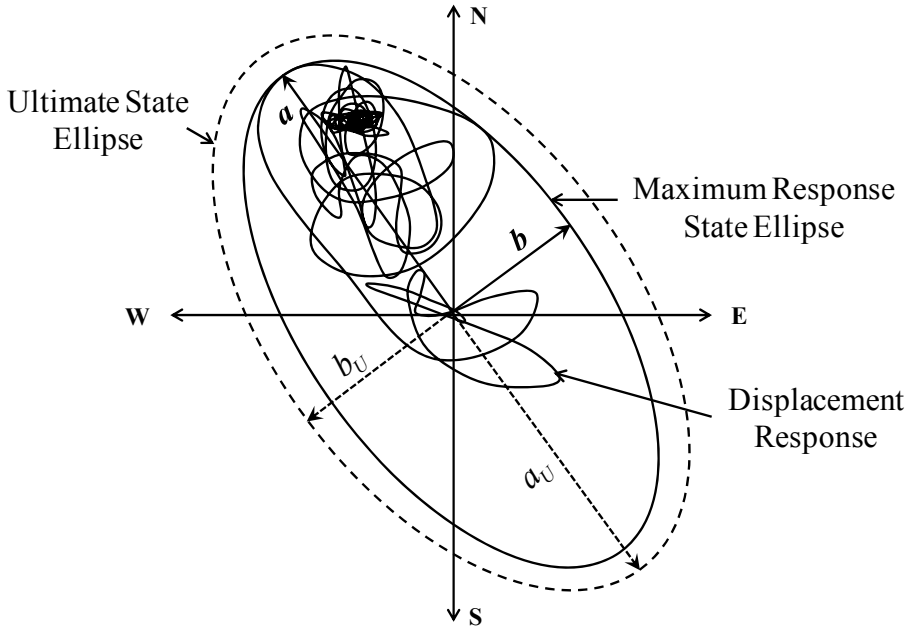

Fig. 3.13 Terminologies used in the Proposed Seismic Design Method

measured from outer profile of the displacement response by using following **Eq. (3.16)**.

$$\frac{\delta_{95)b/a}}{\delta_{95)UNI}} = \left(\frac{\delta_{95)CIR}}{\delta_{95)UNI}} - 1 \right) \frac{b}{a} + 1 \tag{3.16}$$

The terminologies used in the proposed bi-directional seismic design method are illustrated in **Fig. 3.13**. E-W and N-S are the directions along which the seismic forces

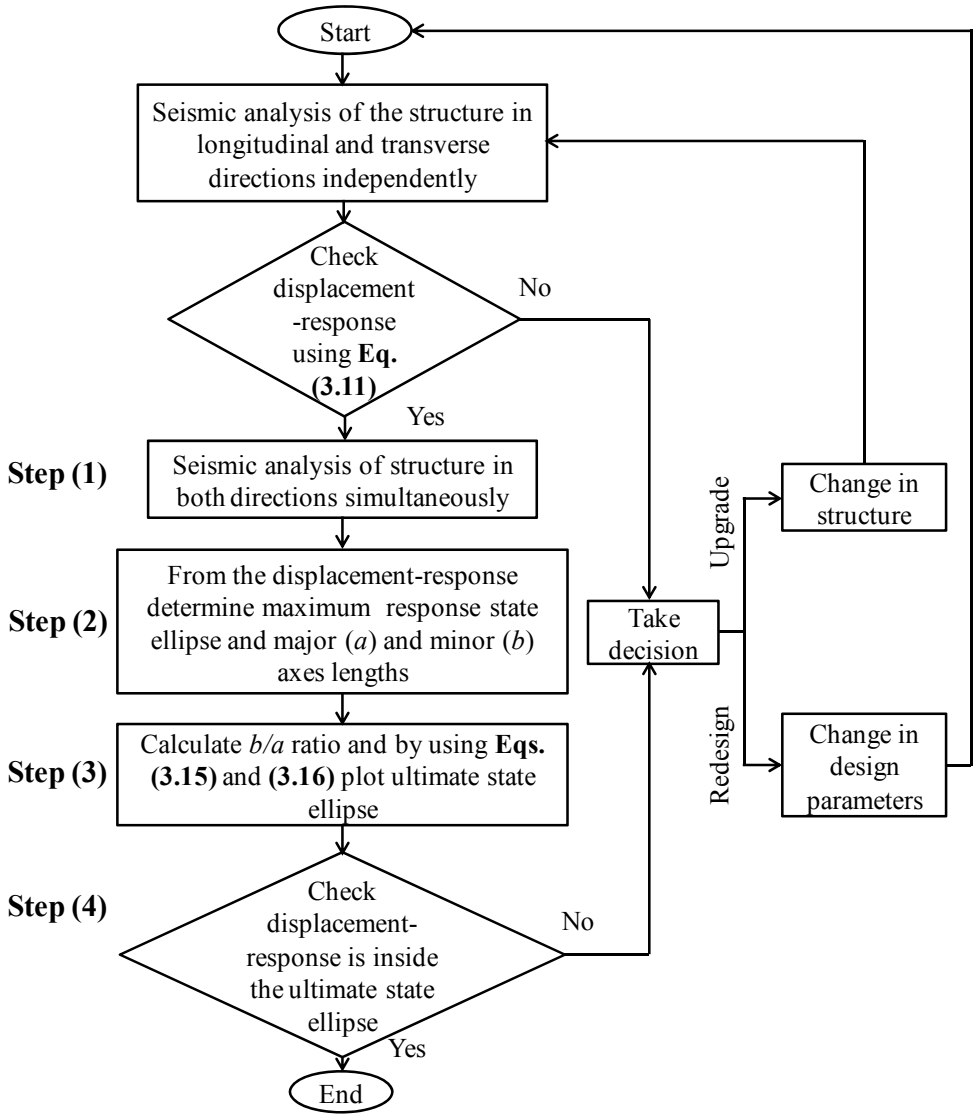

Fig. 3.14 Stepwise Procedure of the Proposed Seismic Design Method

are applied. The displacement response history of top node of the column in E-W and N-S directions is called as 'displacement response'. The 'maximum response state ellipse' is the ellipse which encloses the maximum displacement response. Center of this ellipse coincides with crossing point of E-W, N-S axes and its major and minor axis lengths are a and b respectively. The detailed procedure of plotting maximum response state ellipse is explained in **Appendix C**. a_U and b_U are respective lengths of major and minor axis for 'ultimate state ellipse' which has shown by dashed line in **Fig. 3.13**. The stepwise process of newly defined seismic design method is shown in **Fig. 3.14** and explained as follows;

(1) Since this proposed design method is an extension of traditionally used

uni-directional seismic design method, dynamic displacement response of top of the steel bridge pier in E-W and N-S directions are checked against ultimate ductility calculated from **Eq. (3.11)** by applying respective earthquake components individually.

(2) If the column confirms above check then as shown in Step (1) of **Fig. 3.14**; apply both E-W and N-S components of earthquake simultaneously, which will give displacement response history similar to that shown in **Fig. 3.12**.

(3) Next to that in Step (2), plot the 'maximum response state ellipse' which encircles all extreme points of displacement response keeping its center on crossing point of E-W and N-S directions (see **Appendix C**). Then measure the length of major and minor axis as *a* and *b* respectively of this plotted ellipse.

(4) In Step (3), evaluate the shape factor *b/a* and major axis length of the 'ultimate state ellipse' as $a_U = \delta_{95)b/a} / \delta_y$ from **Eqs. (3.15)** and **(3.16)**. Then draw an ultimate state ellipse by knowing a_U and $b_U = (b/a)a_U$, in the similar manners as the maximum response state ellipse was plotted.

(5) In final Step (4), check whether the ultimate state ellipse lies outside or inside of the maximum state ellipse. If the ultimate state ellipse is outside the maximum state ellipse, the column is assumed to be performed safely under bi-directional earthquake motions and if reverse case happens, the column is supposed to be responded unsafely. In this later case upgrade or redesign of the column is necessary until the safe condition is achieved.

In the succeeding paragraphs, the applicability of this proposed displacement-based bi-directional seismic design method is explained through some illustrative examples of nonlinear dynamic analysis.

3.7 Implementation of Seismic Design Method in Nonlinear Dynamic Analysis

In order to explain the implementation of the proposed seismic design method,

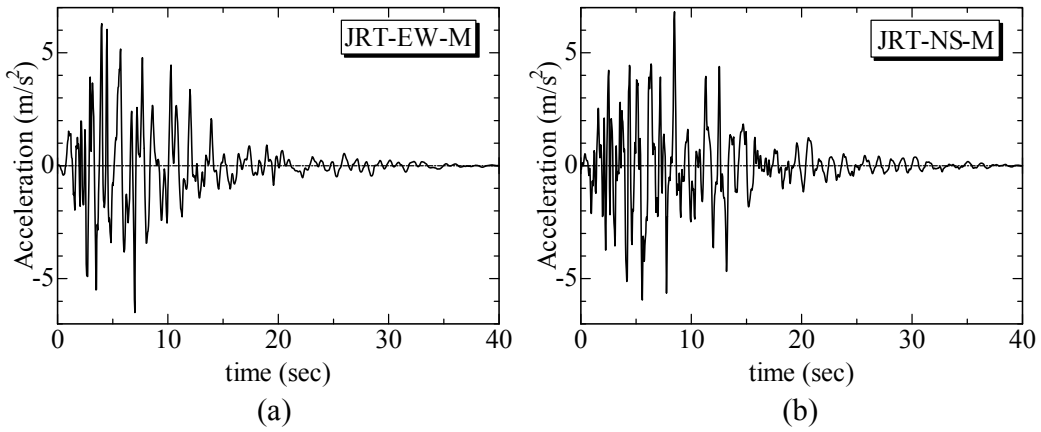

Fig. 3.15 Earthquake Motions Considered in Dynamic Analysis

nonlinear dynamic analyses are performed. Three cases of single bridge piers are selected as: P75-20, P75-40, P75-60, which have different slenderness ratios but same radius-thickness ratios. The beam element models with concentrated mass at the top of the columns are modeled by using ABAQUS software (see **Fig. D.1 (a)** of **Appendix D**). As mentioned before, uniaxial modified two-surface model can be employed in these analyses, to simulate the cyclic nonlinear behavior of steel material. The Rayliegh damping which usually appears in the dynamic analysis consists of mass proportional and stiffness proportional damping coefficient. Here, mass proportional damping coefficient, α is calculated for each pier based on their respective fundamental frequencies. Whereas, the stiffness proportional damping coefficient β is taken as zero, since it can be neglected when, the hysteretic damping due to nonlinear properties of material is considered.

To carry out the dynamic analysis, two strong ground motions on Ground Type-II (Japan Road Association, 2002); JRT-EW-M and JRT-NS-M as shown in **Figs. 3.15 (a)** and **(b)** are used. Following the steps given in the procedure of seismic design method, at first EW and NS earthquake motions are applied to each pier and response histories are plotted for deformations of the top node of the columns as indicated in **Fig. 3.16** and checked against the ultimate ductility δ_u / δ_y defined by **Eq. (3.11)**. It is observed from **Fig. 3.16 (a-c)** that design of all three columns is adequate to safeguard displacement responses within the allowable limits.

Moving ahead to the next step of the procedure, bi-directional dynamic analyses are carried out by applying EW and NS components of earthquakes at the same time. The displacement response histories in X and Y directions are plotted as shown in

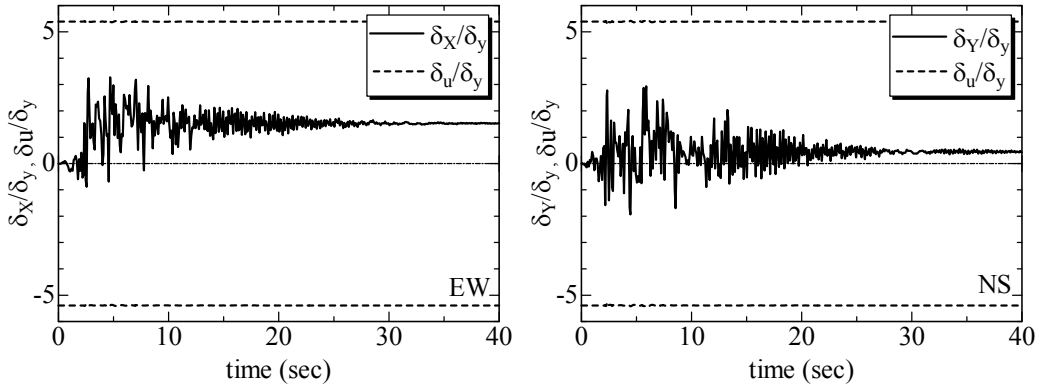

(a) Column P75-20

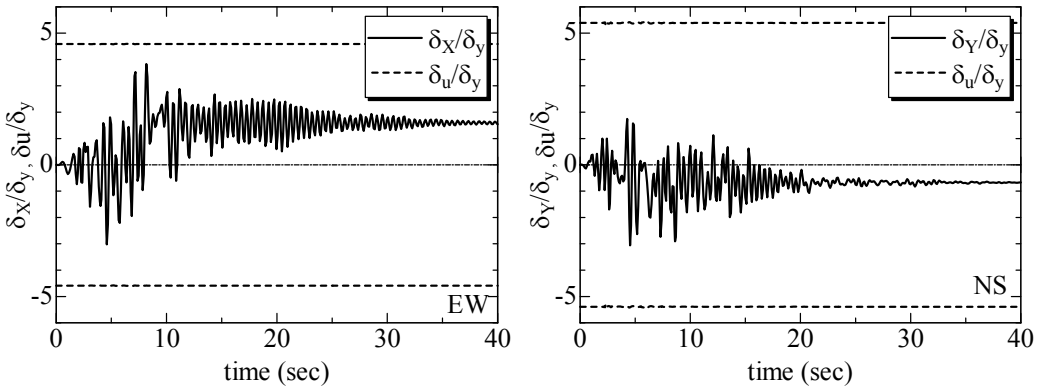

(b) Column P75-40

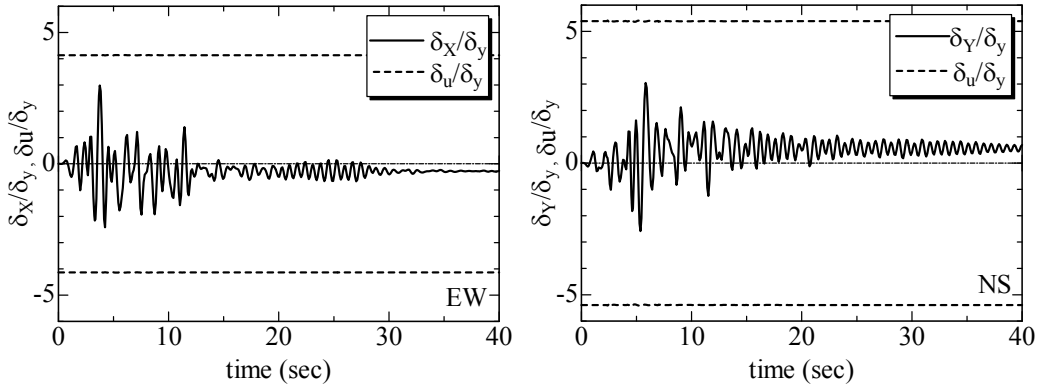

(c) Column P75-60

Fig. 3.16 Displacement Response Histories in Individual Earthquakes

Fig. 3.17. The maximum response state ellipses of solid thick line are drawn covering the displacement response. The major and minor axis lengths respectively *a* and *b* are measured and the shape factor *b/a* is calculated. Then the major axis length of ultimate state ellipse $a_U = \delta_{95)b/a} / \delta_y$ is determined by using the **Eqs. (3.14)** and **(3.15)**. Then minor axis length of ultimate state ellipse is calculated by $b_U = (b/a)a_U$. The ultimate state ellipses in dashed line are drawn coinciding with maximum state

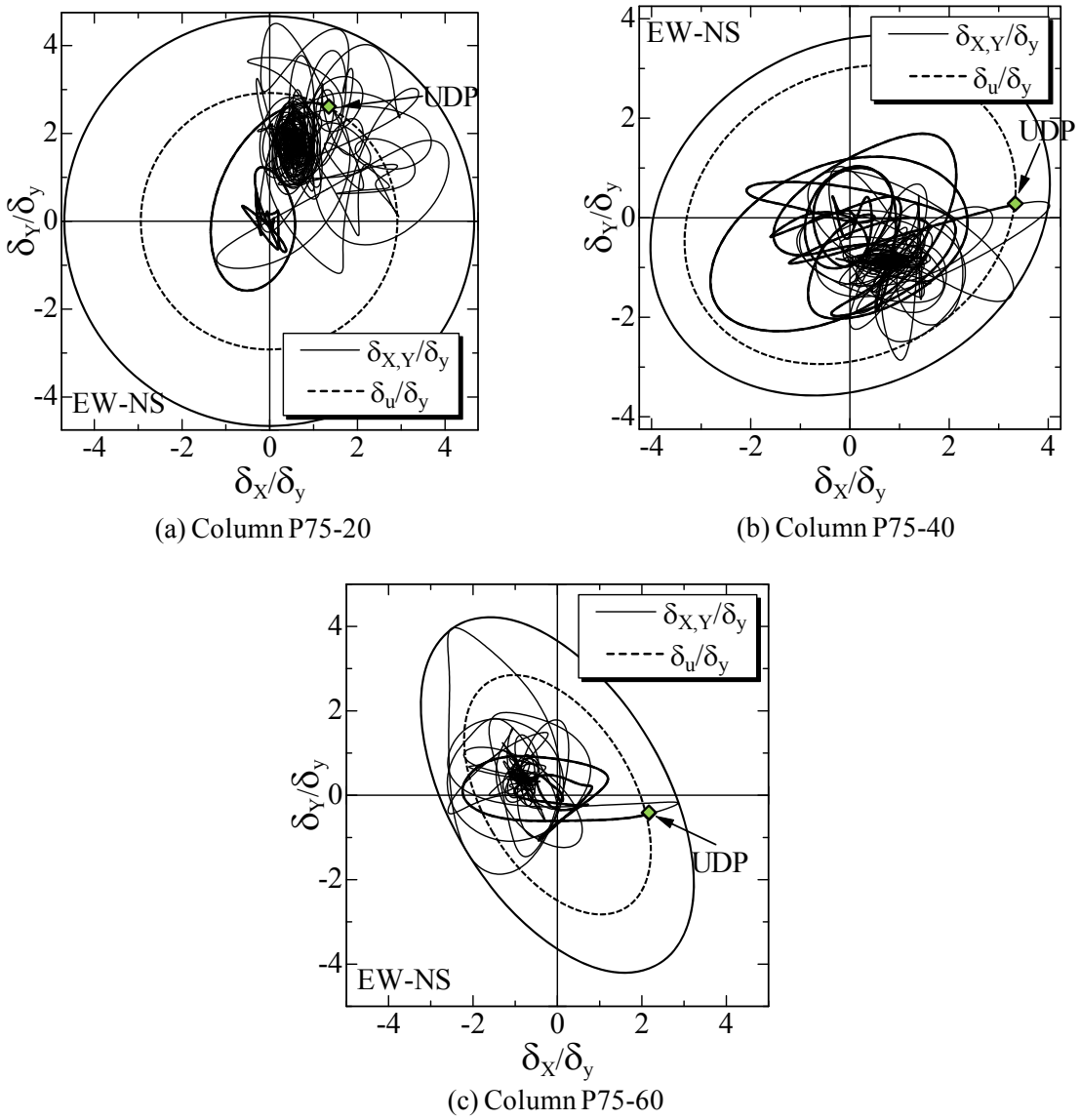

(a) Column P75-20

(b) Column P75-40

(c) Column P75-60

Fig. 3.17 Displacement Response Histories in Bi-directional Earthquakes (Unsafe)

ellipses. **Fig. 3.17 (a-c)** indicates that in all cases the ultimate state ellipse lies inside of maximum response state ellipse. This implies that column designs which have given safe responses during individual earthquake excitations are unable to satisfy the seismic design condition defined for bi-directional seismic response check. The coupling of two earthquake motions amplified the displacement responses; hence the presently designed columns are unsafe in the bi-directional earthquake. In this situation, redesign or upgrade options are suggested in the design procedure. Therefore, redesign option is selected. For keeping the geometrical properties of the columns same in redesign step, instead of altering thickness of each column plates (in

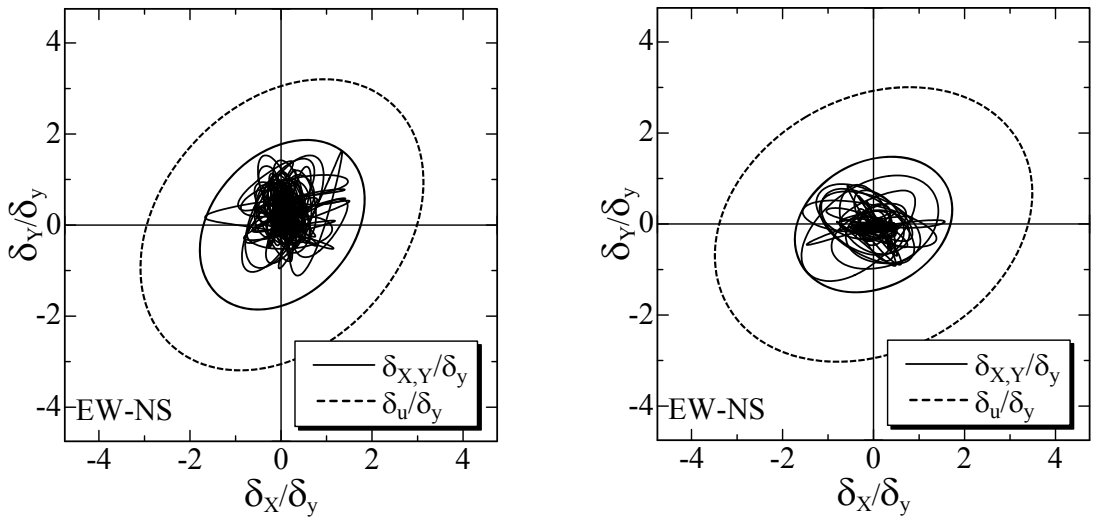

(a) Column P75-20

(b) Column P75-40

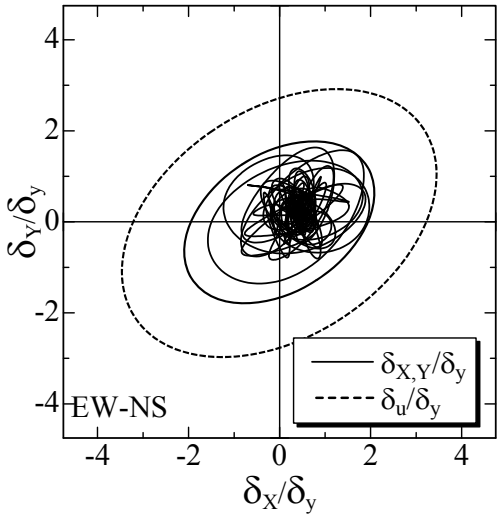

(c) Column P75-60

Fig. 3.18 Displacement Response Histories in Bi-directional Earthquakes (Safe)

other words, radius-thickness ratio), the lumped masses at the top node of the columns are adjusted at this redesign step in such a way that bi-directional response of all three columns satisfy the condition given in the seismic design method. **Fig. 3.18** shows displacement responses are within ultimate state ellipses which mean the columns are performed safely. However, it should be noted that, in the real bridge design process the amount of lumped mass due to superstructure remains fixed and engineers have to alter the thicknesses of column plates.

In addition to the displacement response histories, average compressive strain response histories are also measured in the base part of three columns. The calculation procedure of average compressive strain is explained in **Appendix D**. **Fig. 3.19** shows

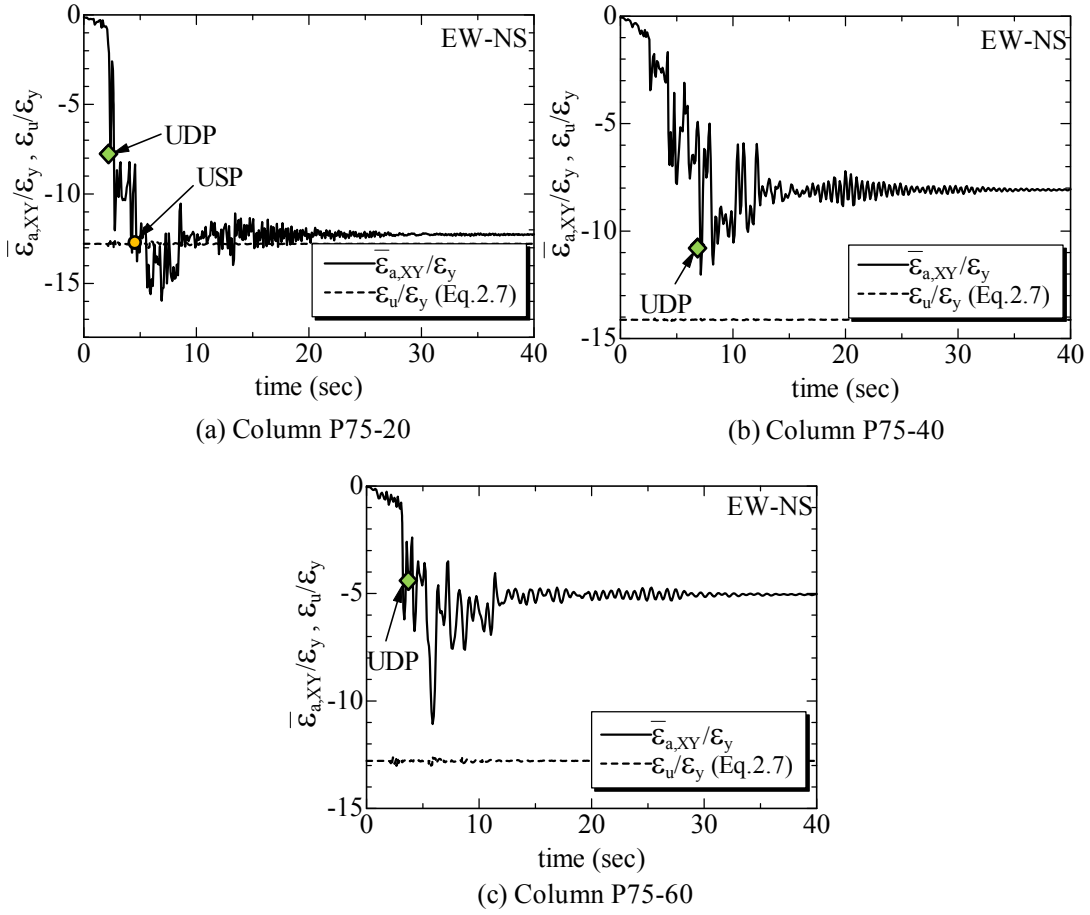

Fig. 3.19 Strain Response Histories in Bi-directional Earthquakes (Unsafe)

strain responses for the same unsafe condition that found for displacements response histories in bi-directional dynamic analyses (see **Fig. 3.17**). Dashed line is plotted for ultimate strain $\varepsilon_u / \varepsilon_y$; which is calculated from **Eq. (2.7)** of Chapter 2 (Ge et al., 2004).

It is noticed from **Fig. 3.19** that the column P75-20 strain response goes beyond the ultimate strain line whereas, for column P75-40 and P75-60, the strain responses remain within the limit of ultimate strain line defined by **Eq. (2.7)**. Moreover, in **Fig. (3.19)** two points are shown by names UDP and USP which indicates crossing points of ultimate displacement and ultimate strain lines to their respective response histories. In case of all three piers UDP appeared on the strain responses which mean that displacement-based design procedure provides minimum allowable limit value than that of strain-based. However, it should be noted that the ultimate strain formula (i.e. **Eq. (2.7)**) used here for comparison is developed by applying combined compression and bending loading on short cylinders. In other words, **Eq. (2.7)** does not include the

effect of cyclic loading and slenderness ratio. Therefore, it is very essential to investigate ultimate strain formulas for steel circular columns which are based on uni- as well as bi-directional cyclic loadings and also take account for all design parameters.

3.8 Summary

The present chapter concerned with the cyclic elastoplastic large displacement FE analysis of uniform thickness circular steel columns modeled for bridge piers. The modified two-surface model is applied to account material nonlinearity. The effect of instability is also included by employing shell elements in the FE model where local buckling occurs. Two kinds of loading patterns considered for comparison; one is conventionally used cyclic uni-directional loading and another is cyclic circular bi-directional loading. The parametric study is carried out to investigate the effects of main parameters such as, the radius-thickness ratio, slenderness ratio, and amount of axial force. Based on the analytical results, the concluding remarks are drawn as follows.

(1) Comparison of local buckling noticed in counter plots drawn at the ultimate state of the column, shows that cyclic circular bi-directional loading produces larger local buckling and hence severe than the cyclic uni-directional loading pattern.

(2) By the parametric study, it is found that both the ultimate strength and ductility are improved with the decrease in R_t irrespective of loading patterns. However, only in the case of cyclic uni-directional loading, the ultimate strength and ductility are improved with decrease in $\bar{\lambda}$, but when loading changes to cyclic circular, the columns with $\bar{\lambda} = 0.2$ has shown lower ultimate strength than the columns with $\bar{\lambda} = 0.4$ and 0.6. The probable reason behind this phenomenon is explained in following chapter. Moreover, the slope of post buckling curve becomes steeper and ductility decreases with increase in axial load. This effect becomes more significant in circular bi-directional loading.

(3) Based on the ultimate values obtained from parametric study, the formulas are

developed for ultimate strength and ductility separately for UNI and CIR loading cases. From these formulas, the value of δ_{95}/δ_y is guaranteed to exceed 4.0 for the column with $\bar{\lambda} = 0.3$ and R_t lies within 0.089 under UNI loading and in case of CIR loading to achieve the same ductility and with same $\bar{\lambda} = 0.3$, the R_t should be less than 0.056. On the other hand to obtain δ_{95}/δ_y = 4.0 and if $\bar{\lambda} = 0.5$ then in UNI loading R_t limit value reduces to 0.076, but in CIR loading it increases to 0.060. This reverse phenomenon is observed because, short columns ($\bar{\lambda} = 0.2$) under CIR loading have shown lower strengths and ductility capacity than medium and long columns (i.e. $\bar{\lambda} = 0.4,\ 0.6$).

(4) Although the ultimate ductility formula is proposed in this study for CIR loading, it is not applicable directly in seismic design of bridge pier subjected to two dimensional earthquake motions. Therefore, a new procedure for displacement-based bi-directional seismic design method is proposed considering the characteristics of displacement response history spread in two perpendicular directions.

(5) To check applicability of this proposed seismic design method nonlinear dynamic analyses are carried out for three columns P75-20, P75-40 and P75-60. It is observed that columns which satisfied the safety criteria when individual earthquake motions are applied, the same columns did not satisfy the condition defined in the design method for simultaneously applied two earthquake motions. Therefore, as mentioned the procedure, it was suggested to redesign the columns.

(6) In addition to the displacement responses of the columns, average compressive strain response histories are plotted for the same unsatisfied cases which were obtained in the displacement-based two dimensional dynamic analyses. For verification against allowable strain, the ultimate strain formula developed in the past study is used here. The comparison between occurrence of ultimate displacement and ultimate strain apparently shows displacement-based seismic design method provides minimum allowable limit value. However, for the sake of proof it is very important to investigate the ultimate strain formulas for circular steel columns modeled as bridge piers, considering effect of both uni- and bi-directional cyclic loadings and all design parameters so that the comparative

study between displacement-based and strain-based seismic design method will become feasible.

Chapter 4

STRAIN-BASED BI-DIRECTIONAL SEISMIC DESGN FOR STEEL CIRCULAR PIERS

4.1 Introduction

As mentioned in Chapter 2, the ultimate strain formulas were proposed for steel short-cylinders under various loading conditions (Gao et al., 1998a; Zheng et al., 2000; Cetinkaya et al., 2008). However, it should be noted that in these studies the steel short-cylinders are assumed as critical segments of the bridge piers as shown in **Fig. 4.1** for a cantilever pier and portal frame. Therefore, to investigate the ductility capacity in terms of strain, loading conditions such as pure compression, combined compression and bending, combined bending and axial force fluctuation were applied monotonically on short-cylinders. Whereas, in the case of ductility prediction in terms of displacement, cyclic uni-directional or bi-directional loadings have been applied on the full length steel columns (Gao et al., 1998b; Watanabe et al., 2000; Goto et al., 2006; Kulkarni et al., 2009). This means effect of cyclic loading on the behavior of critical segments in the bridge piers has not been estimated so far. In Chapter 3, seismic design method based on displacement-based capacity was proposed and explained about how to confirm performance of circular steel columns under simultaneous bi-directional earthquake motions. And it was concluded that strain-based seismic design method for circular steel columns under cyclic bi-directional loading is essential to develop, so as to check its performance with formerly proposed displacement-based method. Therefore, objective of this study is to develop ultimate strain formulas and based on that seismic design method for circular steel bridge piers when subjected to uni- as well as bi-directional cyclic loading.

Present work is organized as follows: first, the numerical analysis are carried out for two types of finite element (FE) models, (1) shell element models, (2) beam element models developed for hollow steel circular columns and subjected to horizontal cyclic uni- and bi-directional displacement loading similar to that used in Chapter 3, including material and geometric nonlinearity. Effect of loading patterns on the ultimate strain in shell and beam element models is compared.

Further the ultimate strain formulas are proposed for uni- and bi-directional load-

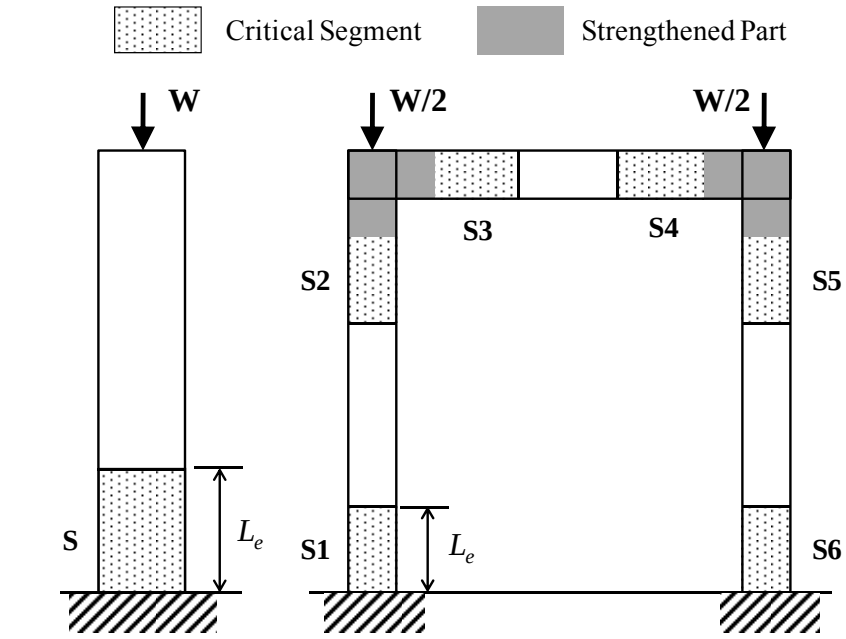

Fig. 4.1 Critical Segments in Bridge Pier

ing based on the results of parametric study. The seismic design procedure is developed and verified by one and two directional nonlinear dynamic analysis.

4.2 Numerical Method

Geometrical properties of the analytical FE models used in the present study are exactly similar to that considered in **Table 3.1** of Chapter 3. The material properties of steel grade SM490 are employed through M2SM constitutive law. The cyclic uni- and bi-directional loadings similar to that shown in **Fig. 3.2** are applied to the top node of FE models with constant axial force. The analysis techniques are also similar to that explained in Chapter 3.

In addition to the shell element models that used in previous chapter, here the beam element models as indicated in **Fig. D.1 (a)** of **Appendix D** are employed, because in engineering practices, to check dynamic performance of bridge systems beam elements are usually selected for modeling. It should be noted that, as the shell element model of bridge pier judges the local buckling in the base part, the beam element model ignores the local buckling effect; however, axial stress and strain in these elements are measurable. Therefore, instead of shell element model, the strain is observed from beam element models to develop the ultimate strain formulas. Hence,

the numerical analyses are carried out for these two types of FE models by applying horizontal cyclic displacement loadings and constant axial force. Further, it is important to point out that strength and equivalent strain are measured from shell element models and average compressive strain are taken from the beam element model, so that behavior of both types of FE models is automatically get included in the ultimate strain formulation which is discussed in the following section. The concept of evaluation of average compressive strain in beam element model and equivalent strain in shell element model are explained in **Appendices D** and **E** respectively.

4.3 Concept of Ultimate Strength and Ultimate Strain

During static analysis, each FE model is subjected to the cyclic lateral displacement with constant axial load and observations are taken for strength and strain.

The shell element models of steel columns are purposefully selected to include the local buckling effect into the ultimate strength quantity. However, ultimate strain values are measured from average compressive strain in the beam element models. Because, even if the concept of equivalent strain incorporate local buckling, this concept is based on nodal deformation in the direction parallel to column height and not on the stress-strain behavior within individual shell element. On the other hand, average compressive strain concept represents stress-strain relationship at each integration point in the cross-section of beam element. Further, in most of the dynamic analysis, instead of shell elements, beam elements are generally preferred by engineers to construct the FE models of bridge systems which decrease complexity in modeling and also reduce analysis run time. Hence, concepts of FE modeling used in static analysis to predict the capacity and in dynamic analysis to find the demand both synchronize well with each other.

Following the same process described in Chapter 3, the strength envelop curve can be plotted as shown in **Fig. 4.2 (a)** and the ultimate strength is defined at 95% of maximum strength on post peak curve. Envelop curves for equivalent strain factor $\bar{\varepsilon}_{ms}/\varepsilon_y$ and average compressive strain factor $\bar{\varepsilon}_{mb}/\varepsilon_y$ are obtained from shell and beam element models respectively and are plotted as shown in **Fig. 4.2 (b)**. The ultimate strain factors $\bar{\varepsilon}_{ms,95}/\varepsilon_y$ and $\bar{\varepsilon}_{mb,95}/\varepsilon_y$ are the points on strain envelop

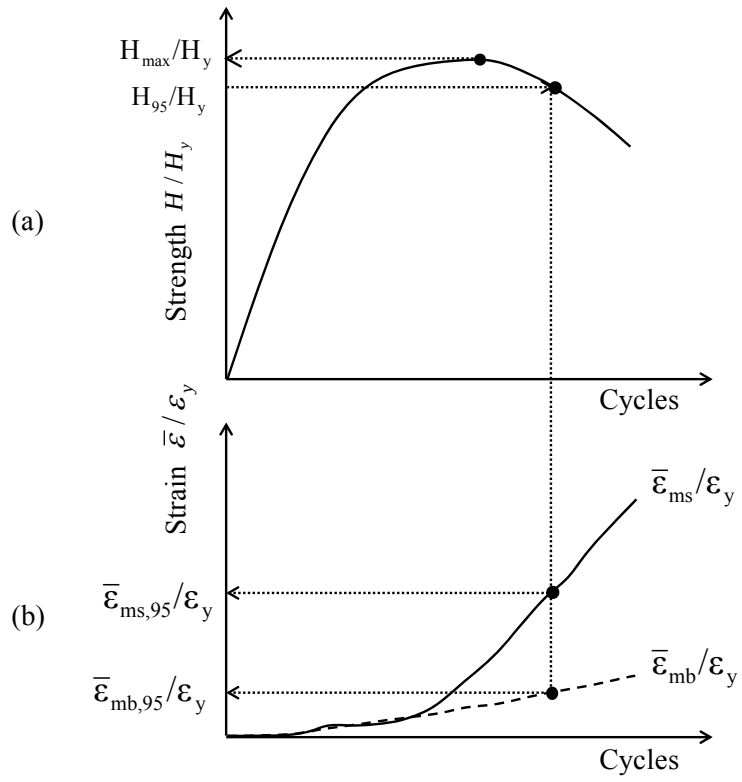

Fig. 4.2 Definition of Ultimate Strength and Ultimate Strains

curves corresponding to the ultimate strength factor H_{95}/H_y. Moreover, in **Fig. 4.2 (b)**, it is observed that, the ultimate equivalent strain has higher amplitude than that of average compressive strain. This difference is appeared due to local buckling in shell element model and which is ignored in the beam element model. Above described procedure of ultimate strain evaluation is applied for each model mentioned in **Table 3.1** to find out influence of various parameters.

4.4 Effect of Loading Patterns on Ultimate Strains

To understand the effect of bi-directional cyclic loading on ultimate behavior of both shell and beam element models, seven loading patterns are selected by substituting *b/a* = 0, 0.1, 0.25, 0.5, 0.75, 0.9, 1 in **Eqs. (3.1)** and **(3.2)**, which include uni-directional (UNI) and perfectly circular bi-directional (CIR) patterns. Only one axial force case $P/P_y = 0.15$ is taken here to explain this effect of loading pattern.

The graphs are plotted for the ultimate strains normalized by ultimate strains for UNI loading versus *b/a* and for each radius-thickness ratio separately as illustrated in **Fig. 4.3**. Left side graphs are shown for equivalent strain ratio i.e. $\bar{\varepsilon}_{ms,95}/\bar{\varepsilon}_{ms,95)UNI}$

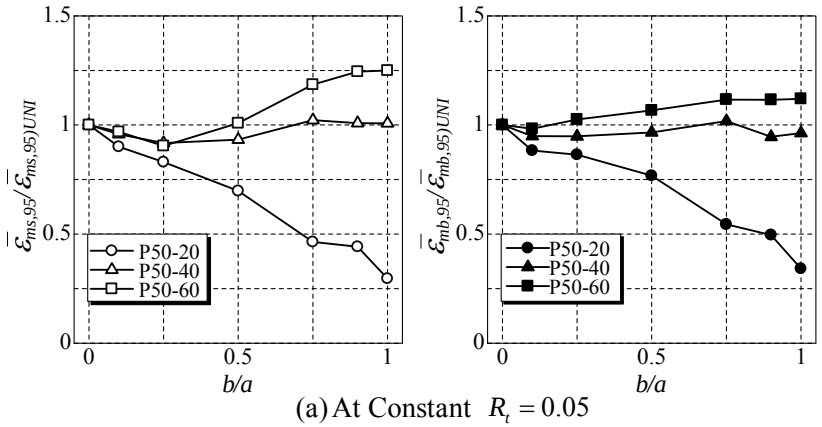

(a) At Constant $R_t = 0.05$

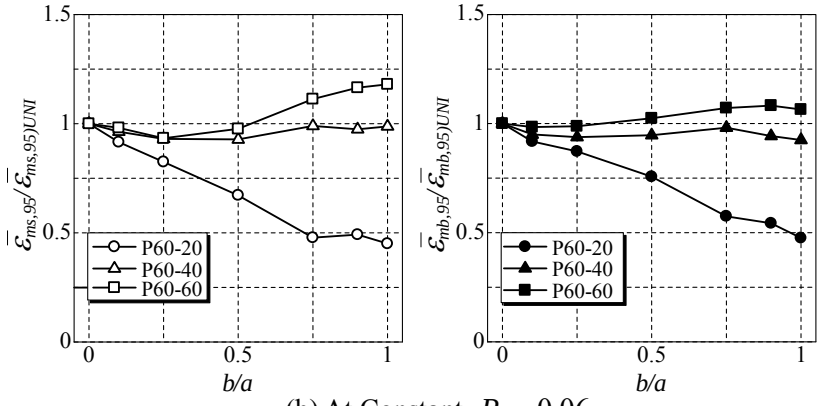

(b) At Constant $R_t = 0.06$

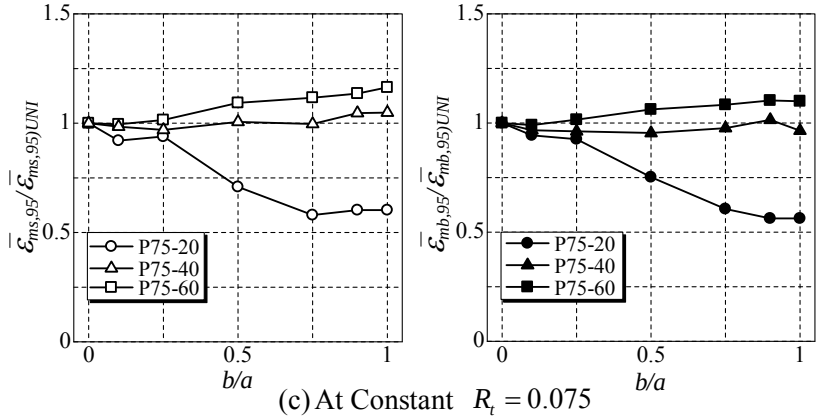

(c) At Constant $R_t = 0.075$

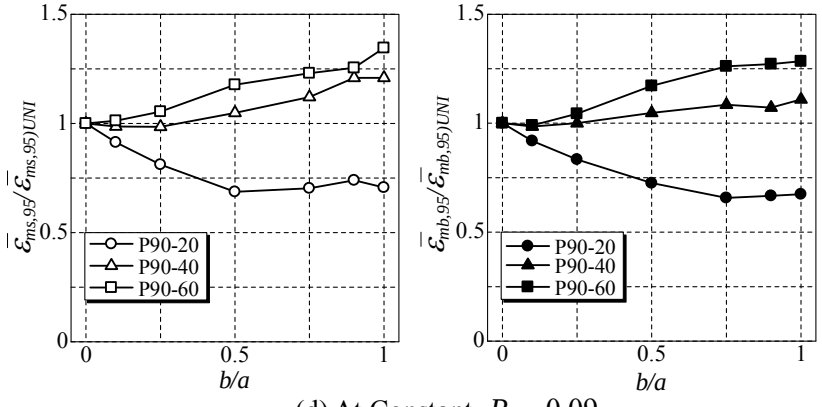

(d) At Constant $R_t = 0.09$

Fig. 4.3 Effect of Loading Patterns on Ultimate Strain Ratios

whereas, right side graphs are for average compressive strain ratio i.e. $\bar{\varepsilon}_{mb,95} / \bar{\varepsilon}_{mb,95)UNI}$. Some significant observations from these plots are summarized as follows;

(1) The effect of ratio b/a, on the behavior of ultimate equivalent and average compressive strain factors has shown considerable similarity. This implies that, shell element model and beam element model perform in similar way almost for all cases of the columns demonstrated in **Fig. 4.3**.

(2) In each graph of **Fig. 4.3**, it is observed that as the loading pattern changes from *b/a* = 0 to *b/a* = 1, ultimate strain for the short columns (i.e. $\bar{\lambda}$ = 0.2) goes on decreasing than its uni-directional ultimate strain. Whereas, for the medium and long columns (i.e. $\bar{\lambda}$ = 0.4, 0.6) that respectively remains nearly constant and increases gradually. This means, slenderness ratio is an important parameter in ultimate behavior of the columns and which further involves its significance in the ductility formulation.

To understand the reason behind this observed phenomenon for various slenderness ratio parameters, it is required to investigate in detail the strain behavior in the columns at their ultimate states. For this purpose, contour plots obtained from ABAQUS/CAE (Dussault Systems Simulia Corp., 2007) are used here to compare strain in shell element models. The averaging method available in ABAQUS/CAE is employed to generate the strain contour plots which calculates average values at nodes common to two or more contributing elements. The average threshold percentage is assigned to 75% to confirm smoother effect with less discontinuities from element to element.

The contour images for logarithmic normal strain ε_z^L, in the direction of local axis of an element parallel to *Z* axis of column and logarithmic shear strain γ^L, in the direction of mutually perpendicular local axes along the plane of the shell element, are shown in **Figs. 4.4** and **4.5** respectively, for the P75-20, P75-40 and P75-60 models. To identify the actual averaged maximum normal and shear strain in the shell elements at the ultimate state of the column, the absolute maximum strain values $\left|\varepsilon_z^L\right|_{max}$ and $\left|\gamma^L\right|_{max}$ shown in the enlarged boxes are taken from each legend of contour plots and then they are normalized by normal yield strain ε_y and shear yield

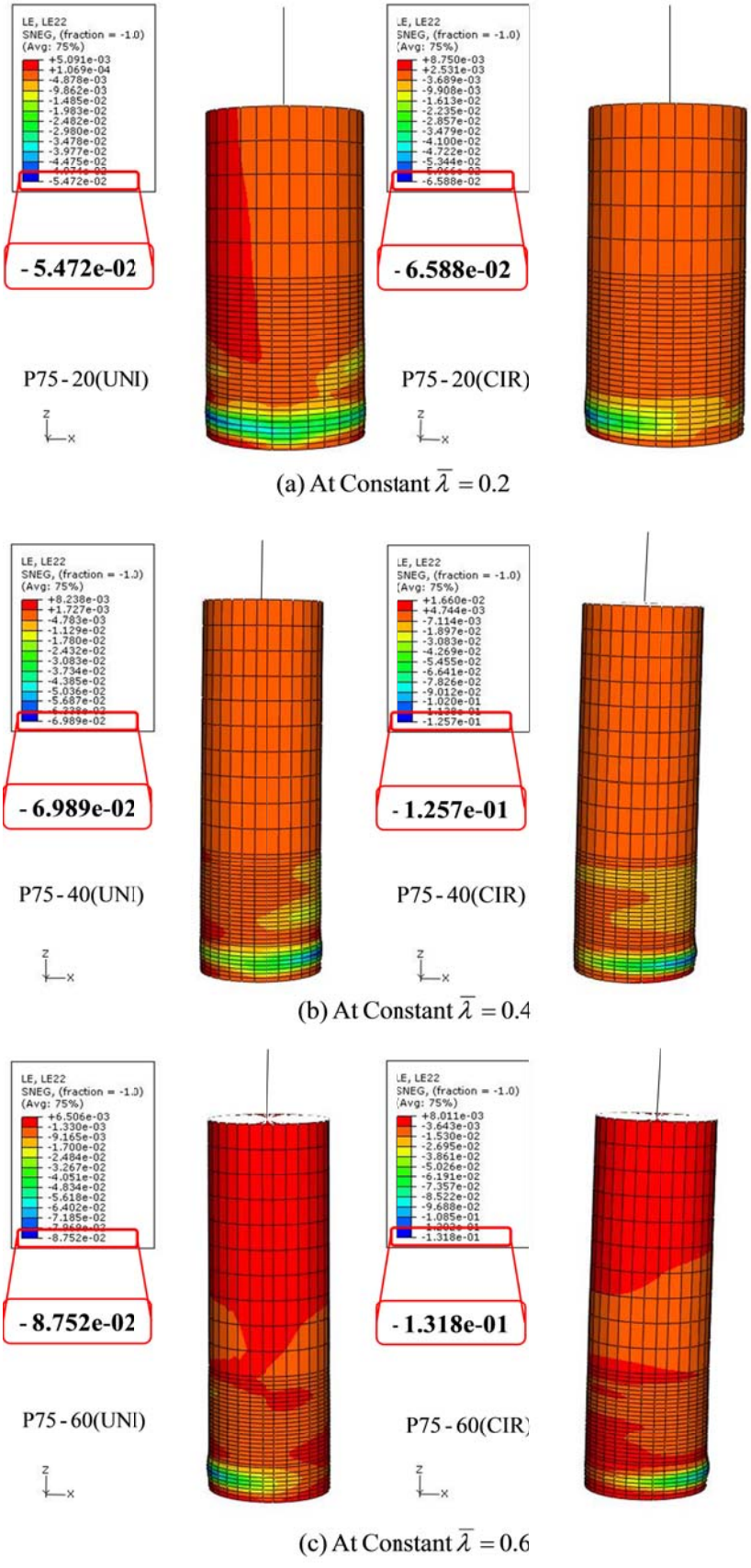

Fig. 4.4 Contour Plots for Normal Logarithmic Strain ε_z^L

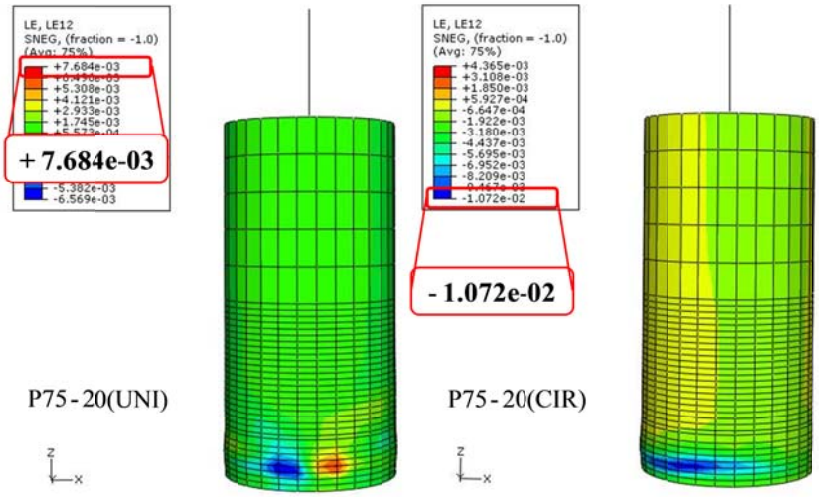

(a) At Constant $\overline{\lambda} = 0.2$

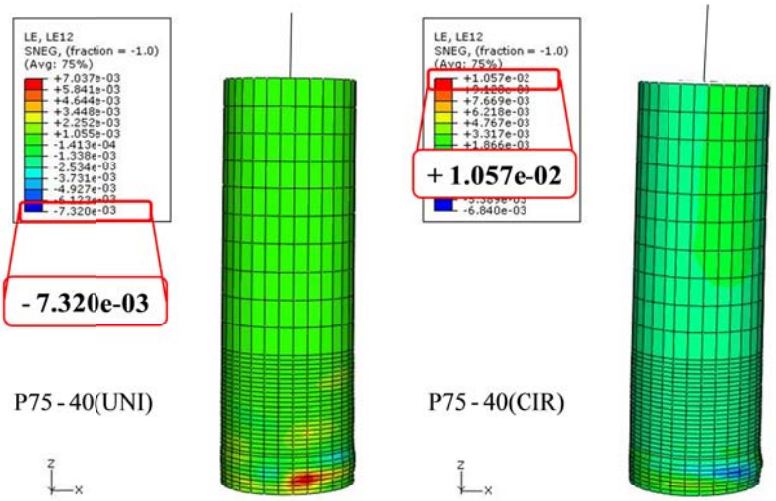

(b) At Constant $\overline{\lambda} = 0.4$

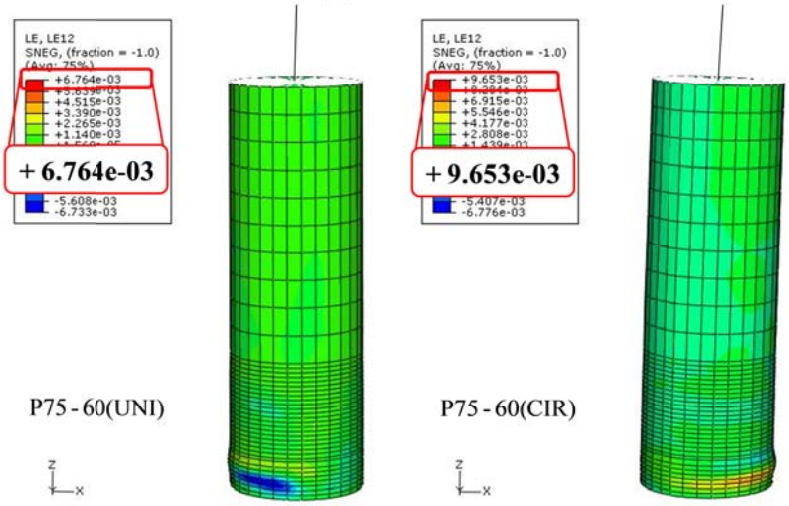

(c) At Constant $\overline{\lambda} = 0.6$

Fig. 4.5 Contour Plots for Shear Logarithmic Strain γ^L

strain γ_y respectively which are tabulated in **Table 4.1** for UNI and CIR loadings. The major findings from this investigation are as follows,

(1) Logarithmic normal strain factor $\left|\varepsilon_z^L\right|_{max}/\varepsilon_y$ which considers tension and compression mechanism; increases as the slenderness ratio parameter $\bar{\lambda}$ increases for both UNI and CIR loadings cases.

(2) On the other hand, the logarithmic shear strain factor $\left|\gamma^L\right|_{max}/\gamma_y$ which accounts for sliding action, decreases as the height of column increases.

Table 4.1 Normalized Absolute Maximum Logarithmic Normal and Shear Strains in Shell Element Models

Models	(a) Normal strain $\left\|\varepsilon_z^L\right\|_{max}/\varepsilon_y$		(b) Shear strain $\left\|\gamma^L\right\|_{max}/\gamma_y$	
	Loading patterns		Loading patterns	
	UNI	CIR	UNI	CIR
(1)	(2)	(3)	(4)	(5)
P75-20	34.85	41.96	3.25	4.54
P75-40	44.52	80.06	3.10	4.47
P75-60	55.75	83.95	2.87	4.09

Note: γ_y = yield shear strain; $\gamma_y = \tau_y / G$; where, τ_y = yield shear stress and G = shear modulus

From this comparison between strains behavior in columns with different slenderness, it can be stated that in short columns shear strains are dominant at their ultimate state and as loading changes from UNI to CIR this strain becomes even larger. Hence, decreasing trend of the ultimate strains was observed in **Fig. 4.3** for short columns, in which strain values are calculated from movement of nodes in normal direction and not in the shearing direction. However, for the medium and long columns normal strains are principle at their respective ultimate states. Therefore, constant and gradually increasing trends were observed in **Fig. 4.3**, as loading changes from UNI to CIR for medium and long columns respectively.

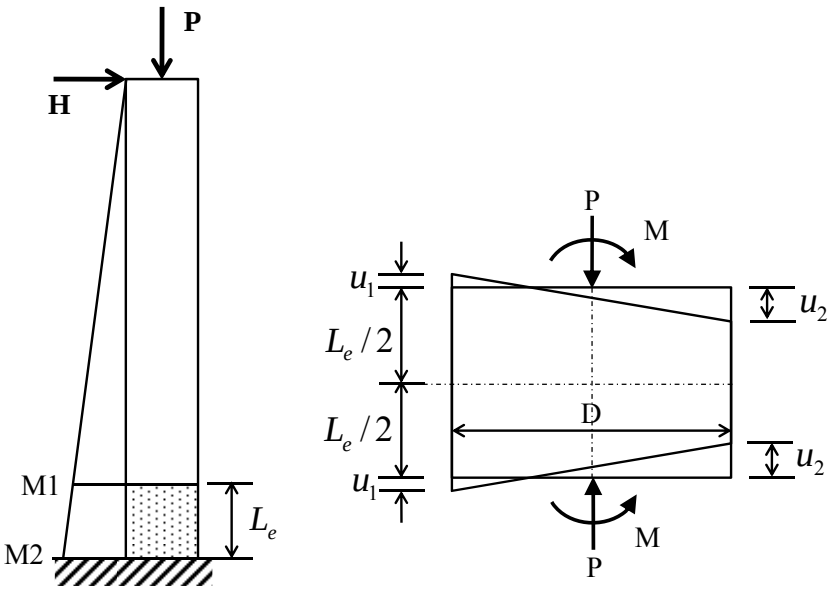

Fig. 4.6 Concept of Strain Observation Considered in Past Studies (Gao et al., 1998a; Zheng et al., 2000)

4.5 Ductility Formulation and Seismic Design Method

4.5.1 Ultimate Strain Formulas

Modified two-surface material constitutive law which is used in the present study is basically developed to capture cyclic behaviour of structural steel especially in the yield plateau. The applicability of the M2SM was confirmed by comparing experimental and analytical results for uni-directional cyclic loading on circular and box steel columns (Gao et al., 1998b; Usami and Ge, 1998) as given in **Appendix A**. Hence, it is believed that the performance of M2SM in bi-directional loading on circular steel columns is well accepted.

The ultimate strain formulas developed for steel columns so far, were concerned to the strain behaviour in the critical part i.e. effective failure height region as shown in **Fig. 4.6** (Gao et al., 1998a; Zheng et al., 2000). Therefore, the effect of the entire height of the column i.e. the slenderness ratio was neglected in ultimate strain formulation. However, in the present work, it is found that slenderness ratio parameter has significant effect on the ductility behavior of steel columns. Therefore, R_t, $\bar{\lambda}$ and P/P_y are very important parameters to get involved in ultimate strain formulas. Moreover, in the past study, the FE models using shell elements were constructed for the critical part of the column and analyzed for compression and bending loads so as to consider local buckling effect in the ductility formulation. Whereas, in the present

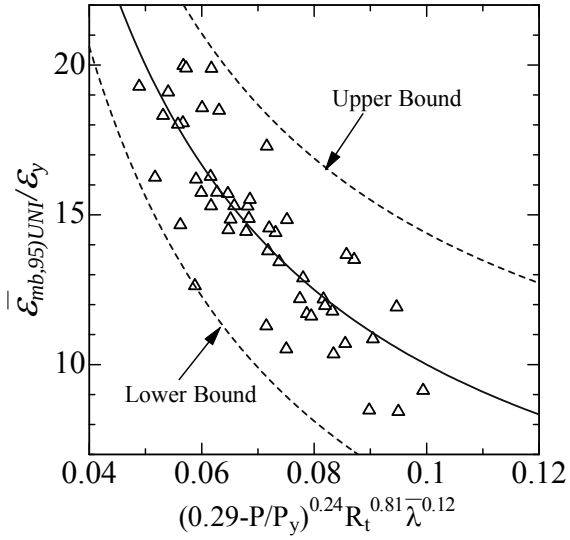

(a) Cyclic uni-directional loading

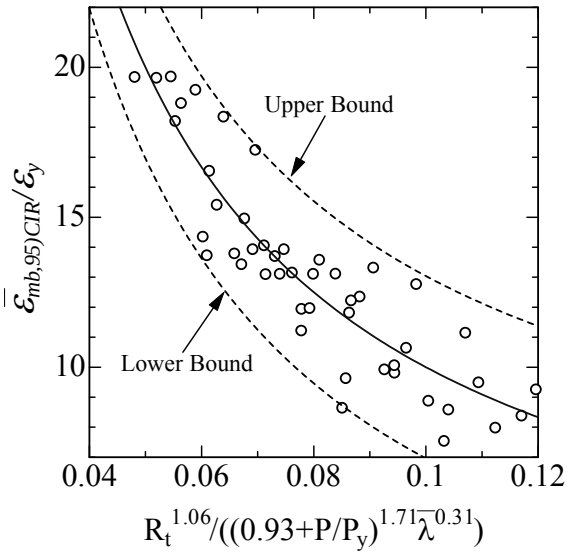

(b) Cyclic circular bi-directional loading

Fig. 4.7 Proposed Ultimate Strain Formulas for Circular Steel Bridge Piers

work, the ultimate strain formulas are derived from the strains observations of beam element models which ensures coordination between FE modeling used in the ductility prediction process and seismic design process i.e. dynamic analysis.

The ultimate average compressive strain factors $\bar{\varepsilon}_{mb,95)UNI}/\varepsilon_y$ and $\bar{\varepsilon}_{mb,95)CIR}/\varepsilon_y$ are plotted against a combined value of R_t, $\bar{\lambda}$ and P/P_y as shown in **Figs. 4.7 (a)** and **(b)**, respectively. These combined values are determined from the nonlinear regression analysis. **Eqs. (4.1)** and **(4.2)** are written for ultimate strains in UNI and CIR loading cases fitted for 99% and 97% confidence levels respectively.

$$\frac{\bar{\varepsilon}_{mb,95)UNI}}{\varepsilon_y} = \frac{1}{(0.29 - P/P_y)^{0.24} R_t^{0.81} \bar{\lambda}^{0.12}} \pm 4.13 \qquad \leq 20.0 \tag{4.1}$$

$$\frac{\bar{\varepsilon}_{mb,95)CIR}}{\varepsilon_y} = \frac{(0.93 + P/P_y)^{1.71} \bar{\lambda}^{0.31}}{R_t^{1.06}} \pm 3.04 \qquad \leq 20.0 \tag{4.2}$$

Valid for the ranges, $0.05 \leq R_t \leq 0.09$, $0.2 \leq \bar{\lambda} \leq 0.6$ and $0.0 \leq P/P_y \leq 0.2$.

The dashed lines in **Fig. 4.7** are the lower bound and upper bound levels for the proposed equations and it is recommended here, to select the lower bound values from **Eqs. (4.1)** and **(4.2)** which will provide the minimum ultimate strain for the steel circular columns under UNI and CIR loading. In these equations maximum limit for ultimate strain is set to 20.0 because, in case of the higher failure strain, low cycle fatigue may initiates in the material. In other words, ultimate strain which is in fact an average compressive strain, if exceeds this limit, the local maximum strain would be very large and such numerical results would become unreliable. Hence, the upper bound for ultimate strain is limited to 20.0 (Usami et al., 2000).

4.5.2 Strain-based Seismic Design Method

It is well known that the earthquake generates multidirectional motions in the ground; therefore it is important to verify structural response due to more than one simultaneous earthquake components. Similar to the previously proposed displacement-based seismic design method (Kulkarni et al., 2009), the strain-based seismic design method is proposed here with considering the ultimate strain equations for UNI and CIR loading i.e. **Eqs. (4.1)** and **(4.2)** respectively. The step by step procedure of this method is indicated in **Fig. 4.8** and explained as follows,

(1) As explained in previous chapter, the present seismic design method is an extension to the conventional uni-directional design method, hence in first step, apply the earthquake motions in longitudinal and transverse directions to the structure and check whether the maximum response of average compressive strain in the effective failure region L_e, of the column remains within the ultimate strain limit calculated by **Eq. (4.1)**.

(2) If the column confirms Step (1), then apply earthquake motions in both directions

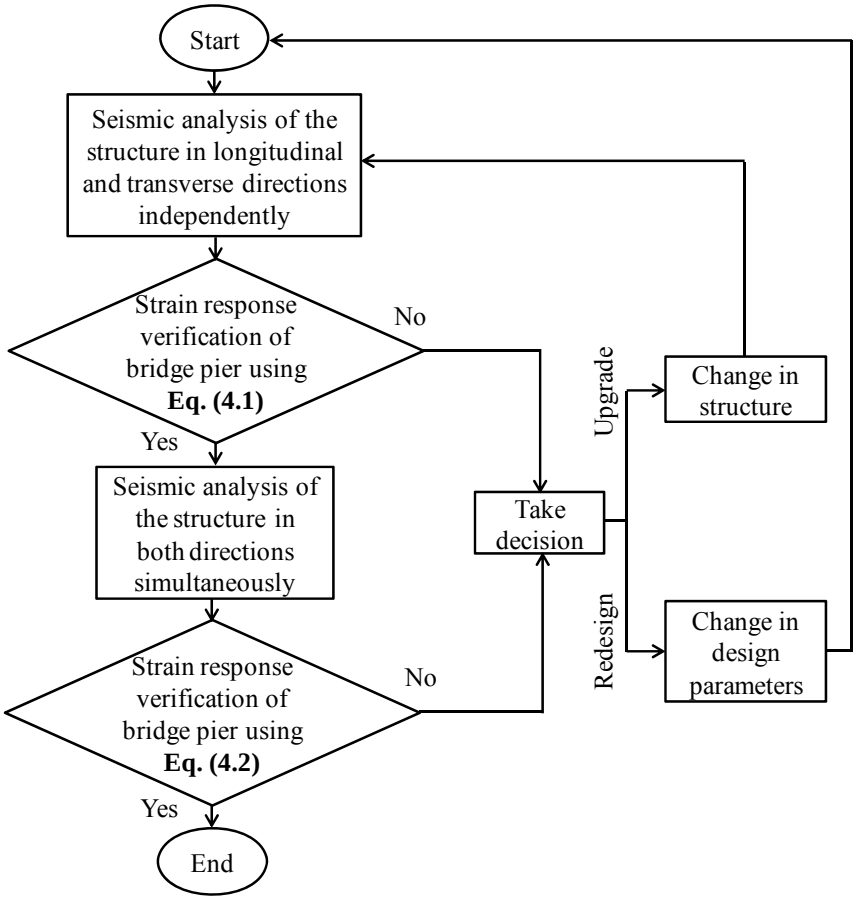

Fig. 4.8 Procedure of Strain-based Seismic Design Method

simultaneously, and again check that the maximum average compressive strain response is less than the ultimate strain value from **Eq. (4.2)**.

(3) At any step, if the column does not satisfy the condition then it is recommended to upgrade or redesign the column.

The functionality of this strain-based seismic design method and comparison with the formerly proposed displacement-based design method, are explained through some illustrative examples of nonlinear dynamic analysis in the following sections.

4.6 Implementation of Seismic Design Method in Nonlinear Dynamic Analysis

Nonlinear dynamic analyses are performed to explain the functionality of strain-based seismic design method which is proposed in this study and at the same time comparing this method with former displacement-based design method

(Kulkarni et al., 2009). Three cases of single bridge pier are selected here as: P60-20 (where, P60-20 means a pier having $R_t = 0.060$ and $\bar{\lambda} = 0.2$), P60-40, P60-60, which have different slenderness ratio but same radius-thickness ratio parameter. Beam element model as shown in **Fig. D.1 (a)** of **Appendix D**, with concentrated mass at the top of the pier is constructed and modified two-surface model is used to simulate the cyclic behaviour of steel material.

Rayleigh damping, which usually appears in the dynamic analysis, consists of mass proportional and stiffness proportional damping coefficient. Mass proportional damping coefficient α is calculated for each pier based on their respective fundamental frequencies. Eigen value extraction analysis is performed to evaluate natural frequencies and corresponding mode shapes. First 10 modes are selected which ensures the total effective mass in each direction is more than 90% of total mass of the structure. Stiffness proportional damping coefficient β is not considered in these dynamic analysis. However, the hysteretic damping comes into action because of material nonlinearity.

In the dynamic analysis, before applying the actual earthquake forces, gravity forces are made activated on the pier including concentrated mass at the top. Since, this pier model is assumed to be isolated from rest of the bridge system; mass at the top gets vibrated like a cantilever structure during the earthquake motions. Two kinds of strong earthquake motions on Ground type II JRT-EW-M and JRT-NS-M as shown in **Fig. 3.15** of Chapter 3 are selected. The dynamic analyses are performed for three cases of the piers but, the results only for pier P60-40 are discussed here.

As described in the strain-based design method, at first EW and NS earthquake motions are independently applied on the pier P60-40, and response histories are observed for displacement of top of the pier (δ_X / δ_y and δ_Y / δ_y) and average compressive strain in the effective failure region ($\bar{\varepsilon}_{a,X} / \varepsilon_y$ and $\bar{\varepsilon}_{a,Y} / \varepsilon_y$) as shown in **Fig. 4.9**. The displacement response histories are found to be bounded between ultimate displacement limits δ_u / δ_y defined by **Eq. (3.11)** and shown by dashed line in **Fig. 4.9 (a, b)**, which confirms that displacement response of pier is safe during individual earthquake component. In **Fig. 4.9 (c, d)**, the average compressive strain time histories are checked against two ultimate strain limits ($\varepsilon_u / \varepsilon_y$), one is defined by **Eq. (4.1)** and another is by **Eq. (2.7)**. **Fig. 4.9 (c, d)** indicate that one directional earthquake response histories of average compressive strain are within both ultimate strain limits defined by **Eqs. (4.1)** and **(2.7)** and hence, confirm the first step of

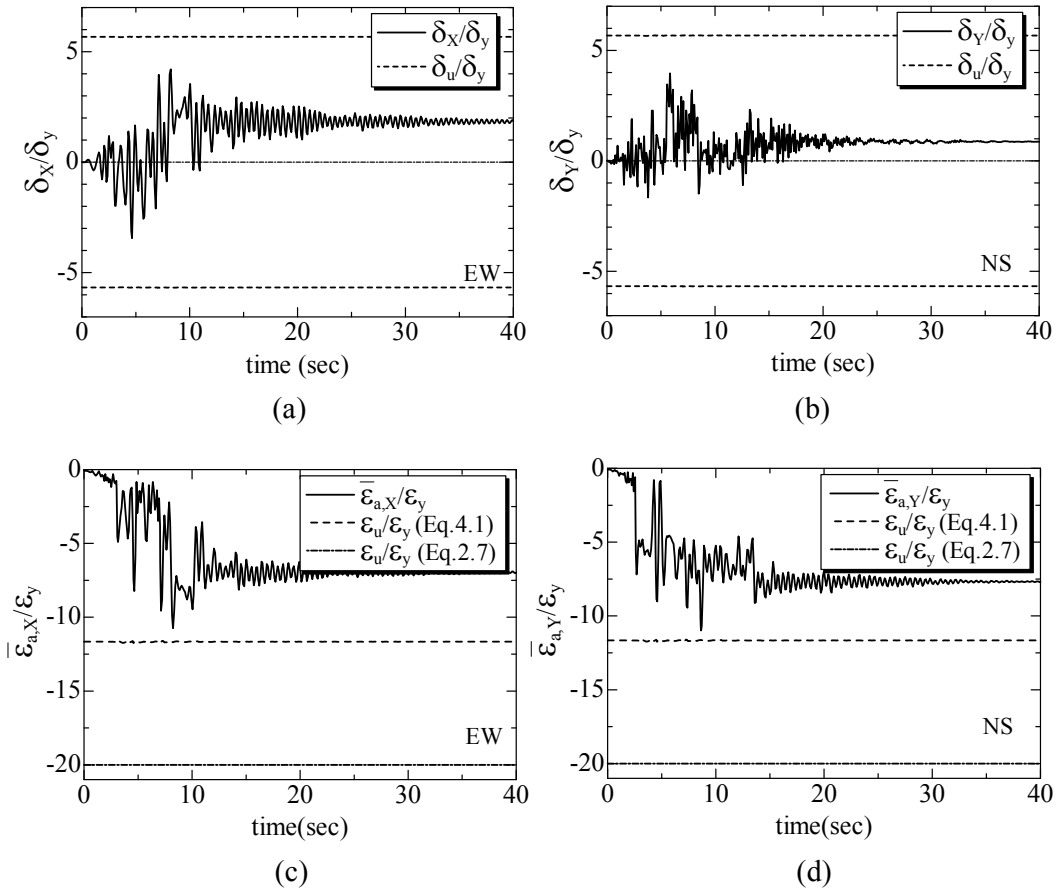

Fig. 4.9 Uni-directional Seismic Response for P60-40 due to EW and NS Earthquake Components (Initial Design)

seismic design method. In addition, it is observed that **Eq. (4.1)** calculates smaller limit value to check safe performance of pier than that of **Eq. (2.7),** which means the ultimate strain formula derived for uni-directional loading, gives critical design for bridge piers. Here, critical designing stands for the minimum plate thickness (i.e. radius-thickness ratio) of bridge pier, for which seismic performance remains within lowest allowable limit.

In the next step, dynamic analysis is performed by applying EW and NS components of the earthquake at the same time. The displacement-based seismic design method developed in Chapter 3, is used to check bi-directional displacement response of top of the pier. **Fig. 4.10 (a)** shows the trajectory of displacement response, which crosses the ultimate state ellipse (shown by dashed line). In **Fig. 4.10 (b)**, average compressive strain response-history is found to be passing through the ultimate strain limit defined by **Eq. (4.2)** but not through the line of **Eq. (2.7)**. From **Fig. 4.10** it can be said that currently designed pier P60-40 which was performed

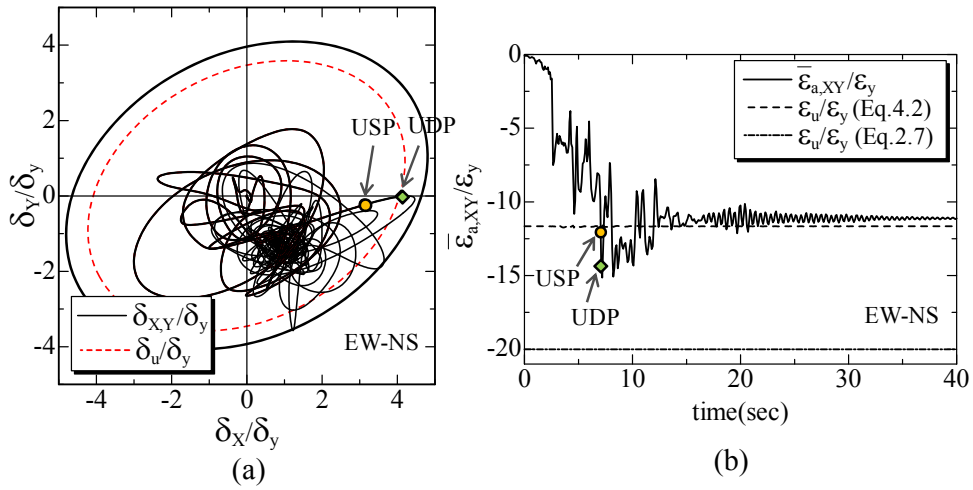

Fig. 4.10 Bi-directional Dynamic Response for P60-40 due to EW-NS Earthquake Components (Initial Design)

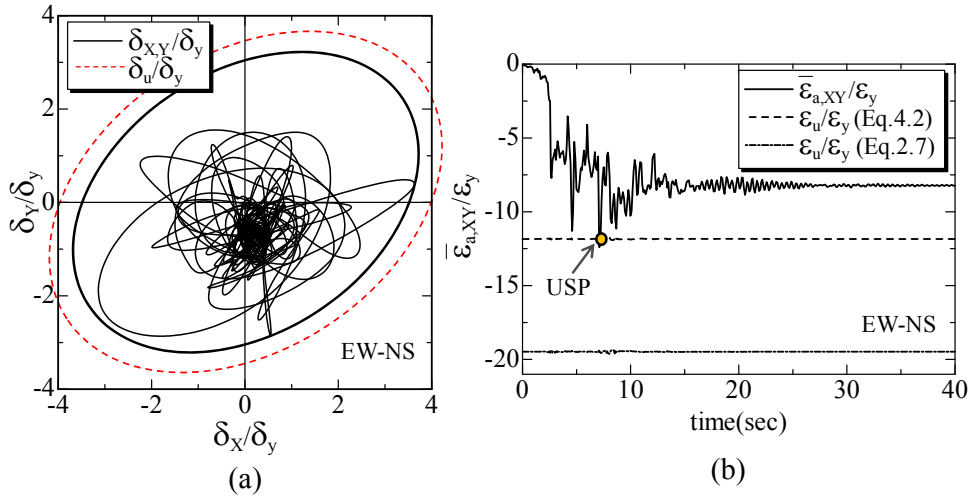

Fig. 4.11 Bi-directional Dynamic Response for P60-40 due to EW-NS Earthquake Components (Trail-1 Design)

safely in individual earthquake excitation, could not satisfy the safe performance in two-dimensional earthquake excitation. The points denoted by UDP and USP are the time instances where displacement response and strain response trajectories crosses their respective ultimate limit lines indicating pier has arrived at ultimate state. In currently designed pier P60-40, USP appears earlier than UDP which apparently indicates that strain-based design method provides critical seismic design than displacement-based method. Therefore to verify this hypothesis, redesign option given in strain-based design method (see **Fig. 4.8**) is selected.

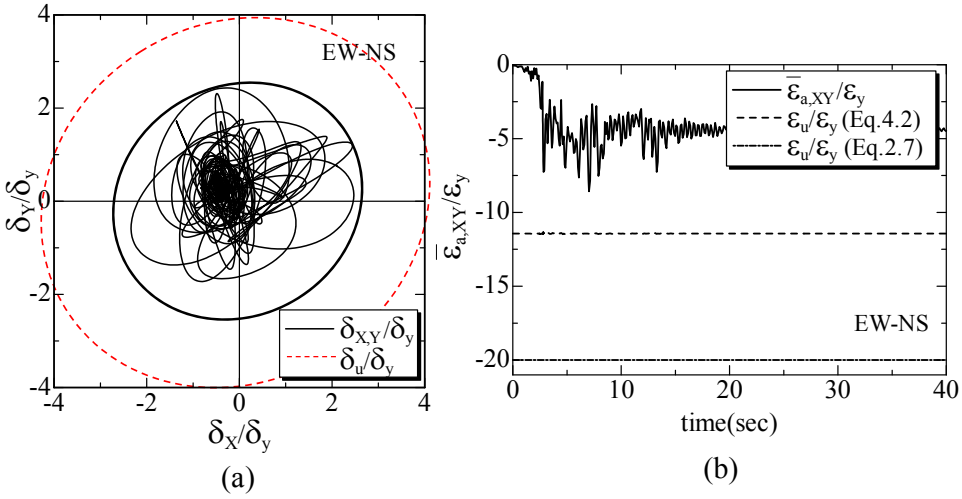

Fig. 4.12 Bi-directional Dynamic Response for P60-40 due to EW-NS Earthquake Components (Trail-2 Design)

Ideally in design practices, redesign means to alter the radius-thickness ratio i.e. the plate thickness of the pier, because height of the pier and lumped mass at the top due to superstructure weight are predefined and remain unchanged at each redesign step of designing process. However, in the present case it is decided to keep the geometrical properties of pier same because, if pier dimensions are changed then it will not be feasible to maintain consistency in comparison of performances in different steps of redesigning. For example, at one step of seismic design, pier P60-40 (i.e. R_t = 0.06, $\bar{\lambda}$ = 0.4) shows unsafe performance and hence in next step, if R_t changes to 0.05 then it will become P50-40 pier which has different geometrical properties than former pier. Therefore, instead of changing R_t, the lumped mass at the top is adjusted so as to expect safe performance of the pier when subjected to bi-directional earthquake. This step is named as Trail-1. The bi-directional dynamic analysis is carried out and the displacement and strain response histories are plotted as illustrated in **Fig. 4.11**. The pier designed for Trail-1 step has shown safe performance against displacement-based check (see **Fig. 4.11 (a)**), but still could not able to satisfy strain criteria and USP is appeared when strain response crosses the ultimate strain line (see **Fig. 4.11 (b)**) which means strain-based design provides minimum allowable limit than that of displacement-based method.

In the next step which is called as Trial-2, pier P60-40 is redesigned again by changing the lumped mass and then analyzed for bi-directional earthquake. Displacement and strain responses are checked against their respective ultimate limits

as indicated in **Fig. 4.12**. In this step, it is noticed that the pier P60-40 has shown safe response with respect to both displacement and strain criteria.

Above mentioned uni-directional and bi-directional dynamic analysis steps are carried out for other two piers: P60-20 and P60-60. These piers have also shown similar behaviour with that of pier P60-40 in each step and proved that strain-based method is a critical seismic design method for the piers studied herein (see **Appendix F** for results of P60-20 and P60-60). Moreover, it is verified that ductility formulas derived in present study i.e. **Eqs. (4.1)** and **(4.2)** provide lower limit values of ultimate strain in comparison with formula developed in the past study i.e. **Eq. (2.7)**. Hence, these observations indicate that strain-based seismic design process developed herein, designs the bridge piers in such a way that they can assure safe performance in severe conditions generated due to coupling of two horizontal earthquake components.

4.7 Summary

Similar to Chapter 3, the present chapter also dealt with the cyclic elastoplastic large displacement FE analysis of uniform thickness circular steel columns. Two types of FE models are constructed namely (1) shell element model which accounts for local buckling and (2) beam element model where local buckling is absent. The uniaxial and multiaxial M2SM are used for nonlinear material properties of beam and shell elements respectively. The cyclic uni-directional and elliptical/circular bi-directional loading patterns with constant axial force are applied to the columns. The effect of gradual change in loading pattern on the strain behavior in shell and beam element models is observed. The parametric study is carried out and based on the ultimate average compressive strain in the beam element models, the ductility formulas are developed separately for uni-directional and circular bi-directional loading cases. Further, the strain-based seismic design method is proposed and it compared with displacement-based method by performing some nonlinear dynamic analysis. Following are the concluding remarks drawn from this study.

(1) The effect of gradual change in loading pattern from purely uni-directional to elliptical and then to circular bi-directional showed that ultimate strains in shell and beam element models behave in similar manners. Moreover, it is also observed that the short column with circular bi-directional loading losses its

ductility considerably faster than with uni-directional loading. The reason behind this phenomenon is revealed by comparing logarithmic normal strain and shear strain in short, medium and long columns. The result of this comparison has indicated that in short columns shear strains are dominant and responsible for yielding of material. However, for medium and long columns, normal strains seem to be principal than shear strain. This implies that the slenderness ratio plays an important role in the ultimate behavior of steel circular columns and hence becomes necessary to include in the ductility formulation.

(2) The ultimate strain formulas are developed by curve fitting method, based on the observations of ultimate states of the beam element models, instead of shell element model, because it synchronizes the FE modeling technique used in dynamic analysis and ductility prediction by static analysis. The seismic design method for bi-directional earthquake is proposed based on the ultimate strain formulas.

(3) Applicability of proposed ultimate strain formulas in the seismic design method is compared with formerly developed displacement-based method and also with the ultimate strain formulation defined in past research by conducting nonlinear dynamic analysis on three different piers. The results revealed that even if the performances of certainly designed piers are found to be safe under uni-directional earthquake motion, they are unable to secure their displacement and strain responses when bi-directional earthquake motions are applied. This implies that pier responses are considerably amplified due to bi-directional earthquake motions and hence it becomes necessary to design bridge piers for simultaneously applied two directional earthquake components. The dynamic analysis on redesigned piers has shown that bi-directional strain-based seismic design method is critical than that of displacement-based method particularly for these studied sample piers.

(4) Comparison between ultimate strain formulas derived in the past study and present work has indicated that formulas from present work provide minimum ultimate strain value in both cases when earthquake motions are applied in one direction and in two directions simultaneously. As these formulas are based on all important parameters which govern designing of steel circular bridge piers, they

are adequate to use in seismic design process of steel circular bridge piers.

Chapter 5

COMPARISON BETWEEN 2D AND 3D EARTHQUAKE RESPONSE OF BRIDGE PIERS

5.1 Introduction

It is well known that coupling of two horizontal earthquake components has great influence on the response of bridge piers than when they are considered independently. Contribution of vertical earthquake component to this coupling effect is necessary to investigate because, measurement of past few earthquakes indicated that the vertical accelerations are strong enough and caused considerable damage (Chopra, 1966; Papazoglou and Elnashai, 1996). However, it was neglected from conventional method of dynamic analysis assuming that self-weight of the structure can provide sufficient inertia to resist vertical motions.

Extensive research has been conducted regarding the inelastic seismic analysis and behavior of reinforced concrete bridge piers. In which some studies of varying axial force are carried out to account for the effect of vertical earthquake component on RC columns (Saadeghvaziri et al., 1990; Saadeghvaziri 1995; Sakai and Kawashima, 2002; Galal and Ghobarah, 2003; Asad and Yan, 2004; Lee et al., 2005; Kim et al., 2006; Saadeghvaziri and Foutch, 2006; Sakai and Unjoh, 2006). Whereas, very few work has been done related to steel bridge piers with varying axial force (Yamazaki S. and Minami S., 1999; Como et al., 2003; Chung et al., 2007).

It is easy to see large investigation are carried out in the field of effect of vertical ground acceleration on reinforced concrete bridge piers than the steel piers, because reinforced concrete contents two different materials one is concrete which has good compression capacity but week in tension and another is steel reinforcement which provides confinement to concrete and has good ductility capacity. Therefore, in multidirectional earthquake, the bridge piers may experience large variation in the axial force i.e. tensile-compression cycles along with horizontal deformation cycles. Coupling of these cyclic motions leads to shear and/or flexural failure of RC piers which are also observed in some earthquakes such as 1994 Northridge earthquake, USA and 1995 Hyogo-ken Nanbu earthquake, Japan (Broderick and Elnashai, 1994; Elnashai et al., 1995). Whereas, the steel bridge piers which are popular in Japan, are constructed by plates of homogeneous steel and most of the times partially filled with

concrete. The main role of steel plates is to carry load of superstructure and concrete is to protect the steel plates from buckling in case of any vehicle collides on the pier. When these steel piers experience multidirectional earthquake, the axial force may varies with large amplitude, but as the steel is good at ductile properties, the effect of varying axial force due to vertical earthquake components is assumed to be small when compared to the effect of cyclic horizontal deformation and hence, vertical earthquake motions are generally ignored in the seismic design of steel bridge piers. However, the steel bridge piers which had damaged in the Hyogo-ken Nanbu earthquake showed: the large local buckling initiated the weld tearing and successive loss of load carrying capacity resulted into collapse and brittle fracture due to crack propagation (Miki and Sasaki, 2005). It has also mentioned that although the primary reason of these damages is very strong ground motions never experienced before. Apart from this, many factors contributed to the damage such as material properties, structural systems, details, and qualities of structural elements. Therefore, it is important to evaluate structural responses due to earthquake such as forces, displacements, stresses, and strains carefully.

The objective of present chapter is to investigate the effect of vertical component over two horizontal components of the earthquake on the bridge pier responses. For this purpose, three types of simply supported bridge systems are designed for Seismic Performance Level 1 and Level 2 as recommended in specifications for Highway bridges 2002 Part V (Japan Road Association, 2002). Then the nonlinear dynamic analyses are performed by applying five selective earthquakes from Japan seismic history. The comparative study is conducted for average compressive strain, deformations and axial force variation responses observed for two dimensional (2D) and three dimensional (3D) dynamic analyses. Similar type of comparative study is also performed to understand effect of scale-up and scale-down of earthquake acceleration motions on the pier responses.

5.2 Analytical Model

Any bridge system consists of two main parts: superstructure and substructures. Both parts are equally important in design point of view. Superstructure is made up of deck, safety railing, footpath, curbs, girders, bearings etc. and it provides an elevated plane surface over the ground surface for the transportation of vehicles. Substructure

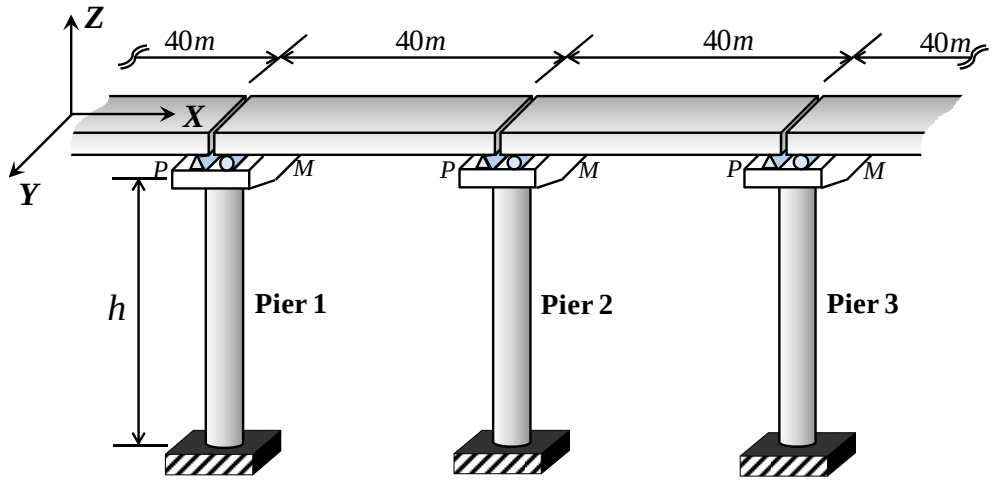

Fig. 5.1 Bridge System Studied in Present Work

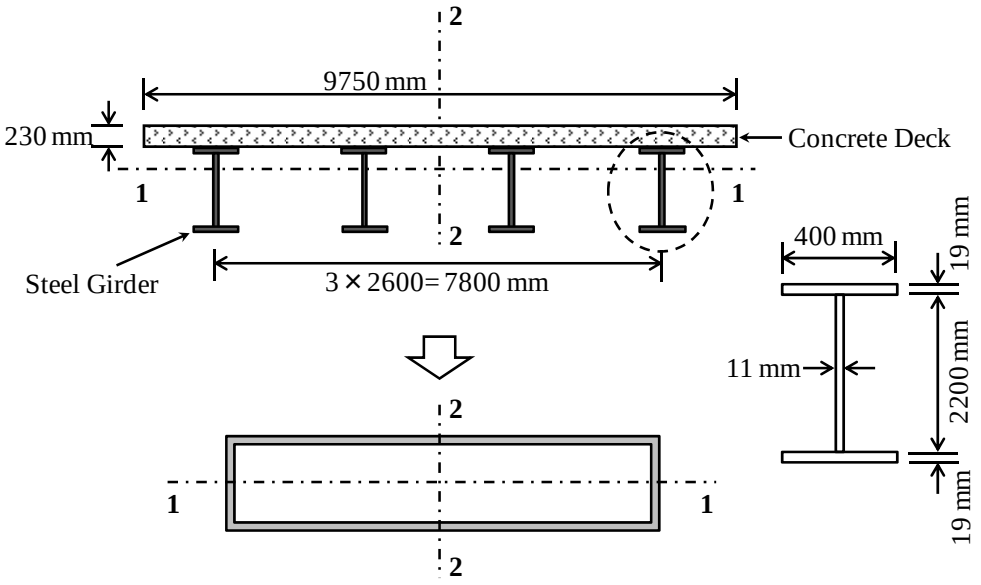

Fig. 5.2 Simplification of Superstructure

parts can cover up piers, abutments, footings, anchors, base isolation if provided, foundations etc. and the main function of substructure is to support superstructure and carry the load to the ground. Bridge system considered in the present work has concrete deck slab rested over steel girders and steel circular piers. Focus of this study is on the behavior of bridge piers and they are designed according to the procedure mentioned in Japanese specification (Japan road association, 2002). Superstructure, bearing systems and foundations are modeled as simple as possible and discussed in

following paragraphs.

(1) Superstructure and Piers

Fig. 5.1 shows assembly of the bridge system. It has four spans with the length l = 40 m and are rested on three steel piers with pipe section. Each span is supported through pin and movable bearings on the pier caps. According to the design principles of bridge systems, the piers should yield first rather than superstructures. Therefore, the bridge systems are designed in such a way that yielding should start first in piers but at the same time superstructure should remains in elastic limits. Mechanical properties of superstructures used in three bridge systems are same with the original superstructure designed by Kawashima et al., (1992), which is composed of reinforced concrete deck and four I-shaped steel girders. The original cross section of superstructure is converted into equivalent steel hollow box section (see **Fig. 5.2**) by confirming two transforming criteria as (1) equal sectional area and (2) equal sectional moment of inertia with respect to neutral axis 1-1 and 2-2. It should be noted that the original sectional area and moment of inertia are computed by using the equivalent steel values of the concrete deck (i.e. dividing the deck area and moment of inertia by the ratio of Young's modulus of concrete to steel).

In dynamic analysis the dead loads are conventionally modeled as lumped masses at the nodal points. However in the present study, instead of using concentrated masses a uniformly distribution of dead load is employed through mass per unit volume of the material (Alaghebandian et al., 2002). Accordingly, the values of mass per unit volume of equivalent steel box section for superstructure and steel piers are 27669.22 and 7851.8 Kg/m^3 respectively.

For modeling superstructure and piers, B31 type beam elements available in the element library of ABAQUS software are used. Each span of superstructure is divided into 10 segments. For piers 5 elements are used in effective failure region, L_e and remaining height of pier is divided into 15 segments. FE model developed for bridge system is shown in **Fig. 5.3 (a)**, in which the pier bases are fixed and earthquake motions are applied at these nodes. The material nonlinearity of piers in dynamic analysis is achieved by employing M2SM and for simplified superstructure, elastic model with same values of E and ν as for pier material are used. The steel grade SM490 is adopted for pier material and its material coefficients are given in **Table A.1** of **Appendix A**.

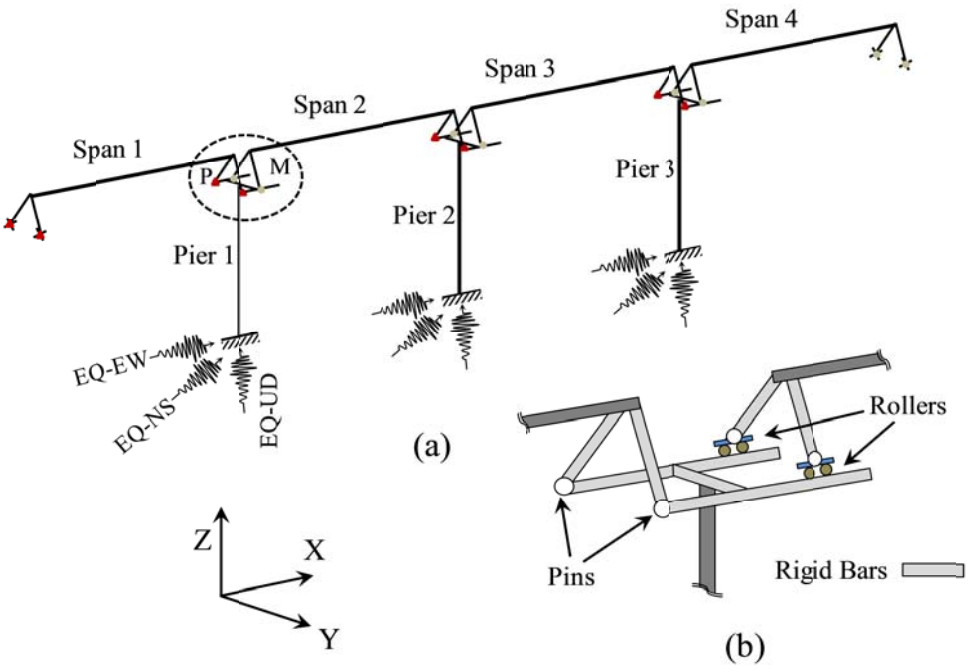

Fig. 5.3 Finite Element Model of Bridge System and Simplified Bearing

(2) Simplified Bearings

The bearings used in these bridge systems are simplified in such a way that, they provide supports between superstructure and pier without any self deformation and self forces distribution. The enlarged view of the bearing support is shown in **Fig. 5.3 (b)**. The rigid bars are used to form a bearing part which do not have any material properties but can transfer forces between elements connected through them. Pin and roller-constraints are defined between vertical and horizontal rigid bars. The pin-constraint avoids displacements in all directions but allows rotation only around Y axis. Whereas, roller-constrain provides displacement along X axis, rotation around Y axis and restricts all other degrees of freedom. Although this bearing system is simplified to some extent, it is made sure to give adequate functional characteristics of bearing between superstructures and piers by using pin and roller-constraints.

5.3 Initial Design of Bridge Piers

As mentioned earlier, three bridge systems are considered here to carry the same superstructure load. Hence, piers are the only members which need initial design. As discussed in Chapter 1, the Japanese specification (Japan Road Association, 2002)

adopted Performance-based design method, and according to this method the initial design of the bridge is categorized into 3 seismic performance levels (abbreviated as SPL). Depending on the importance, the bridges need to satisfy the predefined SPL. In this study, bridges are assumed to have standard importance (i.e. Class B bridges) therefore they require SPL 1 and SPL 2 verification. The stepwise procedure of initial design is as follows.

(1) Seismic Performance Level 1:

In this level, bridge should remain sound during Level 1 earthquake ground motions. Both static and dynamic methods can be used to check the performances in this SPL 1. In the present work seismic coefficient method is employed as static and time-history analysis as a dynamic method.

A. Seismic Coefficient Method

In seismic coefficient method, the inertia force from superstructure which is equivalent to the inertia force generated due to application of earthquake and concentrated axial force from superstructure which is equal to the lumped mass; both are applied together to the top of the single bridge pier as shown in **Fig. 5.4**. The horizontal inertia force H is obtained by following equation.

$$H = k_h W \tag{5.1}$$

where, k_h = design horizontal seismic coefficient, W = dead load from superstructure (kN). Further k_h is calculated by following formula.

$$k_h = c_z k_{h0} \geq 0.1 \tag{5.2}$$

where, k_{h0} = standard value of the design horizontal seismic coefficient for Level 1 earthquake ground motion based on the natural period of the structure and ground type. In present study ground Type II is assumed and piers are designed so as to give natural period ranging from 0.2 to 1.3. For this criteria, specifications suggest value of k_{h0} = 0.25. c_z = modification factor for zones of Japan territory as defined in specification. Zone A is assumed in this study and its value is c_z=1.0.

In SPL 1 the verification criteria suggested that bridge piers should not get yield. For checking this condition maximum axial stress in the bottom most elements is observed and compared with the allowable stress as defined in following equation.

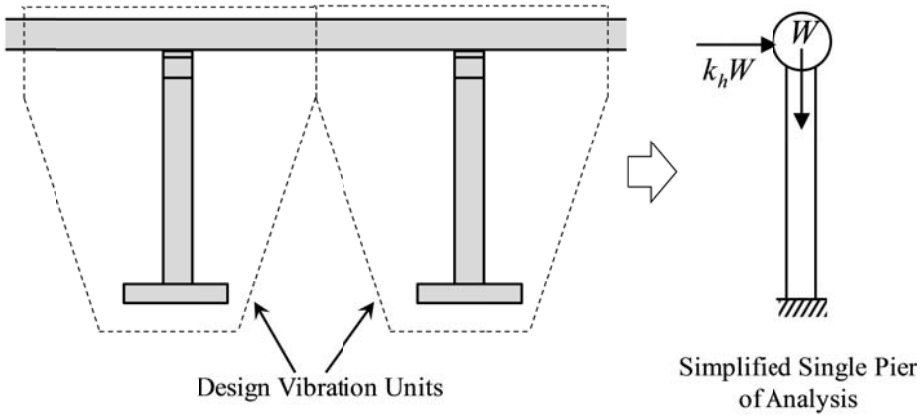

Fig. 5.4 Force Application in Seismic Coefficient Method

$$\sigma_{max} < \sigma_a \tag{5.3}$$

where, $\sigma_a = \sigma_y / \alpha$, α_s = factor based on steel grade (in Japanese called as 'warimashi') and which is taken as 1.12. The observed stress and allowable stress values for the middle pier (Pier 2 in **Fig. 5.3 (a)**) of the three bridge systems is normalized and given in **Table 5.1**. It can be seen clearly that the maximum stresses are less than allowable stress and hence it assures elastic performance of piers during Level 1 earthquake motions.

B. Dynamic Analysis Method

Another method to check SPL 1 criteria is the dynamic analysis. The Level 1 earthquake motions with small to medium magnitude are selected on the bases of high probability of occurrence during the life time of the bridge. Two such earthquake motions JIBAN1 and JIBAN2 are taken for dynamic analysis. Each earthquake motion is applied in bridge longitudinal and transverse direction separately (see **Fig. 5.3 (a)**) and the maximum average compressive strain $\bar{\varepsilon}_{a)max}$ in the effective failure height of the middle pier (i.e. Pier 2) are checked against the yield strain ε_y. The observed values and allowable values are tabulated in **Table 5.2**.

(2) Seismic Performance Level 2:

This SPL 2 recommends for bridge design to sustain limited damages during earthquake and capable of recovery within a short time. As mentioned in Chapter 1,

Table 5.1 Verification Results for SPL 1 (1)

Pier 2 of Models	Seismic Coefficient Method	
	Observed maximum stress σ_{max} / σ_y	Allowable stress σ_a / σ_y
(1)	(2)	(3)
Model-1	0.423	0.893
Model-2	0.571	0.893
Model-3	0.726	0.893

Table 5.2 Verification Results for SPL 1 (2)

Pier 2 of Models	Dynamic Analysis Method				
	Observed maximum average compressive strain $\bar{\varepsilon}_{a)max} / \varepsilon_y$				Allowable strain $\varepsilon_y / \varepsilon_y$
	JIBAN1		JIBAN 2		
	Longitudinal	Transverse	Longitudinal	Transverse	
(1)	(2)	(3)	(4)	(5)	(6)
Model-1	0.42	0.40	0.56	0.77	1
Model-2	0.50	0.43	0.62	0.98	1
Model-3	0.97	0.39	0.80	0.69	1

Table 5.3 Geometrical Properties of Designed Bridge Piers

Property (1)	Model 1 Piers (2)	Model 2 Piers (3)	Model 3 Piers (4)
D(m)	1.66	1.6	1.6
h(m)	5.4	7.45	9.6
t(m)	0.029	0.030	0.034
R_t	0.072	0.067	0.059
$\bar{\lambda}$	0.23	0.33	0.43

Level 2 earthquake motions are required for SPL 2 and there are two types of earthquake motions, namely Type I of plate boundary type earthquake with large magnitude and Type II of an inland direct strike type earthquake. In the present study, 3 earthquakes are selected for each type of recommended earthquake motions and modified for the ground Type II. Type I earthquake motions are namely ONN-TR-M, ITA-LG-M and ITA-TR-M and Type II earthquake motions are respectively FUKIAI-M, JRT-EW-M and JRT-NS-M. Similar to the procedure explained for SPL 1 dynamic analysis, these 6 earthquake motions are applied to the base of the piers in longitudinal and transverse directions and the maximum average compressive strain in the middle pier is compared against allowable strains. The ultimate strain formulas developed by author in Chapter 4 are found suitable in designing process of steel circular bridge piers, hence, the formula for uni-directional loadings (i.e. **Eq. (4.1)**) is employed here as a allowable strain. The strain responses are plotted and compared with the allowable strains for Pier 2 of each model and collectively presented in **Appendix G**. It is observed therein that each pier has satisfied the SPL 2 criteria. In this way, the designed geometric properties of the bridge piers are given in **Table 5.3**. Further, these three designed bridge systems are analyzed for actual earthquake records selected from Japanese seismic database.

5.4 Input Earthquake Motions

Five actual (i.e. unscaled) earthquake motions having significant vertical acceleration magnitude are selected in the present study to understand their effect on behavior of steel bridge piers. The earthquake records listed in **Table 5.4** are taken from reliable online source: Japan Meteorological Agency, K-NET and KiK-NET (NIED). The time-history records of each earthquake component are presented in **Appendix H** along with their acceleration spectra.

5.5 Bridge System under 2D and 3D Earthquake Motions

Nonlinear dynamic analyses are carried out for three bridge systems, using general purpose ABAQUS software. The mass proportional Rayliegh damping coefficient α which is related to the fundamental period of bridge system is employ ed into analysis. Two types of dynamic analyses are conducted for each earthquake

Table 5.4 Input Earthquakes

Outbreak Date and time (1)	Name of the Earthquake (2)	Observation Station (3)	Magnitude (4)	Peak Acceleration (EW, NS, UD) (cm/s^2) (5)	Abbreviation (6)
1995 Jan 17 17:46	The south Hyogo prefecture Earthquake in 1995	JR Takatori Station	M7.3	666, 642, 290	HYG
2003 may 26 18:24	The Miyagi prefecture Hokubu-oki Earthquake in 2003	OShika	M7.0	1112, 1103, 825	MYG
2004 Oct 23 17:56	The Mid Niigata Prefecture Earthquake in 2004	Kawaguchi city	M6.8	1676, 1142, 870	NIG
2004 Nov 29 3:32	The Hokkaido Tokachi-oki Earthquake in 2004	Tsurui East	M7.1	563, 756, 629	TKC
2008 Jun 14 8:43	The Iwate-Miyagi Nairiku Earthquake in 2008	Ichinoseki West	M7.2	1433, 1143, 3866	IWT

listed in **Table 5.4**, one by using only EW and NS components (i.e. 2D earthquake motion) and another is including EW, NS and UD components (i.e. 3D earthquake motions). Therefore, it is possible to observe the effect of vertical component over two horizontal components of the same earthquake. Influence of this vertical component on response of strain, deformations and axial force in the bridge piers are measured and compared in the following paragraphs.

5.5.1 Influence on Average Compressive Strain

Each bridge system assumed in this study consist of three circular piers, out of them the middle pier i.e. Pier 2 is selected to measure responses, because this pier represents behavior of a pier within a multi-span bridge systems. However, Pier 1 and 3 are the adjacent piers to Pier 2; hence their responses may get affected due to their position in the bridge system considered in present study.

Sample response history of average compressive strain $\bar{\varepsilon}_a / \varepsilon_y$ in the effective failure region L_e observed for 2D and 3D earthquake excitations are shown in **Fig. 5.5 (a)**. The maximum strains are marked by circular and triangular dots for 2D and 3D responses respectively. Such absolute maximum strains for three piers when subjected to five different earthquakes are collectively presented in **Fig. 5.5 (b-d)**.

Significant similarity in 2D and 3D absolute maximum strain is noticed for each pier except for the earthquake IWT. It is also noticed that for a particular earthquake the absolute maximum strain response varies from pier to pier, because of their relationship between natural periods and acceleration response spectra. As shown in **Fig. H.1** of **Appendix H**, fundamental natural period of three models differs from each other and hence, they are sensitive to different amplitudes of spectral accelerations. In general it can be observed in **Fig. H.1** that the natural period line of Model-1 crosses higher amplitudes of spectral acceleration and therefore, it has shown large strain response than the others. In case of IWT earthquake as shown in **Fig. 5.5 (b, d)**, piers of Model-1 and 3 have shown slightly higher strain response for 2D than that of 3D earthquake. This implies that 2D earthquake motions can become severe than 3D motions, if the vertical component of earthquake is strong enough which may reduces compression force due to tensile forece effect. Beside all these observations, it endorses that the strain response of piers is related to characteristics of earthquake motions and bridge system.

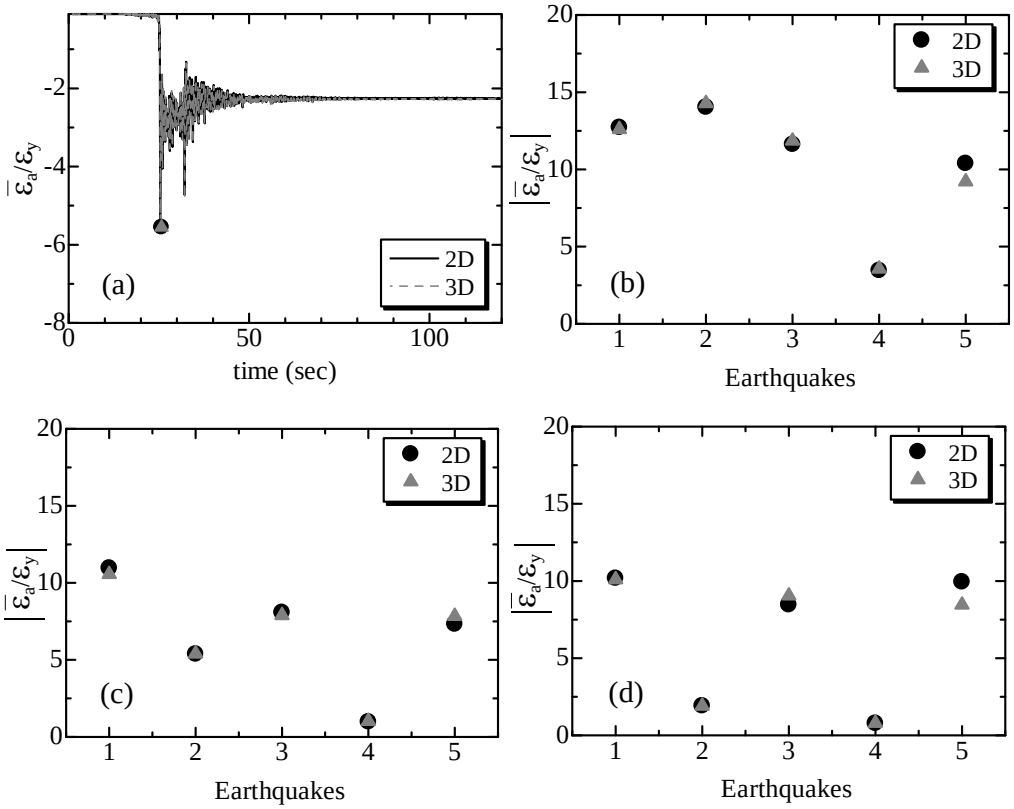

Fig. 5.5 (a) Average Compressive Strain Response of a Pier in 2D and 3D Earthquake Motions, (b)-(d) Comparison of Absolute Maximum Strains in 2D and 3D Earthquake Motions Measured for Middle Pier of Model-1, 2, 3 Respectively

5.5.2 Influence on Deformations

A sample of relative deformation response of top of the pier in X-Y plane, (i.e. δ_X / δ_{y0} and δ_Y / δ_{y0}, where δ_{y0} = yield deformation excluding axial loading effect) is shown in **Fig. 5.6 (a)** for both 2D and 3D earthquake motions. The maximum and minimum deformations in X and Y directions are marked by circular and triangular symbols for 2D and 3D responses respectively. In this way the observed maximum and minimum X directional deformation points are plotted in **Fig. 5.6 (b-d)** for each pier and similarly Y directional deformations are plotted in **Fig. 5.7**. This comparison between 2D and 3D deformation responses has not shown any change due to vertical component of earthquake.

5.5.3 Influence on Axial Force

In the similar way with strain and displacement responses, the axial force

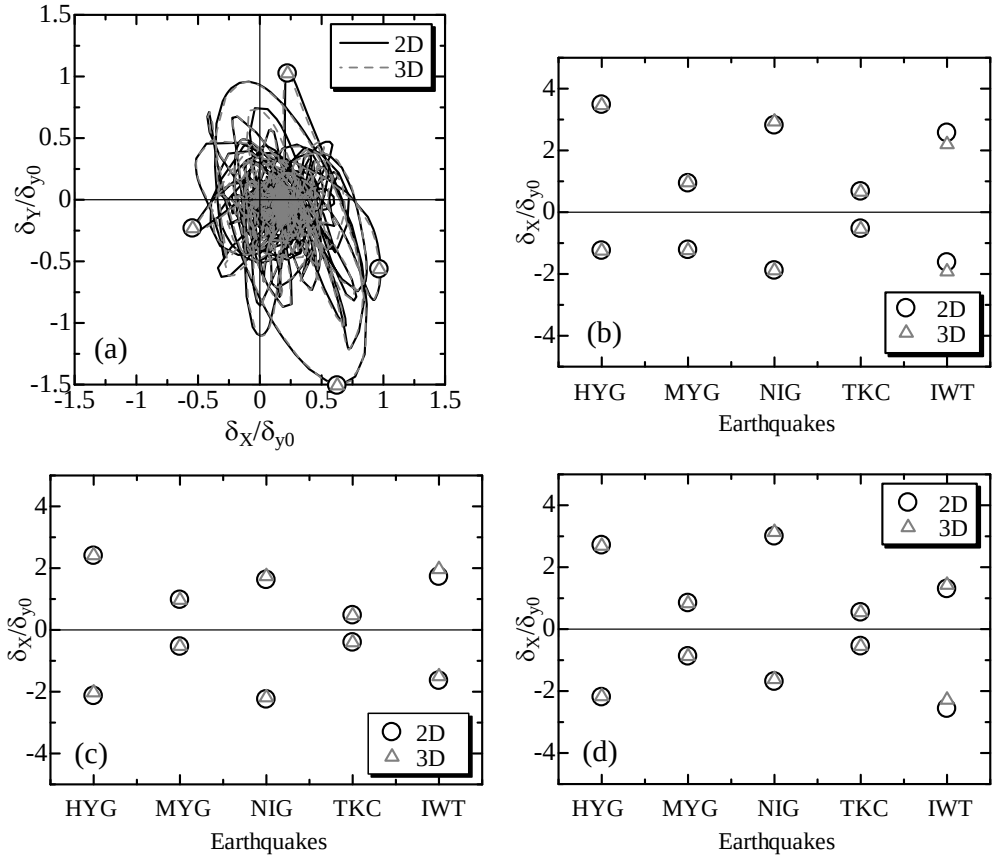

Fig. 5.6 (a) Deformation Response of a Pier in 2D and 3D Earthquake Motions, (b)-(d) Comparison of X directional Maximum-minimum Deformations in 2D and 3D Earthquake Motions Measured for Middle Pier of Model-1, 2, 3 Respectively

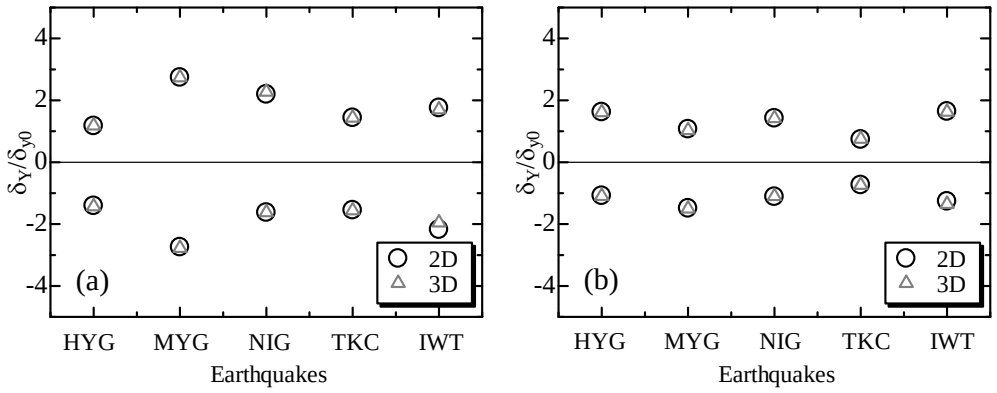

Fig. 5.7 (a)-(c) Comparison of Y directional Maximum-minimum Deformations in 2D and 3D Earthquake Motions Measured for Middle pier of Model-1, 2, 3 Respectively

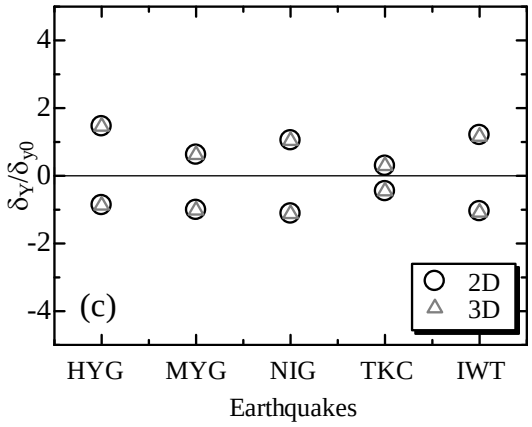

Fig. 5.7 Continued

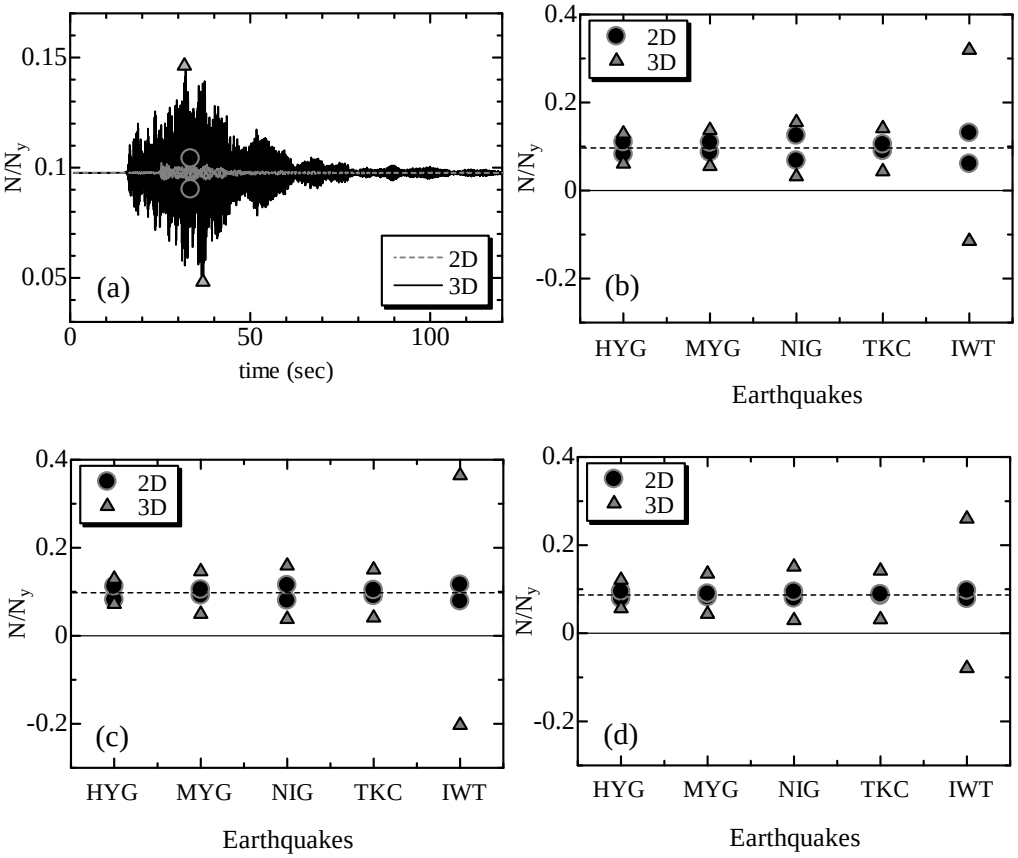

Fig. 5.8 (a) Axial Force Response of a pier in 2D and 3D Earthquake Motions, (b)-(d) Comparison of Maximum-minimum Axial Force in 2D and 3D Earthquake Motions Measured for Middle pier of Model-1, 2, 3 Respectively

responses (i.e. N / N_y where, N_y = squash load = $\sigma_y A$) in a pier are presented in **Fig. 5.8 (a)**, for 2D and 3D earthquake motions and their maximum and minimum points are marked by distinct symbols. In **Fig. 5.8 (b-d)**, the observed maximum and minimum axial force values are collectively plotted for each earthquake and each pier. It is clearly seen that axial force in piers has varied considerably when vertical component of earthquake becomes active. In the case of 3D IWT earthquake, the axial force even reaches on negative side i.e. pier experiences tensile force.

Above mentioned observations reveal that vertical component together with two horizontal components of earthquake has not shown major influence in average compressive strain and deformations but caused large variation in the axial force. However, it should be noted that this dynamic response comparative study is carried out by applying different unscaled or actual earthquake components in two directions and three directions having different vibration characteristics. Hence, to find out the scale-up and scale-down effect of components of single earthquake on the bridge pier response, few more dynamic analysis are performed and their responses are compared again.

5.6 Scale-up and Scale-down Effect of Earthquake Components

Hyogo-ken Nanbu earthquake motions and Model-2 bridge system are selected to observe influence of scale-up and scale-down of components on seismic performance of the pier based on the study carried out by Kawashima et al., (visited on 9th Aug 2010). Two multiplication factors are used for scale-down as 0.50 and 0.75, for scale-up 1.25 and 1.50 and multiplication factor 1 represents for actual motions. 2D and 3D dynamic analysis are carried out by considering four cases of application of multiplication factors (MF) such as (1) MF for all components, (2) MF only for UD component, (3) MF only for EW component, (4) MF only for NS component. Comparison between 2D and 3D earthquake response of the pier is discussed as follows.

Similar to that mentioned in the section 5.5, maximum strain, deformation and axial force responses are compared when 2D and 3D earthquake components are applied on bridge system. **Fig. 5.9** shows maximum strain responses plotted for various scaling MF on earthquake component. It is clearly observed that inclusion of vertical earthquake component has not affected the maximum average compressive strain in the pier. In other words, 2D and 3D maximum strain responses are similar to each other. Moreover, in **Fig. 5.9 (a, c, d)**, the maximum strain is found to be

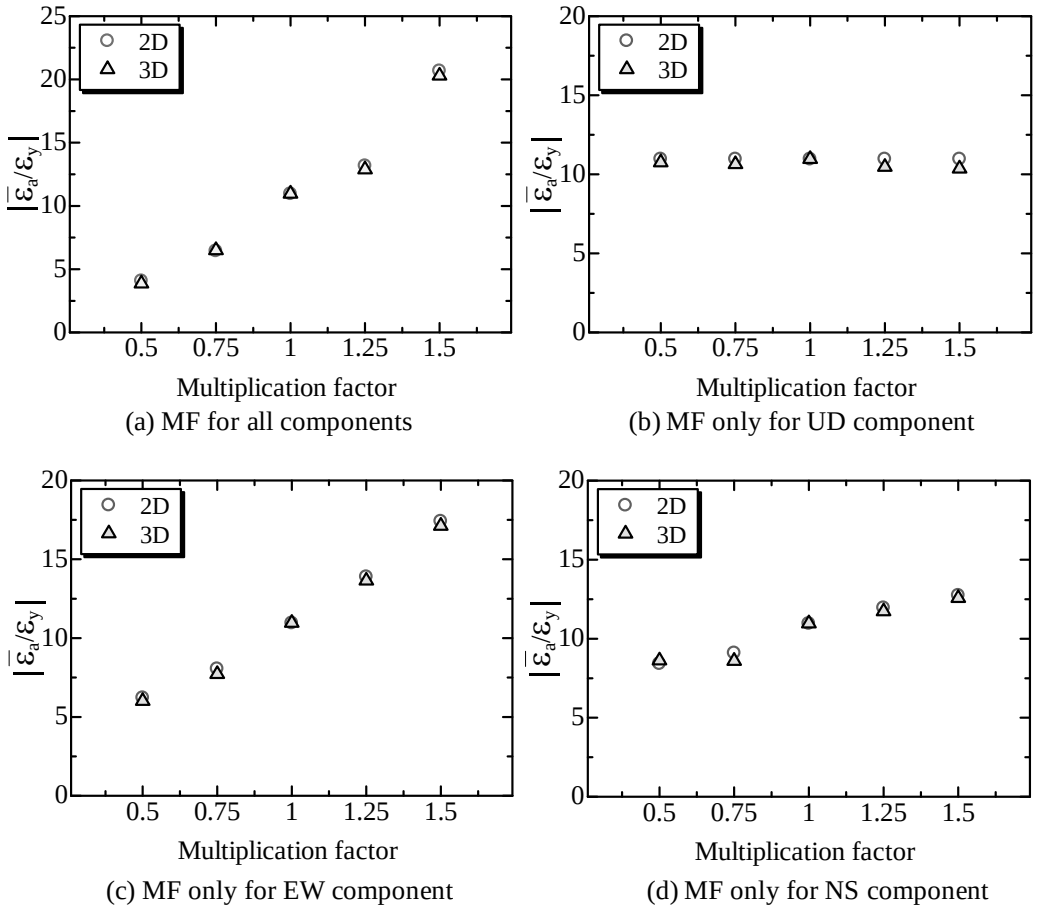

Fig. 5.9 Comparison between 2D and 3D Maximum Average Compressive Strain Responses Observed for Scaling on HYK Earthquake Components

increased as the MF applied respectively on EW-NS-UD, EW and NS components in increasing order. However, in **Fig. 5.9 (b)** maximum strain almost remains unchanged even if MF is applied only on UD component. This means, scaling of vertical earthquake components has no influence on maximum strain response but it depends on the scaling of horizontal components.

Figs. 5.10 and **5.11** indicate the maximum and minimum deformations of top of the pier in X and Y directions respectively. Considerable similarity is observed between 2D and 3D deformation responses which mean coupling effect of vertical component of earthquake with two horizontal components is same with coupling of two horizontal components. Moreover, it is found that scaling of UD component has no effect on deformation response in both directions (see **Figs. 5.10 (b)** and **5.11 (b)**), however, scaling of EW and NS components has shown change in deformation response. Comparison between 2D and 3D earthquake effect on maximum and maxi-

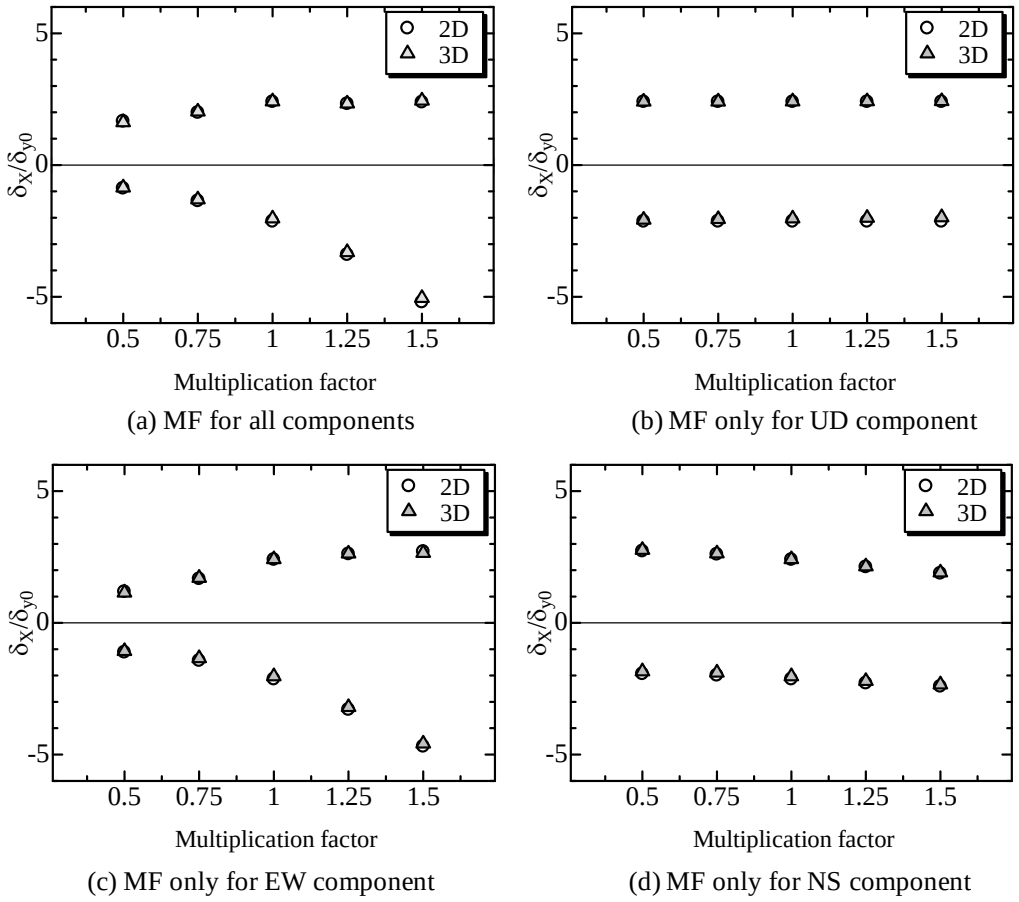

(a) MF for all components (b) MF only for UD component

(c) MF only for EW component (d) MF only for NS component

Fig. 5.10 Comparison between 2D and 3D Maximum and Minimum X Directional Deformation Responses Observed for Scaling on HYK Earthquake Components

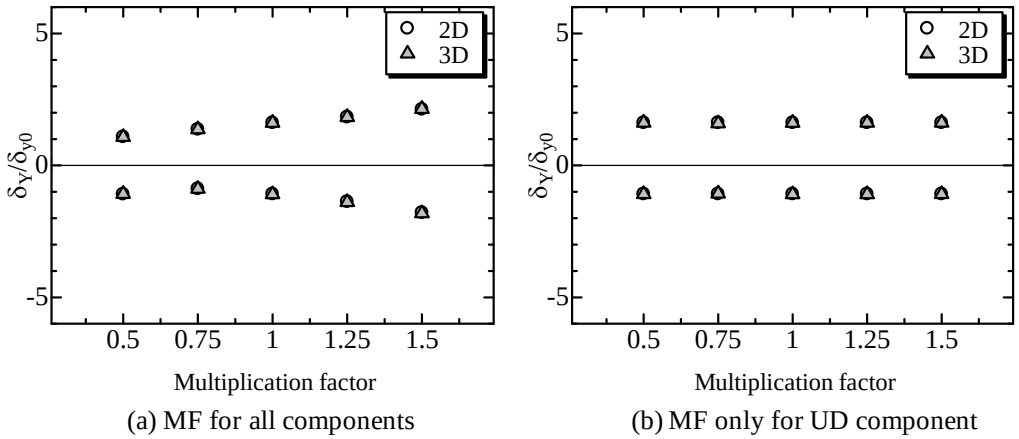

(a) MF for all components (b) MF only for UD component

Fig. 5.11 Comparison between 2D and 3D Maximum and Minimum Y Directional Deformation Responses Observed for Scaling on HYK Earthquake Components

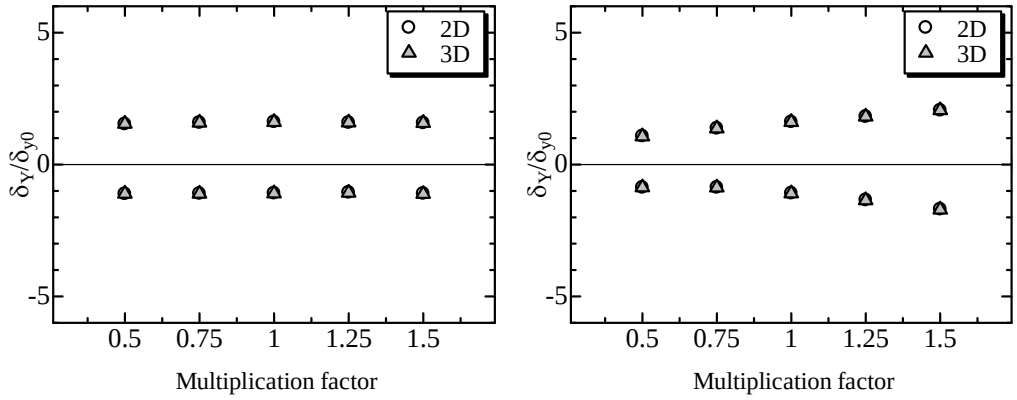

(c) MF only for EW component (d) MF only for NS component

Fig. 5.11 Continued

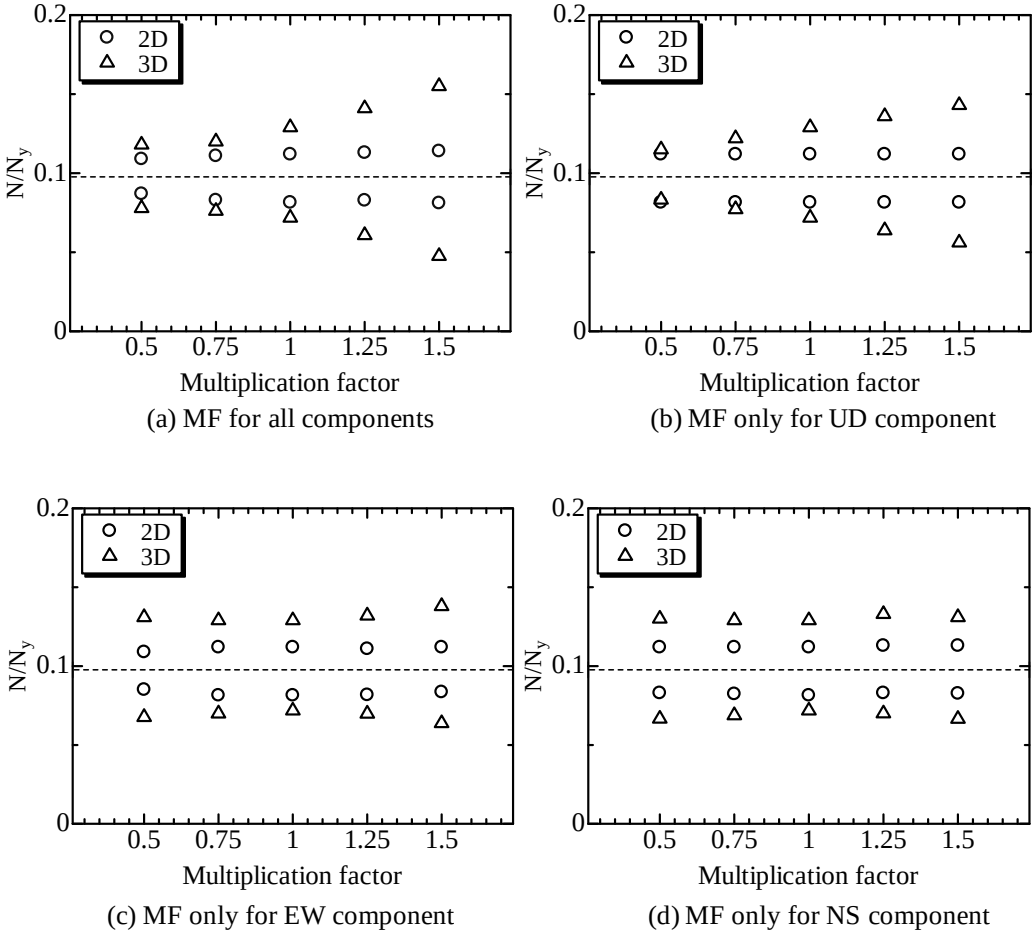

(a) MF for all components (b) MF only for UD component

(c) MF only for EW component (d) MF only for NS component

Fig. 5.12 Comparison between 2D and 3D Maximum and Minimum Axial Force Responses Observed for Scaling on HYK Earthquake Components

mum axial force in the pier is shown in **Fig. 5.12**. It is noticed that amplitude of axial force due to 3D earthquake is always lager than that of 2D earthquake. In **Fig. 5.12 (a, b)**, 3D axial force response is found to be increased as MF increases. However, axial force response almost remains unaffected even if MF is applied on EW and NS components as shown in **Fig. 5.12 (c, d)**.

From these observations it can be stated that UD component of earthquake has close relationship with axial force variation and strain and deformations responses are dependent on horizontal motions i.e. EW and NS earthquake components. However, it should be noted that the present dynamic analysis are carried out on the FE models constructed by beam elements which do not consider local buckling. To check the strain and deformations responses along with buckling modes of the piers due to 2D and 3D earthquake, it is necessary to conduct dynamic analysis using shell elements.

It is discovered from 3D dynamic analysis that axial force in the bridge piers varies with large amplitude and hence it is very important to find out effect of variation in axial force on the capacity of steel columns; so that some measures can be suggested while designing bridge piers. For this purpose, nonlinear static analysis are performed by applying bi-directional horizontal cyclic displacement loading with varying axial force on circular steel columns and which is discussed in following chapter.

5.7 Summary

The present chapter dealt with the comparative study between 2D and 3D seismic effect on the various responses of bridge piers. It has been already proved in Chapters 3 and 4 that, EW-NS earthquake components severely amplify displacement, strain responses of the piers than merely any one component. Hence in the present chapter, the influence of vertical component over the horizontal components of earthquakes is investigated.

Five unscaled strong earthquake motions selected from the seismic database are applied on the initially designed three bridge systems. 2D and 3D nonlinear dynamic analyses are conducted by applying EW-NS components and EW-NS-UD components respectively. The responses of the piers are measured in terms of average compressive strain, displacements and axial force variations. The similar observations are also taken when earthquake acceleration components are increases or decreased by using

multiplication factor. The important findings from these results are summarized as follows.

(1) The maximum average compressive strains observed in 2D and 3D earthquakes have shown great similarity and their amplitudes has indicated close relationship with fundamental natural period. The tensile force developed in 3D earthquake like IWT, might have the capacity to reduce average compressive strain than its 2D components. Neglecting the exceptional cases, it can be said that 3D earthquake has not significant impact on maximum strains in comparison with 2D earthquake.

(2) Maximum and minimum amplitudes of displacements in X and Y directions of top of the piers have not shown any considerable change due to 3D earthquake motions.

(3) The axial force response in each pier revealed that vertical component coupled with two horizontal components of earthquakes has substantial effect on maximum and minimum axial forces. In some rare cases, axial force variation even reached on tensile side (e.g. IWT earthquake).

(4) Scale-up and scale-down of earthquake acceleration components has clearly shown that maximum strain and deformations in the bridge pier are affected due to scaling in horizontal components, whereas, the axial force response is found to be changed when scaling factor is applied on vertical component of earthquake. These results indicate a requirement to understand the influence of varying axial force on the capacity of circular steel bridge piers and which is discussed in next chapter.

Chapter 6

VARYING AXIAL FORCE EFFECT ON CYCLIC BEHAVIOR OF STEEL CIRCULAR PIERS

6.1 Introduction

As observed in Chapter 5 that 3D earthquake motions including vertical and two horizontal components can severely affect the axial force in the steel bridge piers. Therefore, it is very necessary to understand effect of varying axial force along with bi-directional cyclic horizontal loadings on the inelastic behavior of the steel circular columns by performing static analysis. Regarding this topic very few past studies have been reported. One of them was carried out on square shaped steel beam-column by applying one directional cyclic displacement and varying axial loadings simultaneously (Yamazaki and Minami, 1999) but, this study was related to steel beam-columns which are generally used for multi-story buildings. Whereas, the steel columns used as bridge piers behave in very different manners than that of the beam-columns used in multi-story buildings. Therefore, the objective of present study is to observe varying axial force along with bi-directional cyclic effect on the steel circular columns modeled as bridge piers.

The properties of three bridge piers mentioned in **Table 5.3** of Chapter 5 are taken here to perform nonlinear static analysis which follows similar process that used in Chapters 3 and 4. In addition to constant axial force cases varying axial force cases are considered. The comparative study is carried out between influence of constant and varying axial force on hysteresis behavior, strength-displacement envelops and energy dissipation per cycle.

6.2 Analytical Model and Loading Patterns

The FE modeling details of three steel circular columns taken for this study is same with that mentioned in Chapter 3. The main purpose of previous studies (i.e. Chapters 3 and 4) were to find out the ultimate capacity due to bi-directional loading with constant axial force. Whereas, the present work is concerned to understand the varying axial force effect. Therefore, different varying axial force patterns are

considered and their influences over constant axial force are compared.

Variation in axial force with respect to lateral displacement can be classified as: (1) proportional i.e. axial and lateral loads are applied simultaneously and both reach their extreme values at the same time and (2) nonproportional means variations are uncoupled. There is possibility of occurring both coupled and uncoupled axial force variation with lateral loading during earthquake response of bridge piers. Nonproportional axial force pattern has proved severe than proportional pattern, for RC columns (Saadeghvaziri et al., 1990; Saadeghvaziri, 1995). Whereas, in the case of steel columns for which cyclic behavior is different from RC columns, deciding the critical axial force variation pattern was unclear until the comparative study between proportional and nonproportional loading on steel circular column was carried out by authors (Kulkarni and Kasai, 2009; see **Appendix J**). It is found that proportional axial force variation with bi-directional cyclic loading has reduced strength and ductility considerably than that of nonproportional pattern. In proportional axial force, the maximum displacement and maximum axial force are applied on the column at the same time which increases P-Δ effect and hence column experience large compressive and bending forces. Whereas, in nonproportional case the axial force does not reach to its maximum when displacement becomes maximum; therefore, resulting P-Δ effect is smaller than that of proportional case. Moreover, steel material has good ductile properties than RC composite material; hence, even though the nonproportional pattern causes large decrease in strength and ductility of RC columns, it may not create same effect in steel columns. Based on this view point, two types of proportional axial force patterns are assumed for analysis in the present work.

For various axial force cases, 16 patterns are considered keeping the lateral cyclic bi-directional displacement loading same as that used in Chapters 3 and 4. Out of 16 patterns, 6 are for constant and 10 are for varying axial force cases as illustrated in **Fig. 6.1**. In the case of varying axial force, two types are assumed as: (1) one axial force cycle is completed with one displacement cycles i.e. single cycle variation and (2) two axial force cycles are completed with one displacement cycles i.e. double cycle variation (see **Fig. 6.1 (g-p)**). It has been found from Eigenvalue analysis of three bridge systems studied in Chapter 5 that, the ratios of fundamental natural period of vertical vibration to that of horizontal vibration are 1/0.7, 1/1.14 and 1/1.5 (refer **Appendix I**). In which application of 0.7 axial force cycles for each displacement cycle creates a nonproportional pattern therefore it is excluded from the

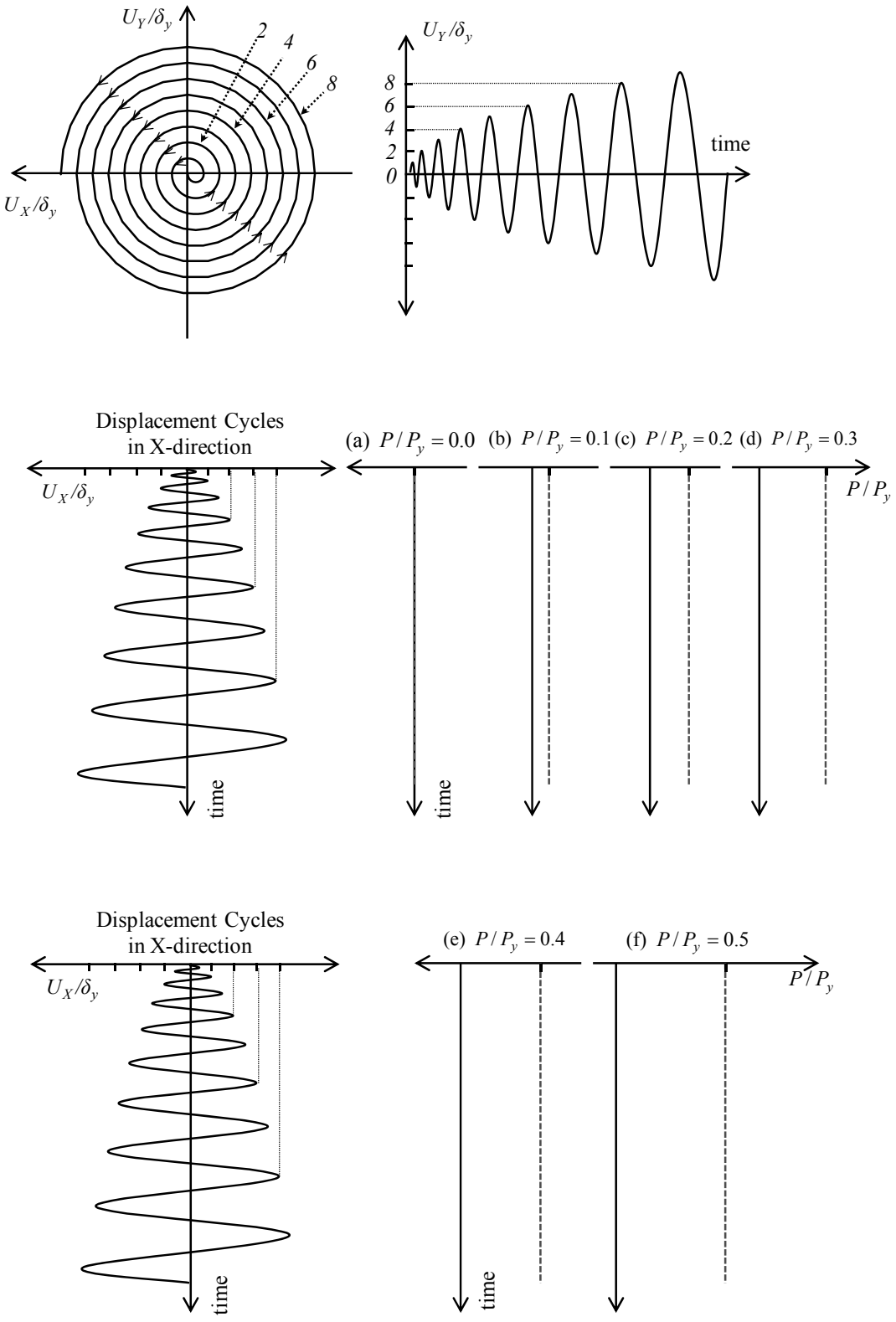

Fig. 6.1 Displacement Loading Patterns and (a) to (f) Constant Axial Force Cases, (g) to (p) Varying Axial Force Cases

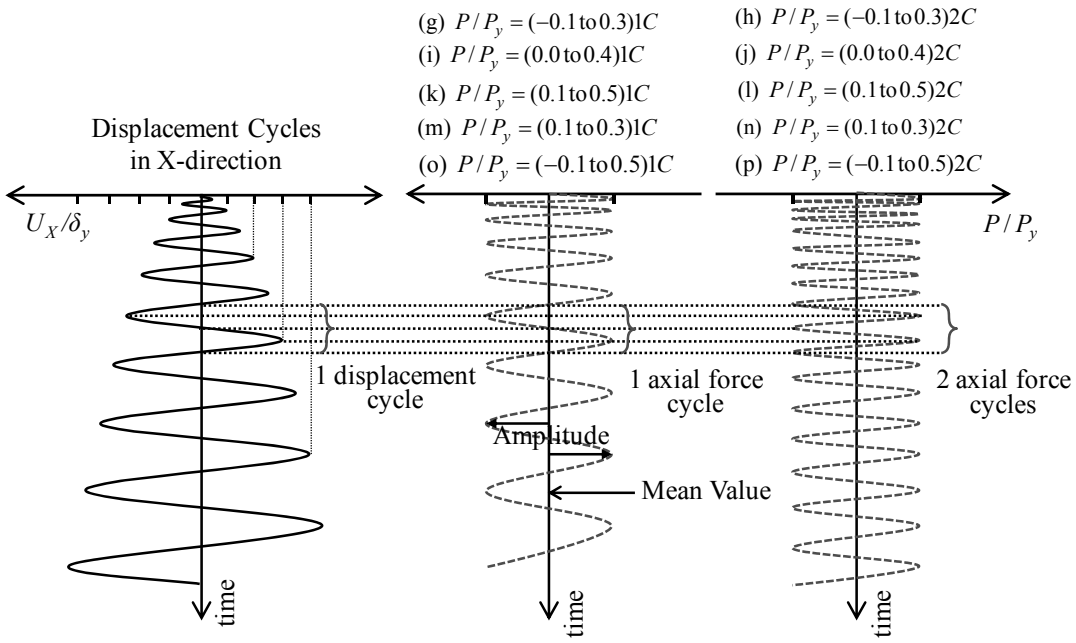

Fig. 6.1 Continued

study. Remaining two cases of 1.14 and 1.5 are lying between two proportional varying axial force patterns as mentioned above. In **Fig. 6.1**, the patterns from **(g)** to **(l)** have constant amplitude of $P/P_y = 0.2$ on both sides of mean value. The mean values are assumed as $P/P_y = 0.1$, 0.2 and 0.3. The patterns from **(m)** to **(p)** have constant mean value $P/P_y = 0.2$ but two different amplitudes $P/P_y =$ 0.1 and 0.3.

During the FE analysis for varying axial force cases, initially the axial force equal to mean value is applied on the top of column when displacement remains zero and in the next step, displacement and axial force variation come into action. Both geometrical and material nonlinearity are considered in the analysis. The results of these analyses are discussed in the following subsection.

6.3 Results and Discussion

The results obtained from analysis for three columns are found to be more or less similar in their behavior, hence, the results from a selected column with $R_t = 0.067$ and $\bar{\lambda} = 0.33$ are presented here. To observe the effect of varying axial force on strength and ductility, they are plotted in their normalized form. Hence, instead of using yield strength H_y and yield displacement δ_y which includes effect of axial force, the similar values like $H_{y0} = M_y / h$ and $\delta_{y0} = (H_{y0}h^3/3EI) + (H_{y0}h/\kappa GA)$

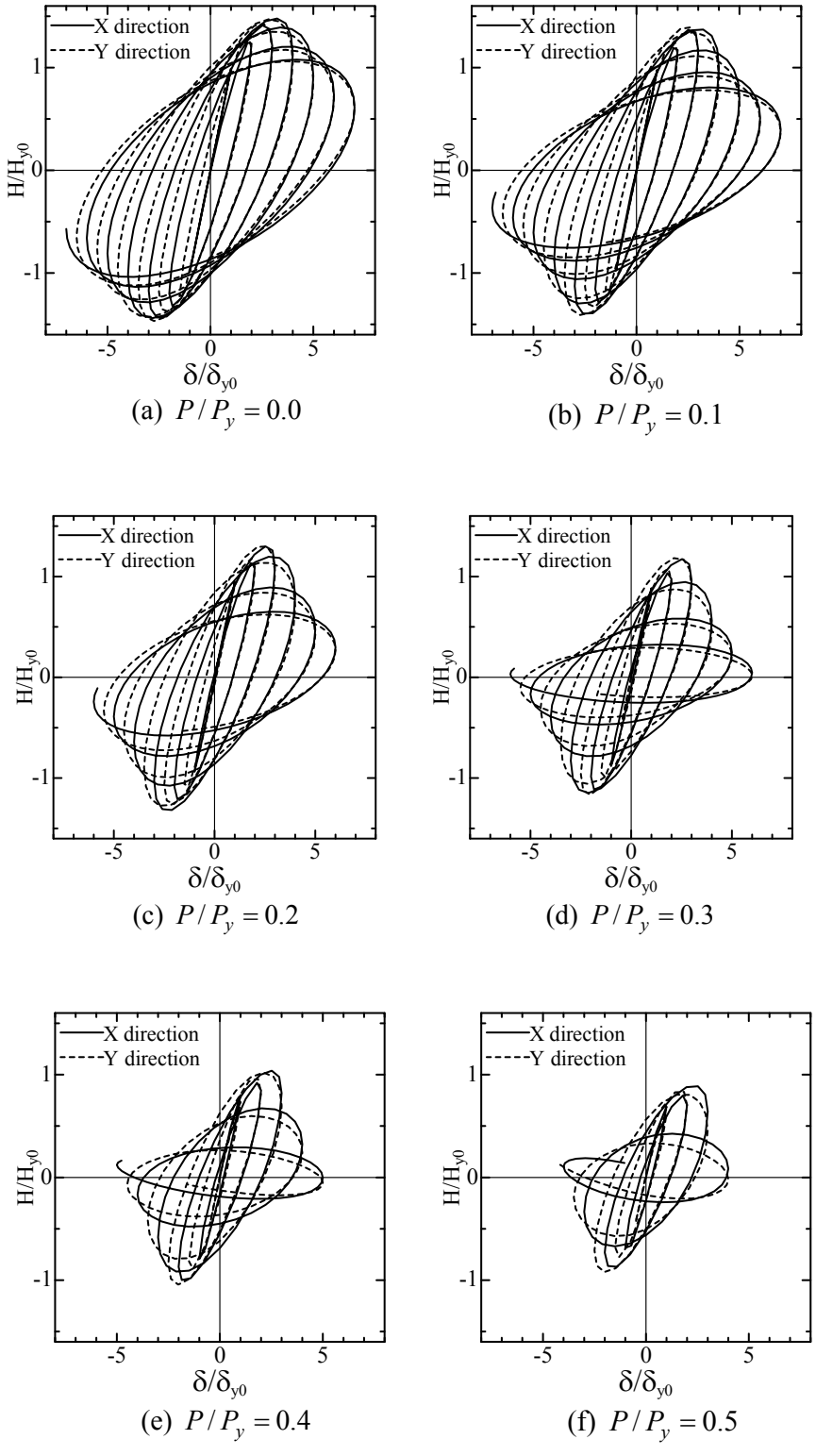

Fig. 6.2 Hysteretic Behavior of a Pier under Various Axial Loading Cases

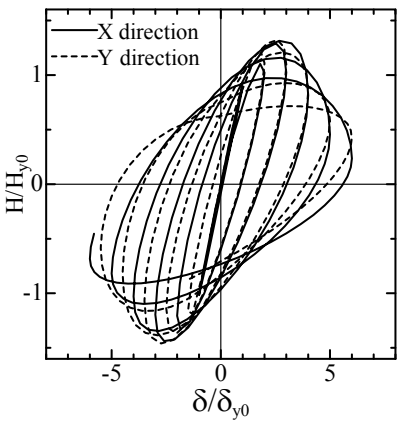

(g) $P/P_y = (-0.1\,\text{to}\,0.3)1C$

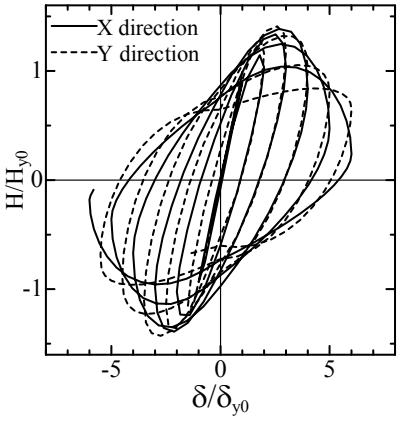

(h) $P/P_y = (-0.1\,\text{to}\,0.3)2C$

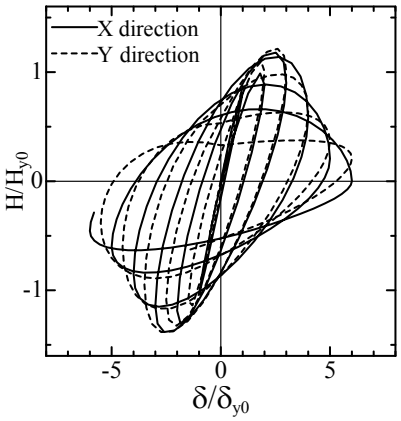

(i) $P/P_y = (0.0\,\text{to}\,0.4)1C$

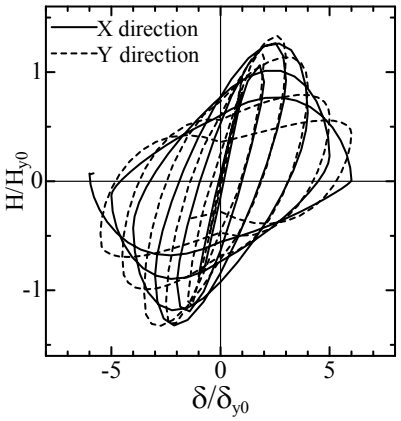

(j) $P/P_y = (0.0\,\text{to}\,0.4)2C$

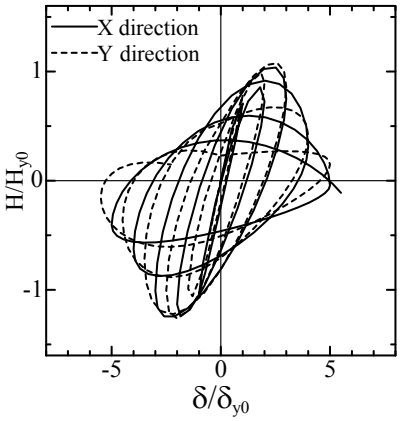

(k) $P/P_y = (0.1\,\text{to}\,0.5)1C$

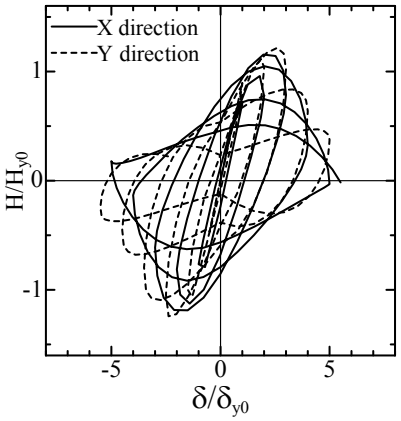

(l) $P/P_y = (0.1\,\text{to}\,0.5)2C$

Fig. 6.2 Continued

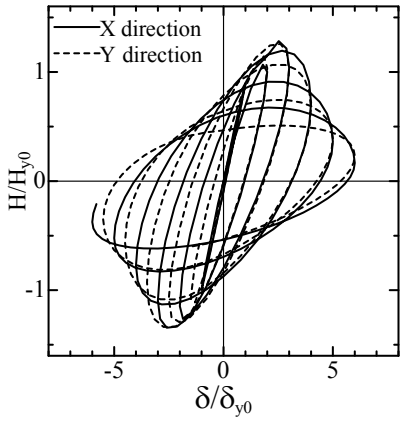

(m) $P/P_y = (0.1\,\text{to}\,0.3)1C$

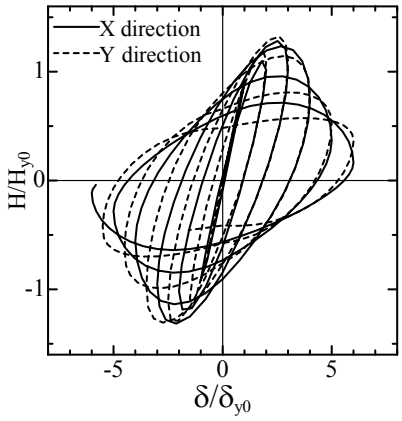

(n) $P/P_y = (0.1\,\text{to}\,0.3)2C$

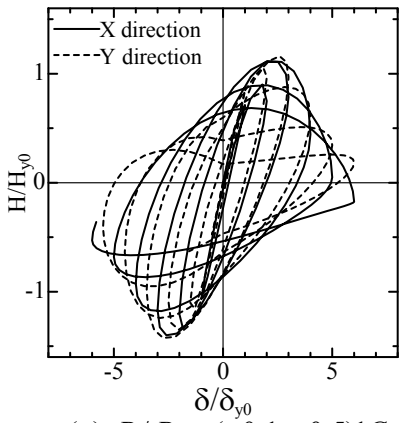

(o) $P/P_y = (-0.1\,\text{to}\,0.5)1C$

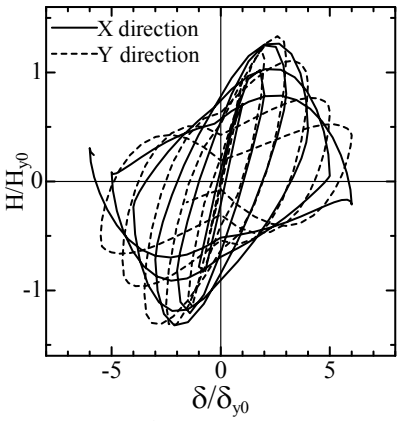

(p) $P/P_y = (-0.1\,\text{to}\,0.5)2C$

Fig. 6.2 Continued

(where, $M_y = \sigma_y z$, z = section modulus, κ = transverse shear stiffness ratio, G = shear modulus and A = cross sectional area) are used which exclude axial force effect.

6.3.1 Hysteretic Behavior

Fig. 6.2 indicates the hysteretic curves of horizontal force-displacements relationships in X and Y directions. Strength and ductility are found to be reduced as the constant axial force increases in **Fig. 6.2 (a-f)** and indicate that the strength-displacement trajectories are spread evenly in both directions. On the other hand, for varying axial force cases, distribution of strength and ductility in X and Y directions are distorted due to unevenness of axial force (see **Fig. 6.2 (g-p)**). However, it can be seen that as the mean value of varying axial force (e.g. mean value P/P_y =

0.1, 0.2 and 0.3 in **Fig. 6.2 (g, i, k)** or **(h, j, l)**) increases, the maximum strength and ductility decreases, which is similar to constant axial force cases. When mean value remains same and amplitude changes (e.g. mean value P/P_y = 0.2 and amplitudes P/P_y = 0.1, 0.2 and 0.3 in **Fig. 6.2 (m, i, o)** or **(n, j, p)**), maximum strength decreases slightly but distortion in Y directional hysteretic curves increases gradually.

The main difference observed in single and double cyclic axial force loading cases, is about distortion shapes. The distortion is noticed on positive side of strength axis for single cycle axial force variation cases (see **Fig. 6.2 (g, i, k, m, o)**) whereas, for double cycle cases distortions can be seen on both sides of strength axis (see **Fig. 6.2 (h, j, l, n, p)**). The amount of distortion is found to be dependent on amplitude and mean value of varying axial force. The most distorted shape can be seen for cases shown in **Fig. 6.2 (l, p)** which have largest mean value and amplitude respectively.

The hysteretic curves explain about distribution of strength and displacement in two perpendicular directions, but to compare this behavior in different way, the envelop curves for maximum strength and displacement are plotted.

6.3.2 Envelop Curves

The envelop curves shown in **Fig. 6.3** are obtained from hysteretic curves in X direction only. From that, **Fig. 6.3 (a)** indicates envelop curves for constant axial force cases, which clearly shows that strength and ductility capacity decreases as the magnitude of constant axial force increases. **Fig. 6.3 (b-f)** are plotted for two types of varying axial force patterns along with a constant axial force case equal to mean value of these varying axial force. It is observed that strength and ductility are larger for single cycle varying axial force than that of constant and double cycle axial force cases. In **Fig. 6.3 (b, c)** even if amplitude of variation remains same (i.e. P/P_y = 0.2), the difference between envelop curves increases when mean value increases from 0.1 to 0.3. Comparing the plots for same mean value cases such as **Fig. 6.3 (e, c, f)** it revealed that as the amplitude value increases from P/P_y = 0.1 to 0.3, the difference between envelop curves also increases.

From these observations, it seems that double cycle varying axial force pattern is severe than constant and single cycle axial force patterns. In other words, it appears that consideration of single cycle axial force pattern may improve strength and ductility capacity of steel columns. But, it should be noted that these envelop curves are plotted for X directional strength and ductility relationship and they are not based

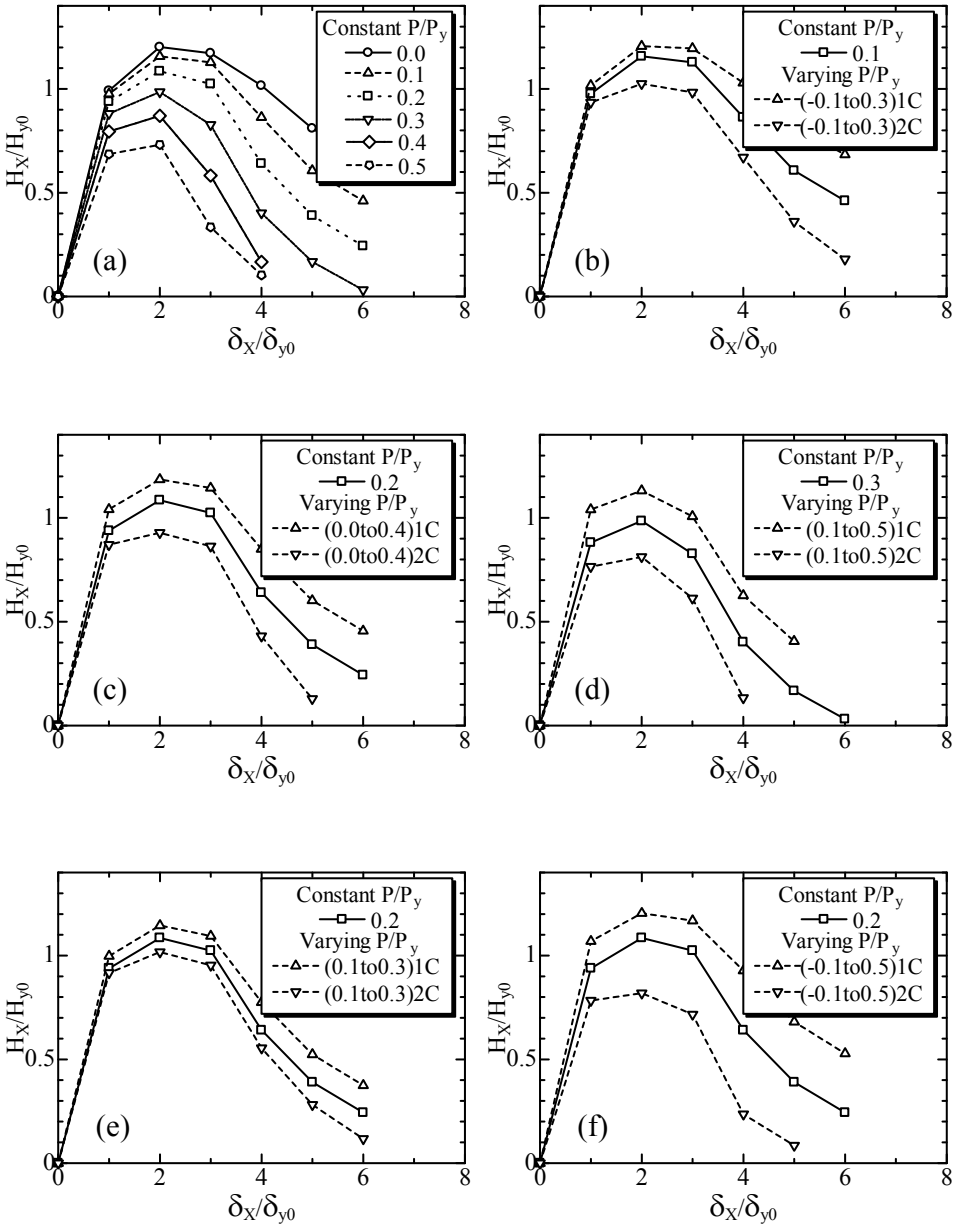

Fig. 6.3 Envelop Curves for a Pier under Various Axial Loading Cases

on representation of both X and Y directional behavior. Therefore, it is necessary to adopt such a quantity for comparison which can measure cumulative effect of strength and ductility. And hence, energy dissipation capacity per cycle during different loading patterns is calculated and presented in the following subsection.

6.3.3 Energy Dissipation Curves

The accumulative dissipated energy is equal to the enclosed area of the hysteretic curves shown in **Fig. 6.4**. Therefore, energy dissipation curve is a better option to

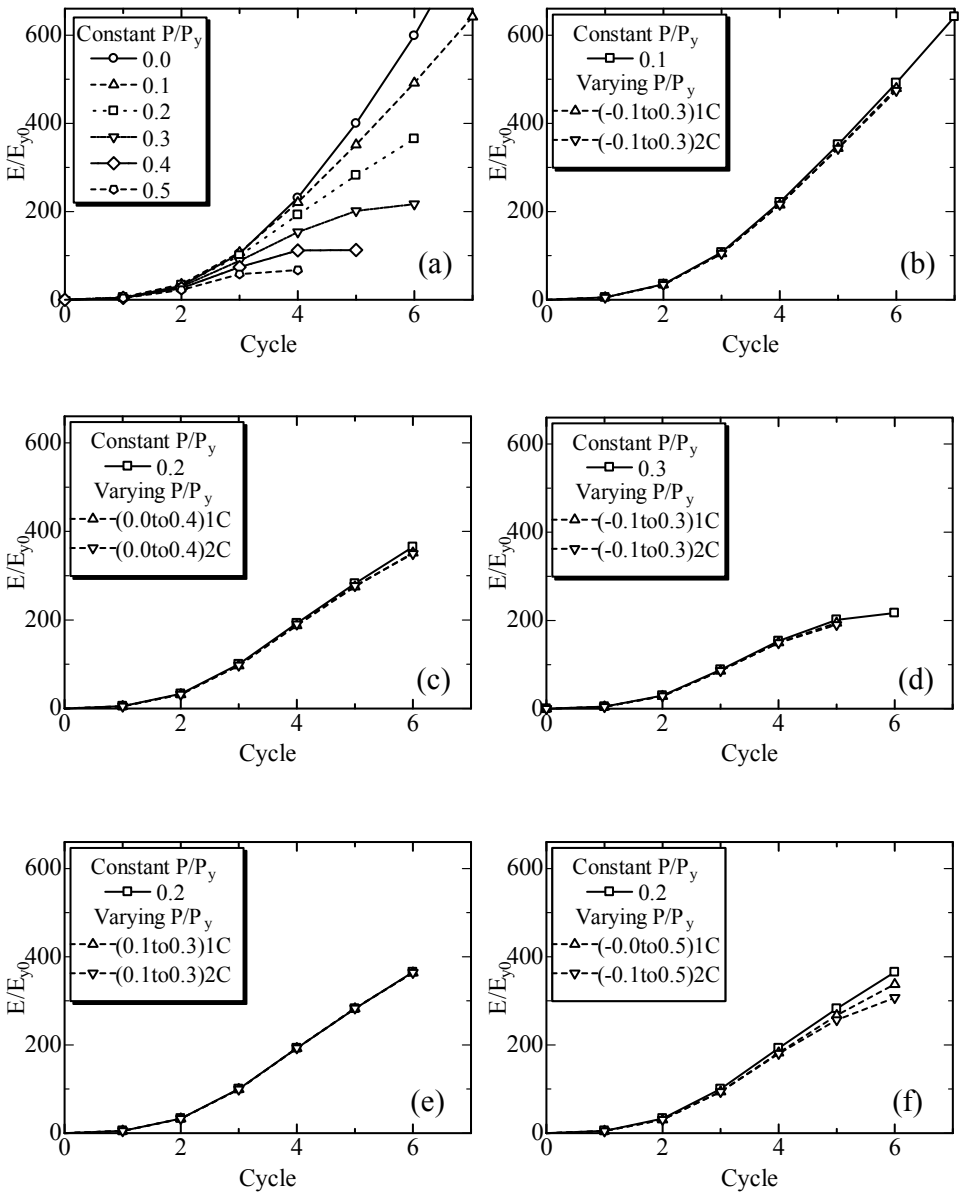

Fig. 6.4 Energy Dissipation Curves for a Pier under Various Axial Loading Cases

represent data for distorted hysteretic curves observed in varying axial force cases. The total energy dissipated during the loading period can be calculated by following **Eq. (6.1)**.

$$\frac{E}{E_{y0}} = 2\left(\int_0^{\delta x} \frac{H_X}{H_{y0}} \frac{d\delta_X}{\delta_{y0}} + \int_0^{\delta y} \frac{H_Y}{H_{y0}} \frac{d\delta_Y}{\delta_{y0}} \right) \tag{6.1}$$

Total dissipated energy curves are plotted against number of loading cycles as

shown in **Fig. 6.4**. The energy dissipation capacity is decreased as the magnitude of constant axial force is increased (see **Fig. 6.4 (a)**). **Fig. 6.4 (b-d)** are illustrated for varying axial force cases having same amplitude P/P_y = 0.2 and three cases of constant axial force equal to mean value of axial force variation. It is clearly observed that single and double cycle axial force loadings dissipate same amount of energy to that case when axial force remains constant during the loading period, which means there is no significant effect of variation in axial forces on energy dissipation capacity, but it only depends on the magnitude of mean value of axial force variation. When the influence of different amplitudes of varying axial force are considered in **Fig. 6.4 (e, c, f)**, it shows no major change except for the largest amplitude case P/P_y = 0.3 (see **Fig. 6.4 (f)**), where curves for axial force variation are slightly differed in the higher cycles of loading.

From these observations it can be concluded that both types of varying axial force cases have almost same energy dissipation capacity similar to the constant axial force which is equal to mean value of variation. Therefore, the capacity formulas defined for bi-directional loadings in Chapters 3 and 4 could be useful in seismic design process when simultaneous 3D earthquake components are used in dynamic analysis. The measured average compressive strain in the analyzed three piers is compared with strain formulation for bi-directional loading in following section 6.4.

6.3.4 Local Buckling

Local buckling near the base of the piers is observable in shell element model of pier. The local buckling images shown in **Fig. 6.5** are obtained at the end of displacement loading cycle with amplitude of U_X/δ_y = 4. **Fig. 6.5 (a-c)** are showing comparison between local buckling for constant axial force and two varying axial force cases with same amplitude of variation. It is noticeable that single cycle varying axial force cases has shown small bulge of buckling than constant and two cycle varying axial force cases. It also shows that constant and two cycle varying axial force cases have produced nearly same amount of buckling. The similar kinds of results can be seen in images of **Figs. 6.5 (d)** and **(e)** which are taken for constant axial force P/P_y = 0.2 and for two types of amplitude values 0.1 and 0.3 respectively keeping the mean value unchanged.

The effect of various axial forces on local buckling as explained above implies that local buckling due to double cycle axial force is equal to that of constant axial

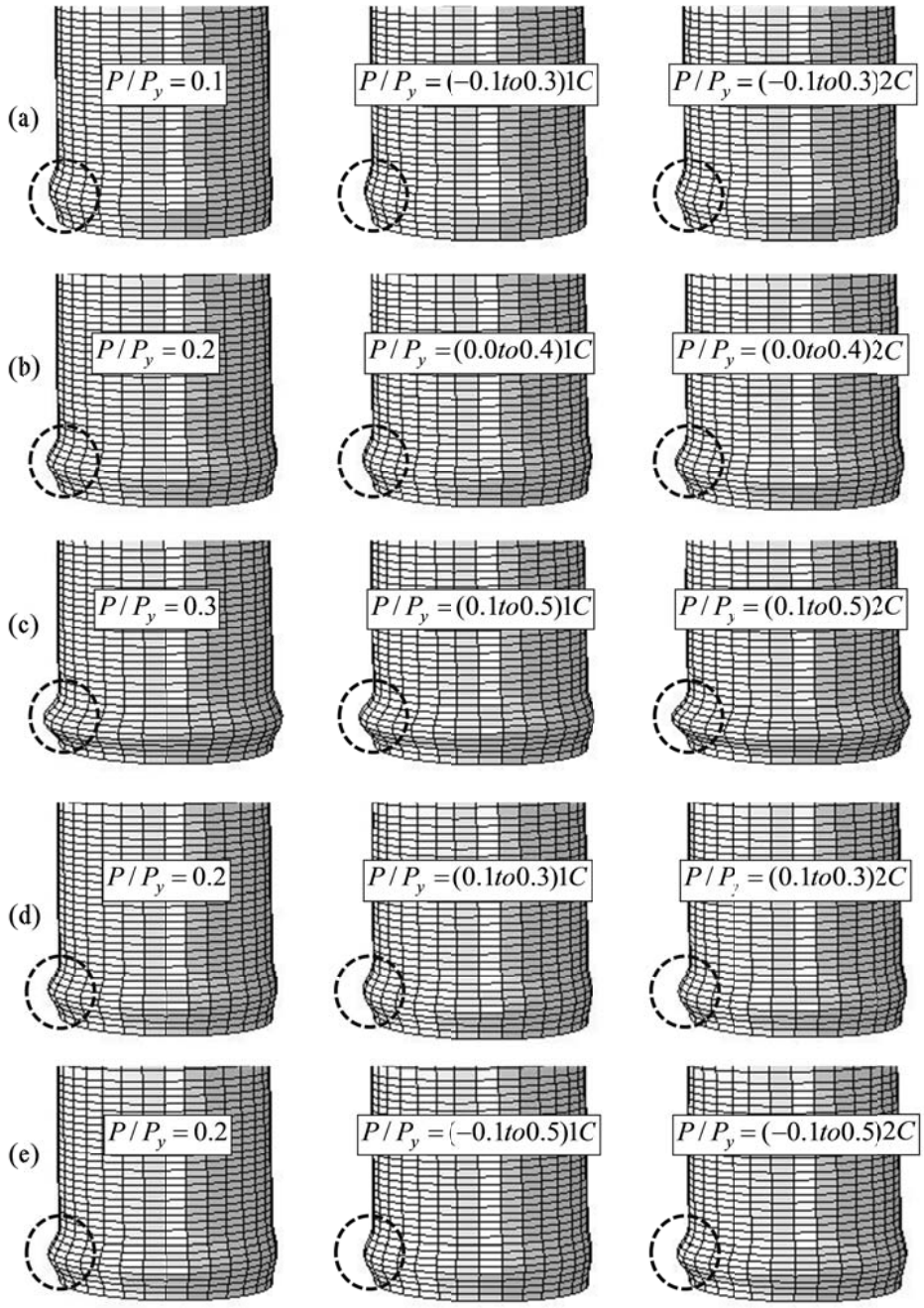

Fig. 6.5 Comparison of Local Buckling of Pier under Various Axial Loading Cases

force which has same magnitude with the mean value of respective varying axial force.

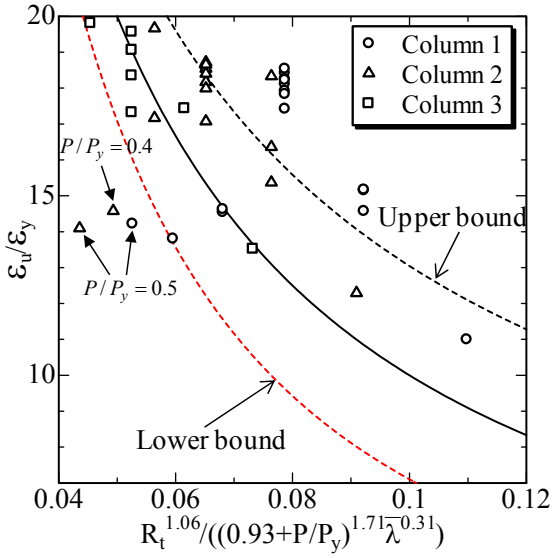

Fig. 6.6 Comparison of Ultimate Average Compressive Strains in Three Piers with the Predetermined Ultimate Strain Formulation

6.4 Comparison of Observed Strain Results with Ultimate Strain Formulation

It has been understood in Chapter 4 that strain-based seismic design method proposed for bi-directional earthquake loading is critical than that of displacement-based design method. Therefore, ultimate average compressive strain values $\bar{\varepsilon}_{mb,95}$ observed in the present work are compared with the ultimate strain formulation proposed previously (i.e. **Eq. (4.2)**). It should be noted that the techniques adopted to measure the average compressive strain are similar with that mentioned in **Appendix D**. **Fig. 6.6** indicates the function lines developed for ultimate strain of the circular steel columns under bi-directional cyclic loading with constant axial force and their equation is rewritten here as follows;

$$\frac{\varepsilon_u}{\varepsilon_y} = \frac{(0.93 + P/P_y)^{1.71}\,\bar{\lambda}^{0.31}}{R_t^{1.06}} \pm 3.04 \qquad (6.2)$$

for the range $0.05 \le R_t \le 0.09$, $0.2 \le \bar{\lambda} \le 0.6$ and $0.0 \le P/P_y \le 0.2$

The lower bound line in **Fig. 6.6** provides minimal ultimate strain value. The measured ultimate strain values for various axial force patterns with bi-directional

cyclic loadings on three different steel columns are also plotted in **Fig. 6.6**. In the case of varying axial force, the mean value of variation is selected to calculate a value on horizontal axis. It can be seen that most of the ultimate strain values are on the safer side of the minimal function line i.e. lower bound line. However, few values are on unsafe side of this minimal line, but these values are for comparatively large constant axial force (P / P_y = 0.4, 0.5) and which are out of the axial force range of proposed **Eq. (6.2)**. Hence, it can be stated that ultimate strain formula developed for seismic designing of steel bridge piers under bi-directional earthquake motions are equally applicable when vertical motion is included with two horizontal earthquake motions.

6.5 Summary

This chapter is mainly concerned with effect of different varying and constant axial force patterns along with bi-directional circular displacements on the behavior of steel circular column. The nonlinear analyses are carried out on shell element model of bridge pier. The major points observed in this comparative study are summarized as follows.

(1) It is observed that hysteretic curves of strength-displacement are found to be distorted in varying axial force cases and the comparison of envelop curves plotted for X directional strength-displacement relationship has shown that double cycle varying axial force pattern is critical than single cycle and constant axial force cases. In addition, increase in amplitude of axial force variation showed increase in difference between envelop curves whereas, increase in mean value of axial force variation indicated decrease in strength and ductility.

(2) The local buckling images are presented for each case and compared. It has observed that amount of buckling bulge is nearly similar for double cycle axial force variation and constant axial force equivalent to its mean value. Change in amplitude of axial force variation has not indicated any significant change in buckling shape. The single cycle axial force variation pattern has shown smaller local buckling than any other cases.

(3) The comparison between energy dissipation curves plotted for two types of varying axial forces and a constant axial force equivalent to their mean value are found identical. This means the use of ductility formulas derived for constant axial force are fairly acceptable to employ as allowable solutions in seismic design of steel bridge pier subjected to 3D earthquake motion.

(4) To verify above statement, the ultimate strain values measured by applying various axial force patterns on steel columns are compared with previously proposed ultimate strain formula which considers bi-directional lateral loading with the range of constant axial force. It is observed that most of the values are laid on safer side of minimal ultimate strain line and hence confirmed the proposed concept given in above point (3).

Chapter 7

SUMMARY AND CONCLUSIONS

Number of steel piers have been designed and constructed as a highway bridge supports in urban area of Japan since more than two decades. The ability of such bridge piers to survive strong earthquake ground motions without collapse depends on their ductility capacity and energy dissipation. These piers are composed of thin-walled steel plates characterized by relatively large radius-thickness ratio, which makes them susceptible for local buckling.

To study the cyclic behavior of such piers into details, precise numerical analytical methods are inevitably required which has been the subject of extensive research work in the past few decades. With the rapid development of computer techniques, the finite element method accounting for both geometric and material nonlinearities is becoming more and more popular. And its accuracy is found greatly dependant on the precision of the material model employed.

Present research was aimed at developing the multi-directional seismic design procedure for circular steel bridge piers on the bases of some ductility formulas. For this purpose, elastoplastic large displacement finite element analyses were carried out by considering material and geometric nonlinearities. A modified two-surface plasticity model developed at Nagoya University was used to model material nonlinearity and to account the local and overall buckling, shell elements were employed. Whereas, beam elements were used to neglect local buckling effects. The parametric study was performed to investigate the effects of loading patterns, radius-thickness ratio, slenderness ratio and axial force on the strength and ductility behavior of piers. As a result, ultimate strength and ductility formulas including the effect of such parameters were proposed. Further, the procedures were developed to explain implementation of proposed formulas in seismic design of steel circular piers. In addition to this, three-dimensional dynamic analyses were performed on bridge systems to understand the influence of vertical earthquake component on response of the bridge piers. In this study, the major effect was observed on axial force variation in the piers, hence it was continued to investigate the influence of varying axial force on strength and ductility behavior of the steel columns used as bridge piers.

The thesis consists of seven chapters. In which Chapters 1 and 2 are related to introduction, historical review of ductility formulations and requirement of the present study. The important concluding remarks from Chapters 3 to 6 are summarized in following paragraphs.

Chapter 3 was concerned with ductility evaluation in terms of displacement, for the steel circular bridge piers subjected to cyclic uni- and bi-directional displacement loading keeping constant vertical compressive load at the top of the pier. The ductility of steel columns under circular bi-directional loading was required to investigate because, it had been proved that, bi-directional loading pattern reduces strength and ductility capacity considerably than that of conventionally used cyclic uni-directional loading pattern and these ductility formulas were needed to used in seismic design of piers when subjected to two directional earthquake motions. The application method of ductility formulas was also developed in this chapter. Following are some important observations in this study;

(1) Local buckling contour maps had shown that circular cyclic bi-directional loading can cause larger buckling than uni-directional cyclic loading.
(2) In the parametric study it had found that ultimate strength and ductility were getting improved when R_t decreases irrespective of loading patterns. The same phenomenon was observed only in cyclic uni-directional loading with decrease in $\bar{\lambda}$, but in case of cyclic circular loading columns with $\bar{\lambda} = 0.2$ had indicated lower ultimate strength than columns with $\bar{\lambda} = 0.4$ and 0.6.
(3) Considering the effects identified in parametric study, the ultimate strength and ductility equations were developed separately for uni- and bi-directional loading and by using nonlinear regression analysis technique. Based on these equations, seismic design method was proposed for the condition when two directional earthquake motions are applied together on the bridge piers.
(4) Implementation of proposed seismic design method was explained through some dynamic analyses. Piers could not satisfy the bi-directional seismic design criteria even though they had shown safe performance when earthquake motions were applied individually.
(5) When an average compressive strain response in critical part of the piers which had shown unsafe performance in bi-directional dynamic analysis, was checked

against available ultimate strain solution, it was found that appearance of displacement and strain-based ultimate state on the response time histories were at different time instant. Therefore, it became necessary to development the ultimate strain formulas under similar loading conditions to compare these two criteria.

Chapter 4 was dealt with prediction of ultimate strain formulas and development of seismic design method when earthquake components are applied in two perpendicular directions. Under similar condition of loadings that used in Chapter 3, the parametric study was carried out on shell element as well as beam element models. Hence, two types of compressive strain quantities were observed depending on shell element and beam element model type. The ultimate strengths were defined from envelop curves of shell element models, however ultimate strain values were taken from envelop curves of beam element models. The reason to select beam element model in prediction of ultimate strains was to synchronize FE modeling method conventionally used in dynamic analysis and capacity prediction static analysis. Some of the significant remarks from this study are as follows.

(1) Ultimate strain in short columns had shown decreasing trend when displacement loading pattern changes from uni-directional to circular bi-directional, whereas in medium or long length columns ultimate strain had remained same or increased slightly than uni-directional ultimate strain values. The comparison between logarithmic shear and axial strains in shell element models at their respective ultimate states had illustrated that in short columns shear strains were predominant and axial strains were major in medium-long columns. Therefore, compressive strains had shown decreasing trend which excludes shearing effect. Taking into account these effects, ultimate strain formulas were derived separately for uni- and bi-directional loadings and based on that seismic design method was proposed.
(2) Dynamic analyses were carried out to explain the proposed strain-based design method and to compare that with former displacement-based method. The applicability of strain-based method was found to be easier and also critical than the former seismic design method proposed in Chapter 3.
(3) Comparison between strain formulas derived in this chapter and derived in past research work, had indicated that formulas from present work provide minimum

ultimate strain value in both cases when earthquake motions were applied in one direction and two directions simultaneously. Hence, the ductility formulas given in this study are useful in seismic design process of steel circular bridge piers, as these formulas are based on all important parameters which govern the design of steel circular bridge piers.

In Chapter 5, the effect due to vertical components over two horizontal components of earthquake on the steel bridge piers was carried out. Three bridge systems were designed according to Seismic Performance Level 1 and 2 requirements. Further, these systems were analyzed using five actual strong earthquake motions. Each unscaled earthquake motion was applied in two ways: first was included only two horizontal components (EW-NS) and second was by employing all three components (EW-NS-UD). In the similar way, observations were also taken when earthquake acceleration components were scaled-up or scaled-down by using multiplication factor. The results observed in these analyses are summarized as follows.

(1) When absolute maximum average compressive strains due to 2D and 3D earthquake motions were compared, it had shown negligible difference between them and their amplitudes were found to be closely related to the fundamental period.
(2) Maximum deformations of piers in both longitudinal and transverse directions had shown great similarity in 2D and 3D earthquake motions. That means there was no effect due to vertical earthquake component on the displacement response of the pier.
(3) Coupling of vertical component with two horizontal components of earthquake had shown significant amplification in axial force response.
(4) The scale-up and scale-down of earthquake acceleration components had clearly shown that maximum strain and deformations in the bridge pier were altered due to scaling in horizontal components, whereas, the axial force response was found to be altered when scaling factor was applied on vertical component of earthquake. This implied to investigate the influence of varying axial force on the capacity of circular steel columns and which was continued in Chapter 6.

Chapter 6 was concerned with the static analysis of shell element models subjected to different varying and constant axial force patterns. The objective of this study was to compare the effect of variation in axial force on strength, ductility and buckling of the pier with that when axial force remains constant. In varying axial force cases two proportional types of patterns were adopted: (1) single cycle of axial force and (2) double cycles of axial force with respect to single displacement cycle. Because for steel columns, non-proportional axial force variation had found less severe than proportional cases. The important findings from this study are summarized as below.

(1) The hysteretic curves in X and Y directions had shown distorted shape for varying axial force cases. Comparing the envelop curves plotted for X directional strength-displacement have indicated that double cycle axial force pattern was severe than single cycle and constant axial force equivalent to its mean value cases. Increase in amplitude of axial force variation had shown increase in difference between envelop curves and increase in mean value of varying axial force pattern had shown decrease in strength and ductility.

(2) Amount of buckling was found nearly similar for double cycle axial force variation and constant axial force equivalent to its mean value. Change in amplitude of axial force variation had not indicated any significant change in buckling shape. The single cycle axial force variation pattern has shown smaller outward deformation than any other cases.

(3) The comparison of energy dissipation curves plotted for two types of varying axial forces and a constant axial force equivalent to their mean value were found to be identical. This further implied that applicability of ductility formulas derived for constant axial force is feasible to employ as allowable solutions in seismic design of steel bridge pier subjected to 3D earthquake motion.

(4) For confirmation, the ultimate strain values measured by applying various axial force patterns on steel columns were compared with previously proposed ultimate strain formula which considers bi-directional lateral loading with constant axial force. It was observed that most of the values were laid on safer side of critical ultimate strain line and hence it was verified that strain-based ductility formulas can be used when multi-directional earthquake motions are applied on circular steel bridge piers.

Although, the present work was extensively related to numerically evaluated ductility formulas and their implementation in the multi-directional seismic design method, future study in this subject is important to focus. Some recommendations are listed below.

(1) These analytical study results must be confirmed by performing some experiments on steel circular piers. However, it needs special experiment set-up which can apply loadings on the steel columns and take measurements appropriately.
(2) The material nonlinearity considered in the present work was modeled by specially developed modified two-surface material constitutive law. It is very essential to confirm its applicability in multi-directional cyclic loading.
(3) In this current work, only unstiffened hollow circular steel columns were considered for evaluation of ductility formulas; but different types of steel columns (for example; stiffened box, L-shaped circular or box, frame type) are also widely used as bridge piers. Therefore, a similar analytical study for these columns is needed to be carried out.
(4) In filled concrete columns are very popular in recent construction practice, hence it also adds another aspect in future work of the present study.
(5) The bridge systems designed in Chapter 5 are very simplified; therefore it requires focusing on more accurate modeling of bridge system to understand multi-directional earthquake effects.

REFERENCES

[1] Anderson E. L. and Mahin S. A., (2004). “An evaluation of bi-directional earthquake shaking on the provisions of the AASHTO guide specifications for seismic isolation design.” *Proc. 13th World Conf. on Eq. Eng.*, Vancouver, B.C., Canada, Paper No. 763.

[2] Asad E. and Yan X., (2004). “Behavior of reinforced concrete columns under variable axial loads.” *ACI Struct. J.*, 101(1), 124-132.

[3] Alaghebandian R., Otani S. and Shiohara H., (2002) “Effect of distributed mass on earthquake response of reinforced concrete frames.” *Proc. 12th World Conf Earthquake Eng, Auckland, New Zealand*., Paper No: 2230.

[4] Broderick B. M. and Elnashai A. S., (1995). “Analysis of the failure of interstate 10 freeway ramp during the Northridge earthquake of 17 January 1994.” *Eq. Eng. Struct. Dyn.*, 24, 189-208.

[5] Bousias S. N., Verzeletti G., Fardis N., et al. (1995). “Load-path effects in column biaxial bending with axial force.” *J. Eng. Mech. ASCE.*, 121(5), 596-605.

[6] Bruneau M., (1998). “Performance of steel bridges during the 1995 Hyogoken-Nanbu (Kobe, Japan) earthquake - North American perspective.” *Eng. Strust.*, 20(12), 1063-1078.

[7] Cetinkaya O. T., Nakamura S. and Takahashi K., (2008). “Bending behavior of short cylinders under axial force fluctuations.” *Eng. Struct.*, 30, 595-604.

[8] Como M., Stefano M. and Ramasco R., (2003). “Effect of column axial force-bending moment interaction on inelastic seismic response of steel frames.” *Eq. Eng. Struct. Dyn.*, 32, 1833-1852.

[9] Chung K., Kobayashi K., Kishiki S. and Yamada S., (2007). “Damage evaluation

on steel columns under combined variable axial force and cyclic moment." *J. Struct. Constr. Eng. AIJ.*, 612, 179-186 (in Japanese).

[10] Chopra A. K., (1966). "The importance of the verticalcomponent of earthquake motions." *Bulletin of the Seismological Soc of America,* 56(5),1163-75.

[11] Dussault Systems Simulia Corp., (2007). "Abaqus/Standard user's manual 6.7-5." Providence, RI, USA.

[12] Dussault Systems Simulia Corp., (2007). "Abaqus/ CAE 6.7-5." Providence, RI, USA.

[13] Dussault Systems Simulia Corp., (2007). "Abaqus/ Theory Mannual 6.7-5." Providence, RI, USA.

[14] Dafalias Y. F. and Popov E. P., (1975). "A model of nonlinear hardening materials for complex loading." *Acta Mech*., 21, 173-192.

[15] Elnashai A. S., Bommer J. J., Baron C. I., Lee D. H. and Salama A. L., (1995). "Selected engineering seismology ad structural engineering studies of Hyogo-ken Nanbu (Great Hanshin) earthquake of 17 January 1995." *ESEE research report,* 95-2; London: Imperial College.

[16] Fujimoto T., Mukai A., Nishiyama K., Nozaki K. and Morino S., (2000). "Biaxial bending behavior of concrete filled square steel tubular stub columns using high strength materials." *J. Struct. Constr. Eng.*, 527, 178-180 (in Japanese).

[17] Gao S. B., Usami T., and Ge H. B., (1998a). "Ductility of steel short cylinders in compression and bending. " *J. Eng. Mech., ASCE*, 124(2), 176-183.

[18] Gao S. B., Usami T. and Ge H. B., (1998b). "Ductility evaluation of steel bridge piers with pipe-sections." *J. Eng. Mech., ASCE*, 124(3), 260-267.

[19] Goto Y., Wang Q., Obata M. and Takahashi N., (1997). "On FEM analysis of

steel bridge piers under cyclic loading based on three-surface constitutive model." *Proc. of Nonlinear Numerical Analysis and Seismic Design of Steel Bridge Piers, JSCE*, 209-216.

[20] Goto Y., Jiang K. and Obata M., (2006). "Stability and ductility of thin-walled circular steel columns under cyclic bidirectional loading." *J. Struct. Eng., ASCE*, 132(10), 1621-1631.

[21] Goto Y., Muraki M. and Obata M., (2009). "Ultimate state of thin-walled circular steel columns under bidirectional seismic acceleration." *J. Struct. Eng., ASCE*, 135(12), 1481-1490.

[22] Ge H. B., Kono T. and Usami T., (2004). "Failure strain of steel segments subjected to combined compression and bending and application to dynamic verification of steel arch bridges." *J. Strct. Eng., JSCE*, 50A, 1479-1488 (in Japanese).

[23] Galal K. E. and Ghobarah A., (2003). "Flexural and shear hysteretic behavior of reinforced concrete columns with variable axial load." *Eng. Stuct*., 25, 1353-1367.

[24] Japan Road Association, (1996). "Specifications for highway bridges, part V, Seismic design." Tokyo, Japan (in Japanese).

[25] Japan Road Association, (2002). "Specifications for highway bridges, part V, Seismic design." Tokyo, Japan.

[26] Japan Meteorological Agency. http://www.seisvol.kishou.go.jp/eq/kyoshin/jishin/index.html, last visited on: 25th July 2010.

[27] Kawashima K. and Unjoh S., (2004). "Seismic design of highway bridges." *J. Japan Assoc. for Eq. Eng.,* 43, 174-183.

[28] Kawashima, K. and Unjoh S., (1997). “The 1996 seismic design specifications of highway bridges.” *Proc. 1st U.S.-Japan Workshop on Eq. Eng. Frontiers in Transportation Facilities, National Center for Eq. Eng. Research*, University of New York, Buffalo, USA.

[29] Kulkarni N. G., Kasai A. and Tsuboi H., (2009). “Displacement based seismic verification method for thin-walled circular steel columns subjected to bi-directional cyclic loading.” *Eng. Struct.*, 31(11), 2779-2786.

[30] Kim T. H., Kim Y. J. and Shin H. M., (2006). “Seismic performance assessment of reinforced concrete bridge columns under variable axial load.” *Magz. of Conc. Research*, 58(00), 1-10.

[31] Kawashima K., Oshima K., Hasegawa K., Unjoh S., Okeda K., and Maehara Y., (1992). “Seismic design examples for road bridges.” Sankaitou (in Japanese).

[32] Kulkarni N. G. and Kasai A., (2009). “Effect of varying axial load on cyclic behavior of circular steel bridge piers.” *Proc. 11th International Summer Symposium, JSCE,* Tokyo.

[33] Kawashima K., Sasaki T. and Kajiwara K., (last visited on: 9th Aug. 2010). “Experimental study on the seismic response of bridge columns using E-defense.” *Public Works Research Institute*., http://www.pwri.go.jp/eng/ujnr/tc/g/pdf/25/1-4.pdf.

[34] Lee D. H., Choi E. and Zi G., (2005). “Evaluation of earthquake deformation and performance for RC bridge piers.” *Eng. Struct.*, 27, 1451-1464.

[35] Mamaghani I. H. P., Shen C., Mizuno E. and Usami T., (1995). “Cyclic behavior of structural steels. I: experiments.” *J. Eng. Mech., ASCE*, 121(11), 1158-1164.

[36] Miki C. and Sasaki E., (2005). “Fracture in steel bridge piers due to earthquakes.” *Steel Struct.*, 5, 133-140.

[37] Nakagawa T., Yasunami H., Kobayashi Y., et al., (1996). “Evaluation of strength

and ductility for box section piers by finite element analysis." *Proc. of Symposium on Hanshin and Awaji Great Earthquake*, 599-604 (in Japanese).

[38] Nakashima M. and Wakabayshi M., (1992). "Analysis and design of steel braces and braced frames in building structures." *Stability and ductility of steel structures under cyclic loading*, Edited by Fukumoto Y., and Lee G. C., CRC Press, Boca Raton, FI, 309-321.

[39] National Research Institute for Earth Science and Disaster Prevention. http://www.k-net.bosai.go.jp/, last visited on: 25th July 2010.

[40] Okazaki S., Usami T. and Kasai A., (2003). "Elasto-plastic dynamic analysis of steel bridge piers subjected to bi-directional earthquakes." *J. Struct. and Eq. Eng., JSCE*, 27, 1-8 (in Japanese).

[41] Oyawa W., Watanabe E. and Sugiura K., (2004). "Finite element studies on hollow columns under multi-directional cyclic loads." *J. Civil Eng. Research and Practice*, 1(1), 33-49.

[42] Onishi A., Aoki T. and Suzuki M., (2005). "Experimental study on the seismic resistance performance of steel bridge subjected to bi-directional horizontal loads." Bulletin of Aichi Institute of Tech., Part B, 40, 121-129 (in Japanese).

[43] Papazoglou A. J. and Elnashai S. A., (1996). "Analytical and field evedance of the damaging effect of vertical earthquake ground motion." *Eq. Eng. and Struct. Dyn.*, 25, 1109-37.

[44] Qiu F., Li W., Pan P., and Qian J., (2002). "Experimental tests on reinforced concrete columns under biaxial quasi-static loading." *Eng. Struct.*, 24, 419-428.

[45] Shen C., Tanaka Y., Mizuno E. and Usami T., (1992). "A two-surface model for steels with yield-plateau." *J. Struct Eng./Eq. Eng., JSCE*, 8(4), 179-188.

[46] Shen C., Mamaghani I. H. P., Mizuno E. and Usami T., (1995). "Cyclic

behaviour of structural steels. I: experiments." *J. Eng. Mech., ASCE*, 121(11), 1165-1172.

[47] Saatcioglu M. and Ozcebe G., (1989). "Response of reinforced concrete columns to simulate seismic loading." *ACI Struct. J*. 86(1), 3-12.

[48] Shen, C. (1993). "Development of a cyclic two-surface model for structural steels with yield plateau," *Doctoral thesis, Civil Engineering Dept*., Nagoya University, Nagoya, Japan.

[49] Saadeghvaziri M. A. and Foutch D. A., (1990). "Behavior of RC columns under nonproportionally varying axial load." *J. Struct, Eng.*, 116(7), 1835-1856.

[50] Sakai J. and Kawashima K., (2002). "Effect of varying axial loads including a constant tension on seismic performance of reinforced concrete bridge piers." *J. Struct. Eng., JSCE*, 48A, 735-746 (in Japanese).

[51] Saadeghvaziri M. A. and Foutch D. A., (2006). "Dynamic behaviour of R/C highway bridges under the combined effect of vertical and horizontal earthquake motions." *Eq. Eng. Struct. Dyn*., 20(6), 535-549.

[52] Sakai J. and Unjoh S., (2007). "Earthquake simulation test of circular reinforced concrete bridge column under multidirectional seismic excitation." *Eq. Eng. Eng. Vibration*, 5(1), 103-110.

[53] Takizawa H. and Aoyama H., (1976). "Biaxial effect in modeling response of R/C structures." *Eq. Eng. Strct. Dyn.*, 4, 523-552.

[54] Timoshenko, S. P., and Gere, J. M., (1961). "Theory of elastic stability." McGraw-Hill Book Co., Inc., New York, N.Y

[55] Usami T., Mizutani S., Aoki T. and Itoh Y., (1992). "Steel and concrete-filled steel compression members under cyclic loading." *Stability and ductility of steel structures under cyclic loading*, Edited by Fukumoto Y., and Lee G. C., CRC

Press, Boca Raton, FI, 123-138.

[56] Usami T. and Ge H. B., (1998). “Cyclic behavior of thin-walled steel structures-numerical analysis.” *Thin-walled Struct.*, 32, 41-80.

[57] Watanabe E., Sugiura K. and Oyawa W., (2000). “Effect of multi-directional displacemnet paths on the cyclic behavior of rectangular hollow steel columns.” *J. Struct. and Eq. Eng., JSCE*, 17(1), 69s-85s.

[58] Wong Y. L., Paulay T. and Priestley M. J. N., (1993). “Response of circular reinforced concrete columns to multi-directional seismic attack.” *ACI Struct. J.*, 90(2), 190-191.

[59] Yamazaki S. and Minami S., (1999). “Experimental study on inelastic behaviour of steel beam-columns subjected to varying axial force and cyclic lateral load.” *J. Struct. Constr. Eng. AIJ.*, 519, 95-102 (in Japanese).

[60] Zheng Y., Usami T. and Ge H. B., (2000). “Ductility of thin-walled steel box stub-columns.” *J. Struct. Eng. ASCE*, 126(11), 1304-1311.

[61] Zahn F. A., Park R. and Priestley M. J. N., (1989). “Strength and ductility of square reinforced concrete column subjected to biaxial bending.” *ACI Strct. J.*, 56(2), 123-131.

APPENDIX A

Review of Modified Two-Surface Model

A.1 Brief Review of Plasticity Models

The concept of yield surface was first introduced by researchers such as von Mises and Tresca. This yield surfaces identify the elastic deformation. The plastic deformation would be induced when the material is loaded beyond this surface.

The isotropic hardening rule proposed by Hill (1950) assumes that the subsequent yield surface is formed by a uniform expansion of the initial yield surface. This model fails to account for the Bauschinger effect, i.e. increase in the yield limit of material in one loading direction due to plastic deformation causes reduction in the yield limit in the opposite loading direction under cyclic loading. To overcome this defect, Prager (1956) and Ziegler (1959) proposed the Kinematic hardening rules which stipulates that the yield surface would translate without any change of the size. However, this model can not accurately account the effect of strain hardening. Mróz (1967) and Iwan (1967) independently proposed multisurface models including few intermediate surfaces with different plastic hardening moduli. These models can represent many cyclic characteristic of the structural steel such as Bauschinger effect. Mróz's multisurface model was modified by Petersson and Popov (1977) by introducing an effective plastic strain concept and a different hardening rule. After that, Minagawa (1987, 1989) developed the Petersson and Popov model by employing the effective plastic strain range concept and the effective plastic strain increment as the state variables to consider the influence of loading history. Above mentioned multisurface models were found to be too cumbersome due to the requirement of excessive amount of storage in keeping track of a large number of yield surfaces at all time in the computer (Hunsaker, et al. 1976).

A two-surface model was first proposed by Dafalias and Popov (1975, 1976). This model had two surfaces, one was yield surface as the inner surface and another was the bounding surface as the outer surface. It was assumed that the yield surface always remain enclosed by the bounding surfaces and the plastic modulus can be obtained by the proximity of the two surfaces in the course of their coupled translation and change in the size during plastic deformation.

In the uniaxial stress case, Dafalias and Popov two-surface model (1975) stipulates that the bounding lines with slope E_0^P exist in both tension and compression sides, and the distance between these lines does not change for any loading path. The plastic modulus E^P in the nonlinear hardening region is defined as follows,

$$E^P = \frac{d\sigma}{d\varepsilon^P} = E_0^P + h\frac{\delta}{\delta_{in} - \delta} \tag{A.1}$$

where, E_0^P =slope of the bounding line = constant; δ=distance between the loading point and the bounding line (say, point Q_2 in **Fig. A.1**); δ_{in}= value of δ at the initial yield state in the current loading path (say, point Q_1 in **Fig. A.1**); and h= shape parameter.

In the multiaxial stress state, the bounding lines in this model are expanded to a bounding surface. The value of δ used in **Eq. (A.1)** is assumed as the distance between the current loading point on the yield surface and the conjugate point on the bounding surface, where the normal of the conjugate point on the bounding surface is the same as that of the loading point on the yield surface.

Besides this two-surface model, many other versions of the two-surface models have been developed by researchers (Ohno 1982; Tseng and Lee 1983; McDowell 1985; Chang and Lee 1986; Shen, et al. 1995).

A.2 Review of Modified Uniaxial Two-Surface Model

The uniaxial stress σ versus plastic strain ε^P curve of the M2SM is shown in **Fig. A.1**. The key definitions and assumptions of this model (Shen, et al. 1992), are briefly reviewed as follows (see **Fig. A.1**):

Calculation of Plastic Modulus

The plastic modulus E^P is calculated by using the same expression as that in the Dafalias and Popov model (1975), as given in **Eq. (A.1)**. It should be noted that E_0^P will no longer be kept constant and is assumed to decrease with plastic work. Moreover, the shape parameter h is assumed to be a linear function of δ as follows,

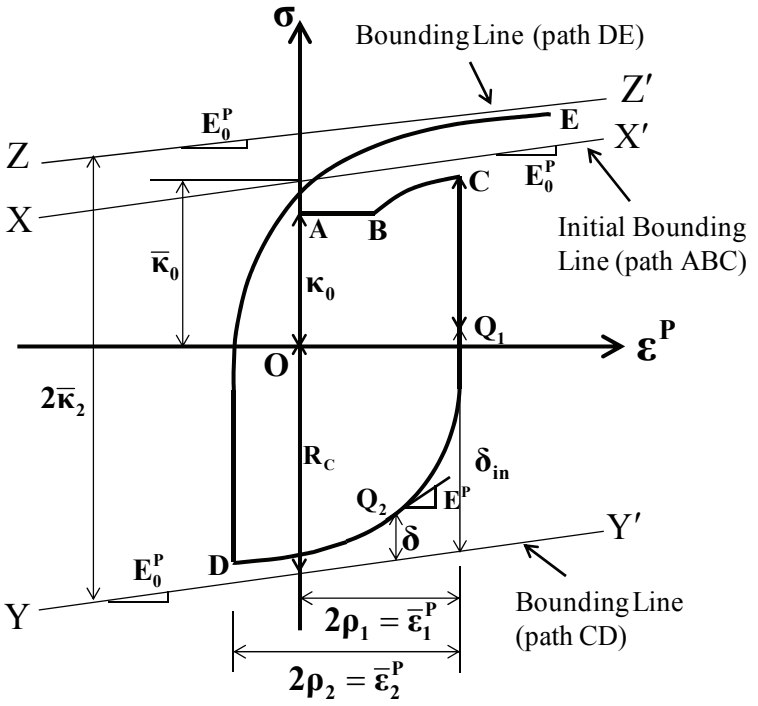

Fig. A.1 Uniaxial Stress σ Versus Plastic Strain ε^P Curve

$$h = e \cdot \delta + f \tag{A.2}$$

where, e and f =material constants.

Reduction of Elastic Range

The reduction of the elastic range is expressed as follows,

$$\frac{\kappa}{\kappa_0} = \alpha - a_1 \cdot \exp(-a_2 \bar{\varepsilon}^P \times 100) - (\alpha - a_1 - 1)\exp(-a_3 \bar{\varepsilon}^P \times 100) \tag{A.3}$$

where κ and κ_0 = half of the current and initial size of the elastic range, respectively ($\kappa_0 = \sigma_y$); σ_y = yield stress; a_1, a_2, a_3, and α =constants; $\bar{\varepsilon}^P$ = effective plastic strain (EPS) range, which is defined as the maximum amplitude of the effective plastic strain that the material has ever experienced before. It is noted that the value of κ is equal to σ_y when $\bar{\varepsilon}^P$ becomes zero and it decreases as the increase in $\bar{\varepsilon}^P$.

Treatment of Yield Plateau

The judgment of the end of yield plateau is an important point in evaluation of

cyclic behavior. The monotonic and cyclic experimental results indicate that the disappearance of the yield plateau depends on EPS range and plastic work. Therefore, termination of the yield plateau can be judged as follows,

$$\left(\frac{\bar{\varepsilon}^P}{\varepsilon_{st}^P}-1\right)-M\cdot\left(\frac{W^P}{W_{st}^P}-1\right) \quad \begin{cases} < 0 & \text{yield plateau still continues} \\ \geq 0 & \text{yield plateau disappears} \end{cases} \tag{A.4}$$

where ε_{st}^P and W_{st}^P = plastic strain and plastic work at the end of yield plateau under monotonic loading, respectively; W^P = plastic work given by $\int \sigma d\varepsilon^p$; and M = material parameter.

Movement of Boundary Line

The size of the bounding lines in the uniaxial case $\bar{\kappa}$, is defined as a function of the EPS range, $\bar{\varepsilon}^P$:

$$\bar{\kappa}=\bar{\kappa}_\infty+(\bar{\kappa}_0-\bar{\kappa}_\infty)\exp(-\xi\rho^2) \tag{A.5}$$

where $\bar{\kappa}_0$ = size of the initial bounding lines; $\bar{\kappa}_\infty$ = limiting value of the bounding line, and is assumed to be equal to the ultimate tensile stress σ_u; ρ = one half of the EPS range = $(1/2)\,\bar{\varepsilon}^P$; and ξ = material constant. From **Eq. (A.5)**, it is observed that for a large plastic deformation, the size of the bounding lines approachs to σ_u. Therefore, σ_u plays an important role in the proposed M2SM.

Virtual Bounding Line and Memory Lines

The virtual bounding line and memory line concepts are proposed to improve the accuracy of the model when cyclic loading is random and the reversed loading point does not reach the memory line, as shown in **Fig. A.2**. It is assumed that the virtual bounding line and memory line for the current loading path (i.e. path *BC*) are parallel to the real bounding line *XX*′. The initial memory line is assumed to pass the initial yield stress σ_y and moves together with the loading point *A*. Therefore, the loading point *A* on the memory line $X_mX'_m$ denotes the point of maximum stress that material ever experienced. Supposing that line $O_XO'_X$ is the center line of the bounding line *XX*′ and *YY*′, the memory line $X_mX'_m$ and $Y_mY'_m$ in tension and compression sides are assumed to be symmetrical with respect to the center line $O_XO'_X$ (Shen, et al. 1992). If the reversal loading point such as point *B* in **Fig. A.1.2**, does not reach the memory

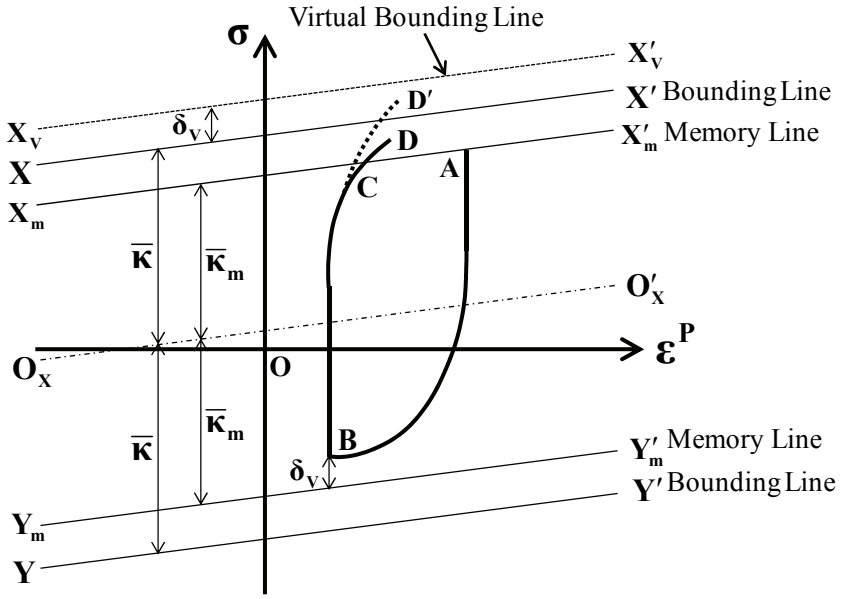

Fig. A.2 Definition of Virtual Bounding Line and Memory Line

line, the virtual line $X_vX'_v$ will be used in the prediction of path BC. The virtual bounding line $X_vX'_v$ is assumed to shift up by a distance δ_y, which is measured from the reversed loading point *B* to the memory line $Y_mY'_m$. In the prediction of path *BC*, the plastic modulus E^P is calculated as follows:

$$E^P = E_0^P + h\frac{\delta + \delta_v}{\delta_{in} - \delta} \tag{A.6}$$

which is obtained by substituting $(\delta + \delta_y)$ and $(\delta_{in} + \delta_y)$ for δ and δ_{in} in **Eq. (A.1)** respectively. It is worth noting that, once the loading point reaches the memory line, the plastic modulus in continuous path *CD* is calculated by **Eq. (A.1)**.

Slope of Bounding Line

The slope of the current bounding line, E_0^P, is assumed to decrease with the plastic work and is expressed as follows:

$$E_0^P = \frac{E_{0i}^P}{1 + \omega W^P} \tag{A.7}$$

where, E_{0i}^P = slope of the initial bounding line determined from the monotonic loading experiment; ω = constant; and W^P = plastic work accumulated from origin O

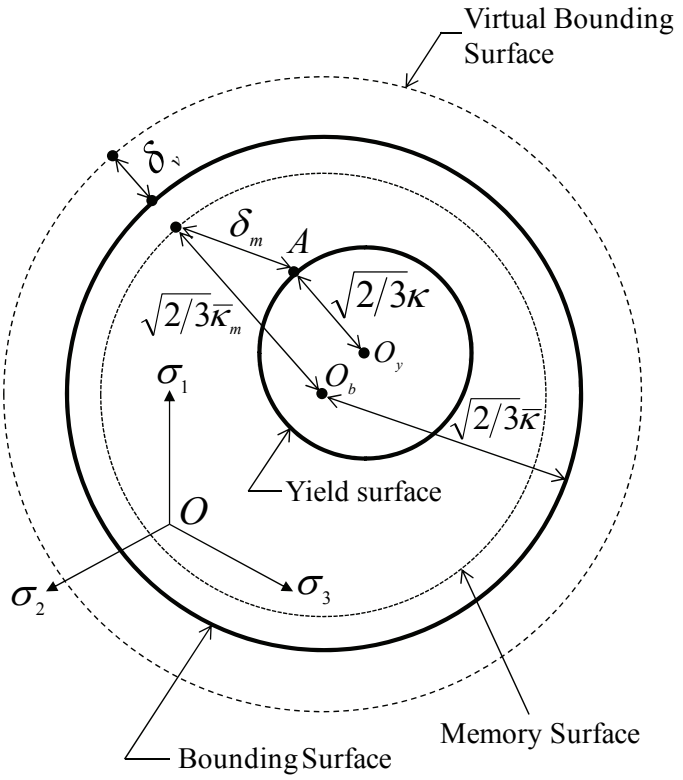

Fig. A.3 Virtual Bounding and Memory Surfaces in M2SM for Multiaxial Stress

to the current loading point. When the material experiences large plastic deformation, the slope of the bounding line E_0^P will become very small.

In the proposed M2SM, there are five material constants ($\sigma_y, E, \nu, \varepsilon_{st}^P, E_{st}$) and twelve model parameters. Here E and ν respectively represent Young's modulus and Poisson's ratio of the material, and E_{st} refers to the initial hardening modulus at the end of yield plateau. All the parameters are obtained from experimental data under relatively simple loading history (Shen, et al. 1992). The obtained values of the model parameters for SM490 grade steel (equivalent to ASTM A242 type steel) are given in **Table A.1**.

By extending the above definitions based on the concept of effective plastic strain range into the multiaxial stress state, a multiaxial M2SM has been developed by Shen et al., (1995) using the similar equations as given in the uniaxial M2SM. The main characteristics of the multiaxial stress state; (1) Definition of EPS surface concept in multiaxial stress state; (2) Definition of yield and bounding surfaces using the Von Mises yield function; (3) Determination of the translation of yield surface; (4) Definition of the motion of bounding surface; and (5) Introduction of the virtual

bounding surface and memory surface. The concept of multiaxial M2SM is explained schematically in **Fig. A.3**.

Table A.1 Two-Surface Model Parameters for Steel Grade SM490

Parameter name (1)	Value (2)	Parameter name (3)	Value (4)
E (GPa)	2.00×10^{6}	e	316
σ_y (MPa)	3.15×10^{3}	f/E	0.484
ν	0.3	M	-0.522
E_{st}^{P}/E	3.335×10^{-2}	E_{0i}^{P}/E	1.01×10^{-2}
ε_{st}^{P}	1.1×10^{-2}	$\omega.\sigma_y$	4.0
a_1	-0.528	$\bar{\kappa}_0/\sigma_y$	1.13
a_2	1.88	σ_u/σ_y	1.61
a_3	18.7	$\zeta\cdot\varepsilon_y^2$	1.52×10^{-3}
α	0.217	-	-

Table A.2 Geometrical and Material Properties of Specimen Steel Column

Geometrical Properties					
h(mm) (1)	D(mm) (2)	t(mm) (3)	R_t (4)	$\bar{\lambda}$ (5)	P/P_y (6)
3403	900	16.1	0.076	0.281	0.138

Material Properties						
σ_y (MPa) (1)	σ_u (MPa) (2)	E (MPa) (3)	E/E_{st} (4)	$\varepsilon_{st}/\varepsilon_y$ (5)	ν (6)	Grade (7)
339.21	537.40	2.03E+5	30	9	0.3	SM490

A.3 Accuracy Check of Modified Two-Surface Constitutive Law for Material

To check the accuracy of proposed two-surface model of material constitutive law, the analytical results of steel column subjected to uni-directional cyclic loading with

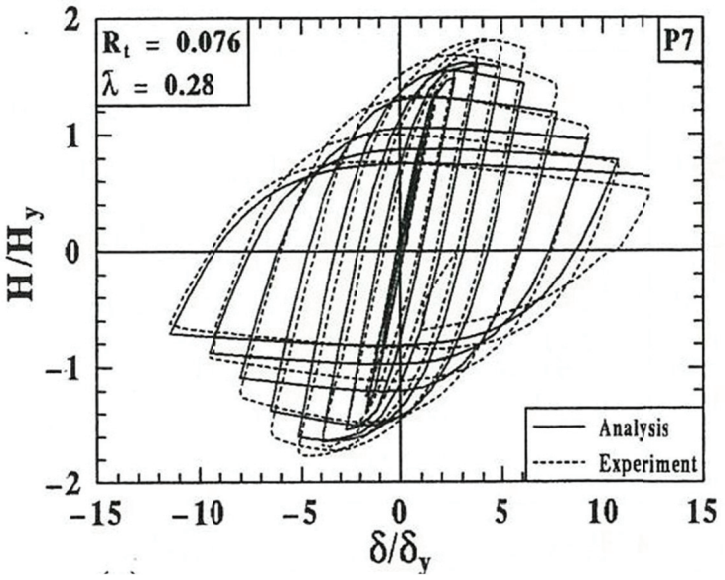

Fig. A.4 Comparison of Hysteretic Curves from Analytical and Experimental Study

constant axial load (Gao, 1998) are compared with experimental results (Nishikawa et al., 1996). The geometrical and material properties of the studied specimen column are shown in **Table A.2**.

Fig. A.4 illustrates the comparison between hysteretic curves of tested specimen P6 and analyzed column using M2SM. It is found that the hysteretic loops of M2SM analysis are little smaller than those of the tests. The possible reasons lie in that: (1) material parameters used in the M2SM analysis are taken from the tension test result. Some errors in uniaxial tension test may result in large discrepancy in structural level; (2) the friction of the test setup may result in higher strength. However, generally speaking, the analytical results coincide well with the experimental results.

References

[1] Chang K. C. and Lee G. C., (1986). "Biaxial properties of structural steel under nonproportional loading." *J. Eng. Mech. ASCE*, 112(8),792-805.

[2] Dafalias Y. F. and Popov E. P., (1975). "A model of nonlinear hardening materials for complex loading." *Acta. Mech.*, 21, 173-192.

[3] Dafalias Y. F. and Popov E. P., (1976). "Plastic interval variables formalism of

cyclic plasticity." *J. Appl. Mech., Trans. ASME*, 43, 645-651.

[4] Gao S. H., (1998). "Numerical study on seismic performance evaluation of steel structures." *Doctoral thesis, Civil Engineering Dept*., Nagoya University, Nagoya, Japan.

[5] Hill R., (1950). "The mathematical theory of plasticity." Oxford University Press.

[6] Hunsaker B., Vaughan D. K. and Stricklin J. A., (1976). "A comparison of the capacity of four hardening rules to predict a material plastic behavior." *J. Pressure Vessel Tech., ASME*, 66-74.

[7] Iwan W. D., (1967). "On a class of model for the yielding behavior of continuous and composite system." *J. Appl. Mech., Trans. ASME*, Sept., 612-617.

[8] Mcdowell D. L., (1985). "A two-surface model for transient nonproportional cyclic plasticity." *J. Appl. Mech., Trans. ASME*, 52, 298-308.

[9] Minagawa M., Nishiwaki T. and Masuda N., (1987). "Modeling cyclic plasticity of structural steels." *J. Struct. Eng./Eq. Eng., JSCE*, 4(2), 361-370.

[10] Minagawa M., Nishiwaki T. and Masuda N., (1989). "Prediction of uniaxial cyclic plasticity behavior of structural steel in plastic flow region." *J. Struct. Eng., JSCE*, 35A, 53-65 (in Japanese).

[11] Mróz Z., (1967). "On the description of anisotropic work hardening." *J. Mech. Phys. Solids*, 15, 163-175.

[12] Nishikawa. K., Yamamoto S., Natori T., Terao K., Yasunami H. and Terada M., (1996). "An experimental study on improvement of seismic performance of existing steel bridge piers." *J. Struct. Eng., JSCE,* 42A, 975-986 (in Japanese).

[13] Ohno N., (1982). "A constitutive model of cyclic plasticity with a nonhardening strain region." *J. Appl. Mech., Trans. ASME*, 49, 721-727.

[14] Petersson H. and Popov E. P., (1977). “Constitutive relation for generalized loading.” *J. Eng. Mech., ASCE*, 104(4), 611-627.

[15] Prager W., (1965). “A new method of analyzing stress and strain in work-hardening plastic solid.” *J. Appl. Mech., Trans. ASME*, 78, Series E, 493-496.

[16] Shen C., Tanaka Y., Mizuno E. and Usami T., (1992). “A two-surface model for steels with yield plateau.” *J. Struct. Eng./ Eq. Eng., JSCE*, 8(4), 179-188.

[17] Shem C., Mamaghani I. H. P., Mizuno E. and Usami T., (1995). “Cyclic behavior of structural steels. II: Theory.” *J. Eng. Mech., ASCE*, 121(11), 1165-1172.

[18] Tseng N. T. and Lee G. C., (1983). “Simple plasticity model of two-surface type.” *J. Eng. Mech., ASCE*, 109(3), 795-810.

[19] Ziegler H., (1959). “The finite element method.” 3rd Ed., McGraw-Hill, New York.

APPENDIX B

Comparison of Strength and Ductility Formulas

B.1 Ultimate Formulas for Uni and Bi-directional Cyclic Loading

As mentioned in Chapter 2, the ultimate strength and ductility formulas derived for a single value of axial force $P/P_y = 0.15$ are compared with past study by Goto el. al., (2006). The fitted curves for maximum strength factor $H_{\max}/H_y$, maximum ductility factor $\delta_{\max}/\delta_y$ and ultimate ductility factor δ_{95}/δ_y are plotted collectively for UNI and CIR loading cases as shown in **Fig. B.1**.

The ultimate formulas developed here and past study can be written in the same common format as follows.

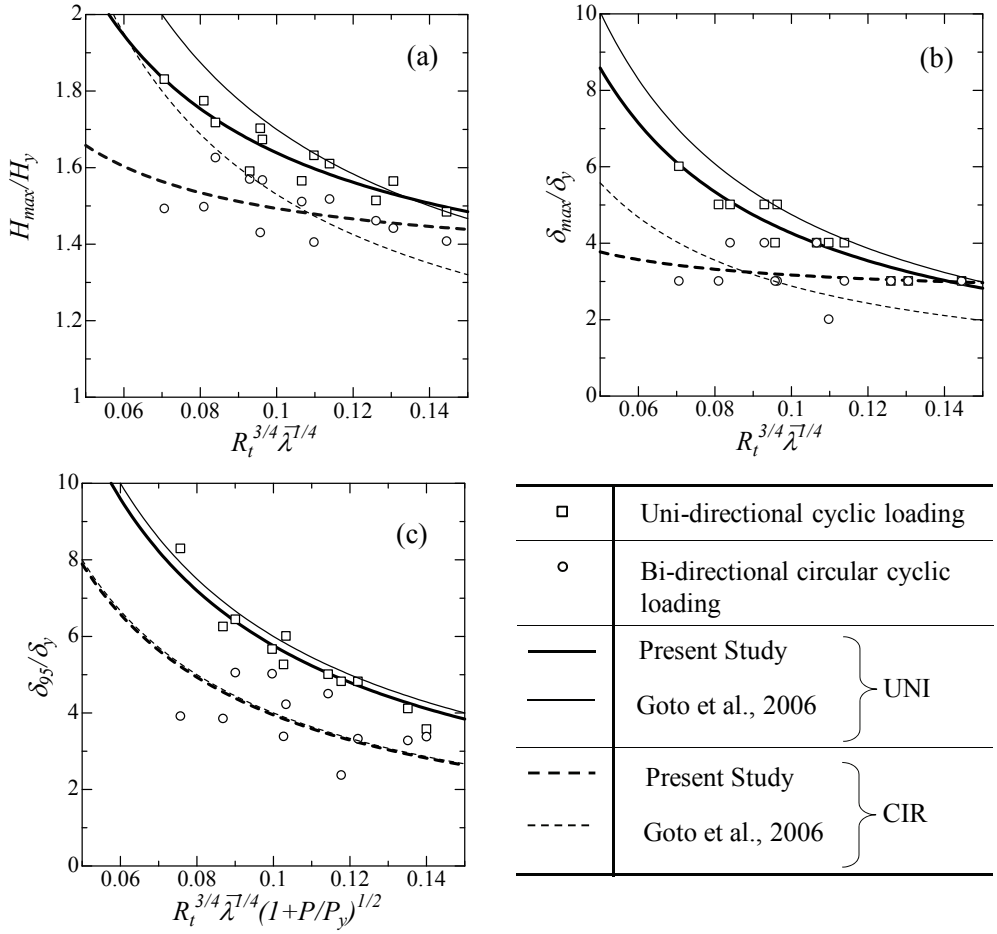

Fig. B.1 Comparison of Proposed Formulas with Past Study

$$f = \frac{C_1^{LoadingType}}{R_l^l \bar{\lambda}^m (1 + P/P_y)^n} + C_2^{LoadingType} \tag{B.1}$$

The constant and power values in **Eq. (B.1)** are given in **Table B.1** for both present study (Kulkarni et al., 2009) and past study.

Table B.1 Constants and Powers of Strength and Ductility Formulas

f	C_1^{UNI}	C_2^{UNI}	C_1^{CIR}	C_2^{CIR}	l	m	n
(1)	(2)	(3)	(4)	(5)	(6)	(7)	(8)
Present study (Kulkarni et al., 2009)							
$H_{\max}/H_y$	0.046	1.18	0.02	1.33	3/4	1/4	0
$\delta_{\max}/\delta_y$	0.43	-0.06	0.06	2.56	3/4	1/4	0
δ_{95}/δ_y	0.58	0	0.39	0	3/4	1/4	1/2
Past study (Goto et. al., 2006)							
$H_{\max}/H_y$	0.07	1.00	0.063	0.90	3/4	1/4	0
$\delta_{\max}/\delta_y$	0.53	-0.55	0.27	0.18	3/4	1/4	0
δ_{95}/δ_y	0.60	0	0.40	0	3/4	1/4	1/2

Although **Fig. B.1 (a)** and **(b)** indicate substantial difference in the present and previous formulas for maximum strength and ductility, however **Fig. B.1 (c)** for ultimate ductility shows fairly good agreement between them.

APPENDIX C

Procedure for Plotting Maximum Response State Ellipse

In Chapter 3, displacement-based seismic design method is proposed in which maximum response state ellipse is suggested to plot around the bi-directional displacement response of bridge pier in such a way that at least two extreme points of displacement response trajectory must lay on circumference of this ellipse. To satisfy this condition and draw an ellipse a stepwise procedure is defined as follows and explained through **Fig. C.1**.

1. Plot the bi-directional displacement response obtained from dynamic analysis on a square plot area as shown in **Fig. C.1 (a)**, with keeping same ranges on horizontal and vertical axis.
2. Draw a circle as shown in **Fig. C.1 (b)**, making the center of circle coinciding with crossing point of horizontal and vertical axis. Radius of circle would be the distance between center and an extreme point on the displacement response trajectory.
3. Sketch a line from center of circle to point of intersection on circumference and measure the length. This line becomes major axis of ellipse as '*a*' (see **Fig. C.1 (c)**).
4. Then assume some value for *b/a* ratio for example 0.8 and calculate minor axis length '*b*'. Plot this from center to outward direction making right angle with major axis (see **Fig. C.1 (d)**).
5. At this step major and minor axes are known. Find out the distance of foci from center by equation $f = \sqrt{a^2 - b^2}$ and plot on major axis as shown in **Fig. C.1 (e)**.
6. Knowing the foci locations and length of major and minor axis, the ellipse can be drawn (see **Fig. C.1 (e)**).
7. Now check that this ellipse is passing through at least two points on displacement response trajectory and if not then alter the value of *b/a* and repeat the steps from 4 to 7 until the condition is assured (see **Fig. C.1 (f)**).

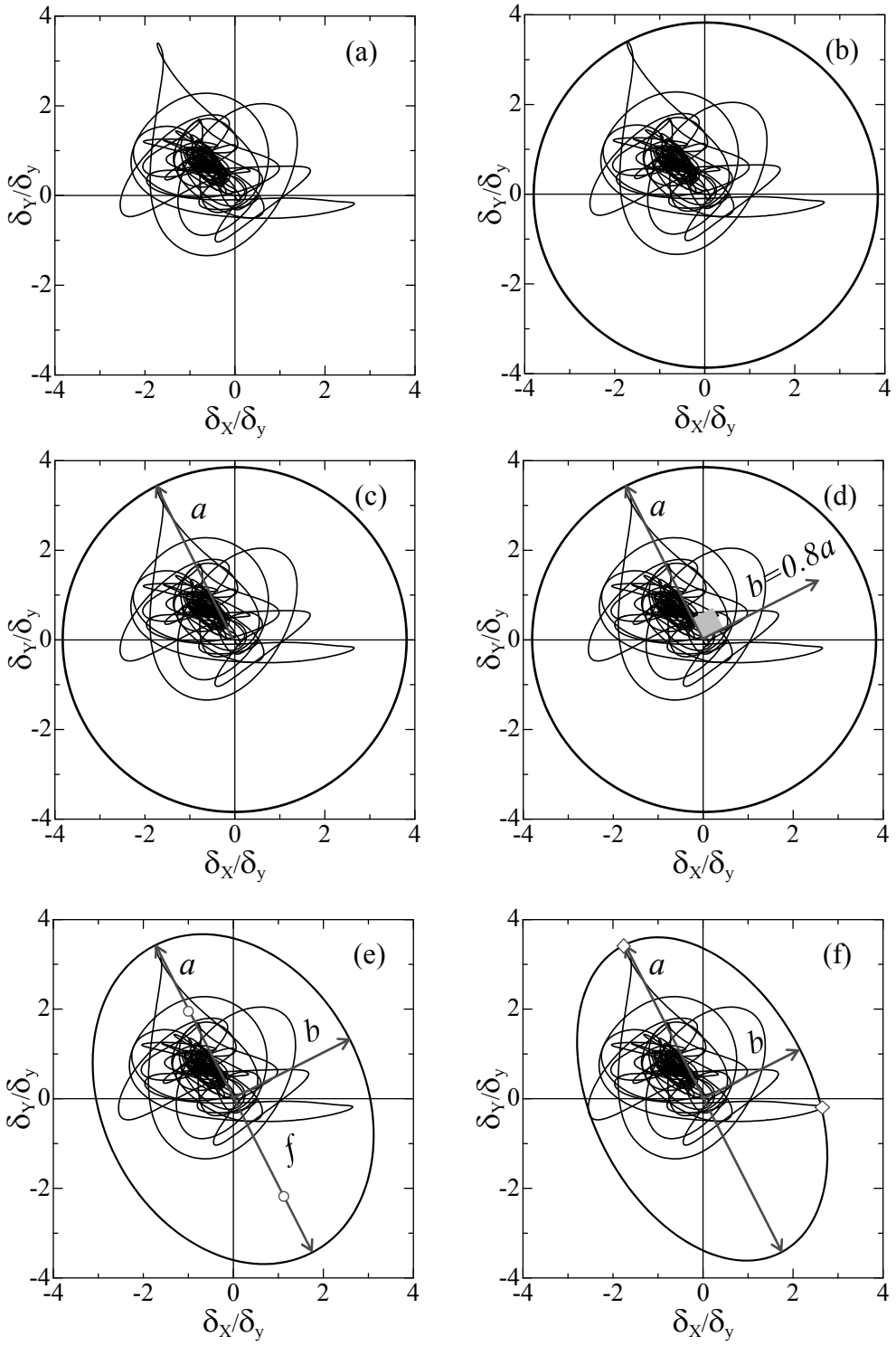

Fig. C.1 Stepwise Procedure to Plot Maximum Response State Ellipse

APPENDIX D

Evaluation of Average Compressive Strain at the Column Base

In the case of beam element model specially adopted for performing dynamic analysis, an average compressive strain $\bar{\varepsilon}_{mb}$ is measured in the bottom part of column. The height of this bottom part is equal to the effective failure length L_e as shown in the **Fig. D.1 (a)**. The L_e length is further divided into N = 5 number of segments. To obtain more precision in calculation, the number of default integration points (i.e. 8) are increased to 24 points along the beam element cross section as indicated in **Fig. D.1 (b)**. After performing the dynamic analysis, the maximum strain envelop $(\varepsilon_{li})_{\max}$ (where, i=1, 2, ... 24 and l = 1, 2, … 5) can be obtained from strain histories at each integration point in a single element. Further, average of such N maximum strain envelops from each segment gives average compressive strain $\bar{\varepsilon}_{mb}$, which can be written in equation form as follows.

$$\bar{\varepsilon}_{mb} = \frac{1}{N}\left(\sum_{l=1}^{N}(\varepsilon_{li})_{\max}\right) \qquad (i=1, 2, \ldots 24) \tag{D.1}$$

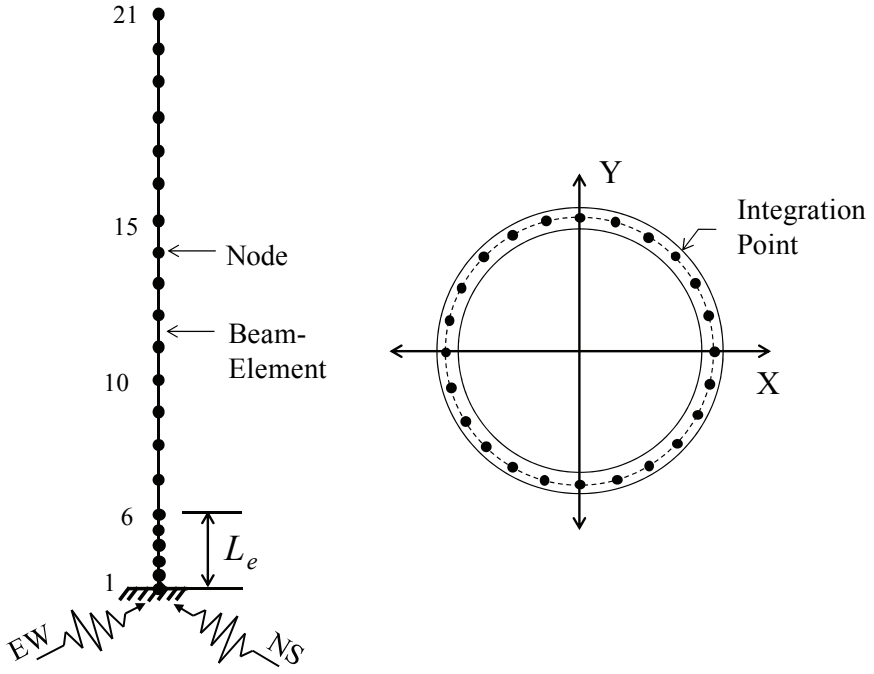

(a) Beam Element Model (b) Integration Points in Cross Section

Fig. D.1 Concept of Average Compressive Strain in Beam Element Model

APPENDIX E

Evaluation of Equivalent Strain in Shell Element Models

The local buckling region at the base part of the column is the place where the material starts loosing strength and undergoes yielding. Therefore, stress-strain behaviour in this base part is very significant to decide the overall strength of the column. The measurement of strain developed due to external loading in base part would give an important index for ultimate state prediction of the steel columns. The height of this base part is defined as $L_e = 1.2D(1/R_t^{0.08} - 1)$ and named as effective failure height. The strain calculation from each shell element comprised in the effective failure height is not feasible to carry out easily. Hence, a simple procedure based on nodal deformation is developed to obtain equivalent strain in L_e height of shell element model. **Fig. E.1 (a)** shows the enlarged cut section of shell element model in which *M* number of nodes are available at height L_e. After time $\bar{t}$ seconds one of the i^{th} node from *M* nodes, gets shifted in *X*, *Y*, *Z* space as shown in **Fig. E.1 (b)**. It can be noticed that, $\Delta L(\bar{t})_i$ deformation of the i^{th} node in *Z* direction, is responsible for axial strain and therefore, *X* and *Y* directional deformations are neglected here. Finally, the equivalent strain $\bar{\varepsilon}_{ms}$, can be evaluated by generating

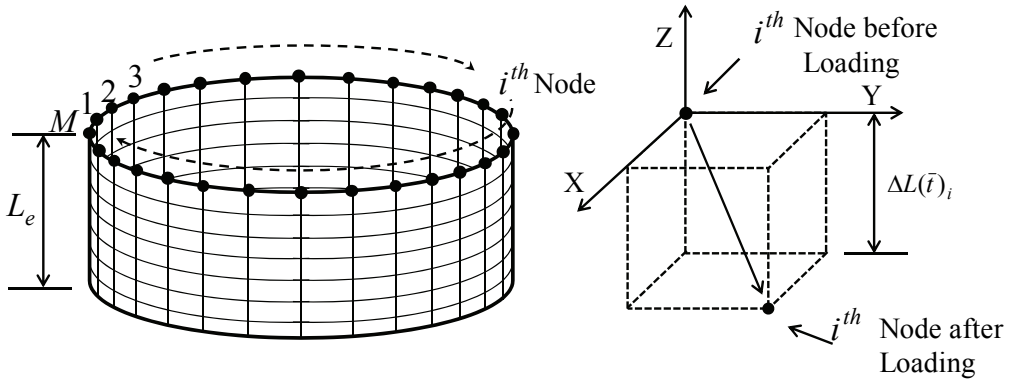

(a) Effective Failure Height Section

(b) Nodal Deformation in X,Y, Z Directions

Fig. E.1 Concept of Equivalent Strain in Shell Element Model

unique maximum envelop for Z directional deformations of M nodes as $Max(\Delta L(\bar{t})_M)$, and then dividing it by effective failure length L_e as given in **Eq. (E.1)**,

$$\bar{\varepsilon}_{ms} = \frac{Max(\Delta L(\bar{t})_M)}{L_e} \tag{E.1}$$

APPENDIX F

Uni-directional and Bi-directional Dynamic Response of the Piers P60-20 and P60-60

F.1 Displacement and Strain Responses of Pier P60-20

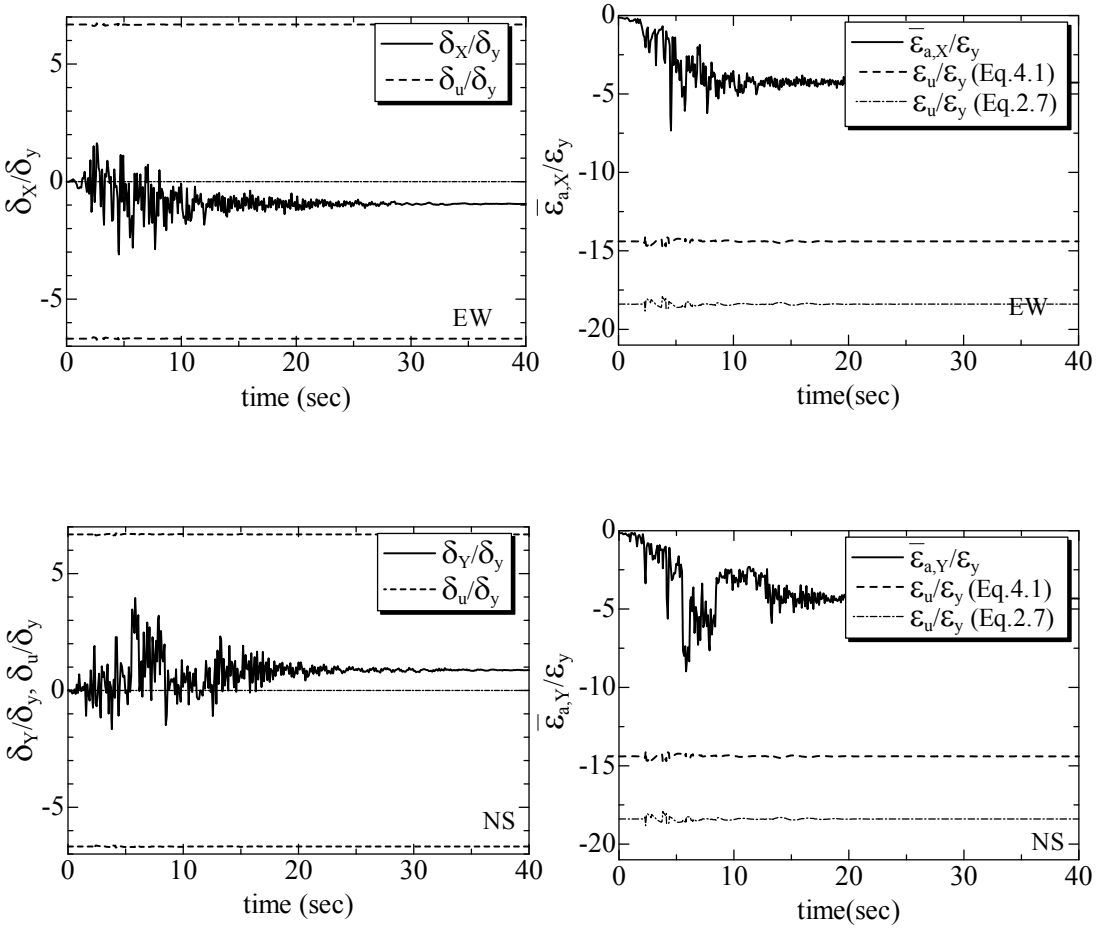

Fig. F.1 Earthquake Components EW and NS Response of P60-20

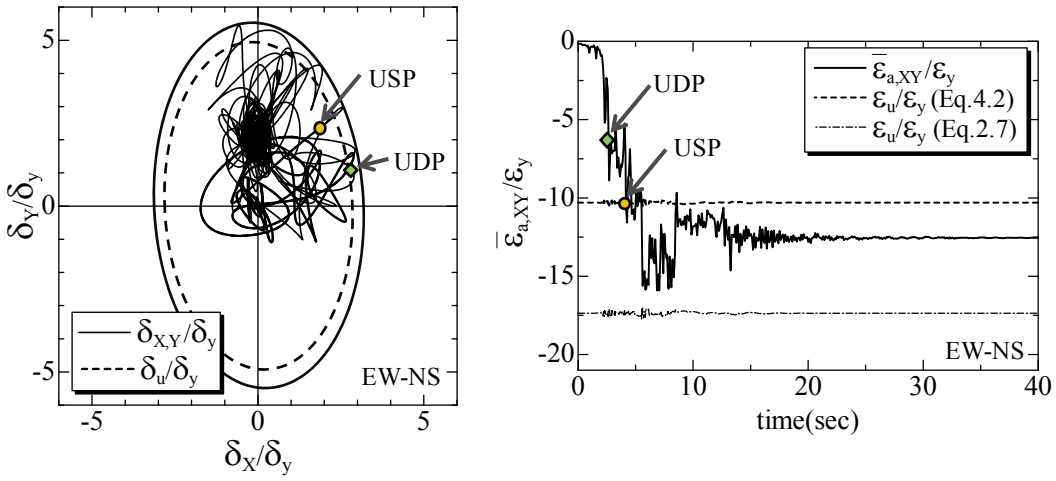

Fig. F.2 Bi-directional Earthquake EW-NS Response of P60-20

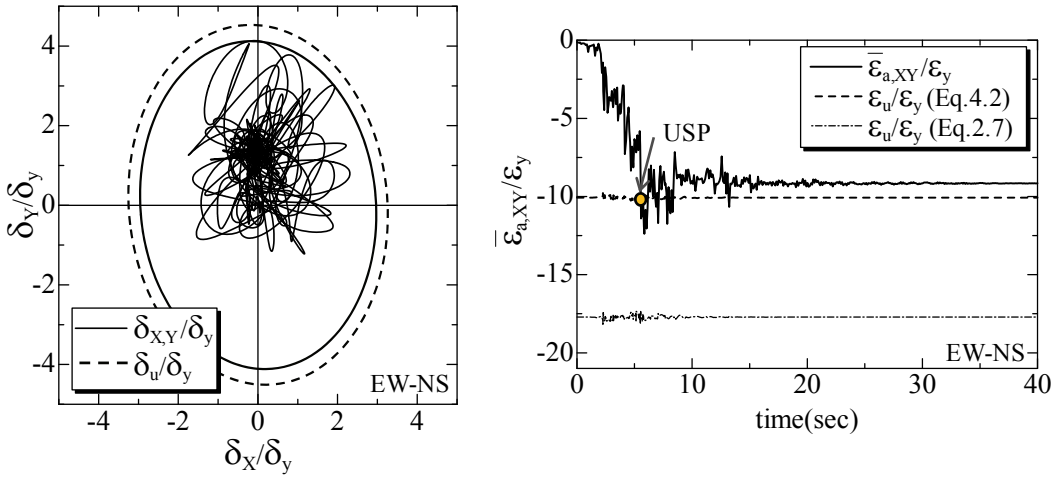

Fig. F.3 Bi-directional Earthquake EW-NS Response of P60-20 (Trail-1)

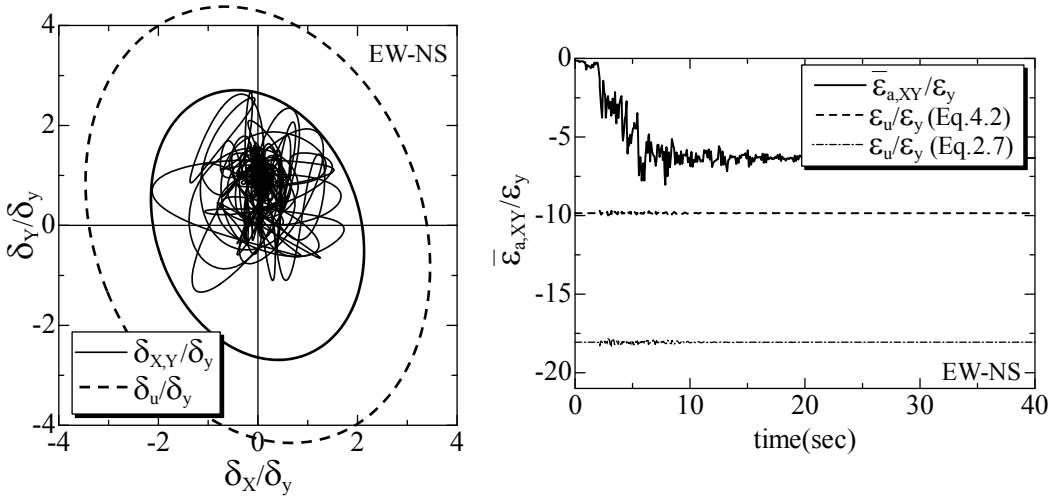

Fig. F.4 Bi-directional Earthquake EW-NS Response of P60-20 (Trail-2)

F.2 Displacement and Strain Responses of Pier P60-60

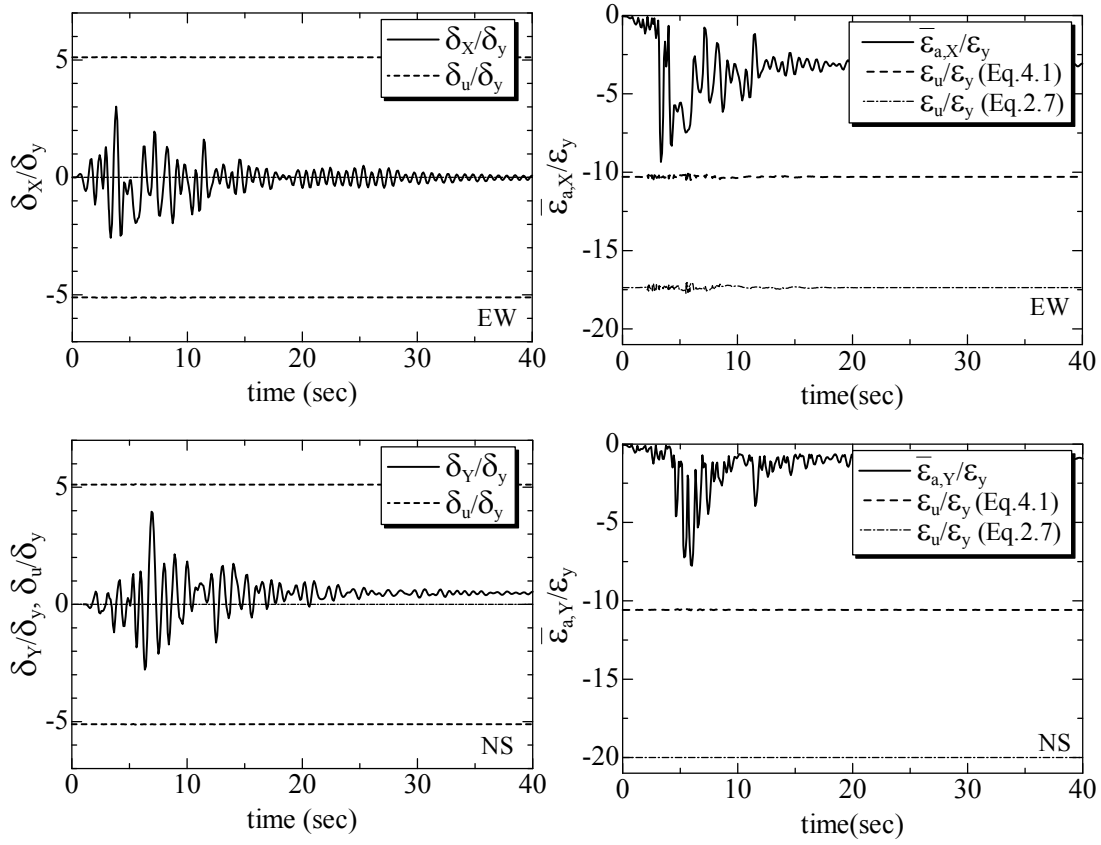

Fig. F.5 Earthquake Components EW and NS Response of P60-60

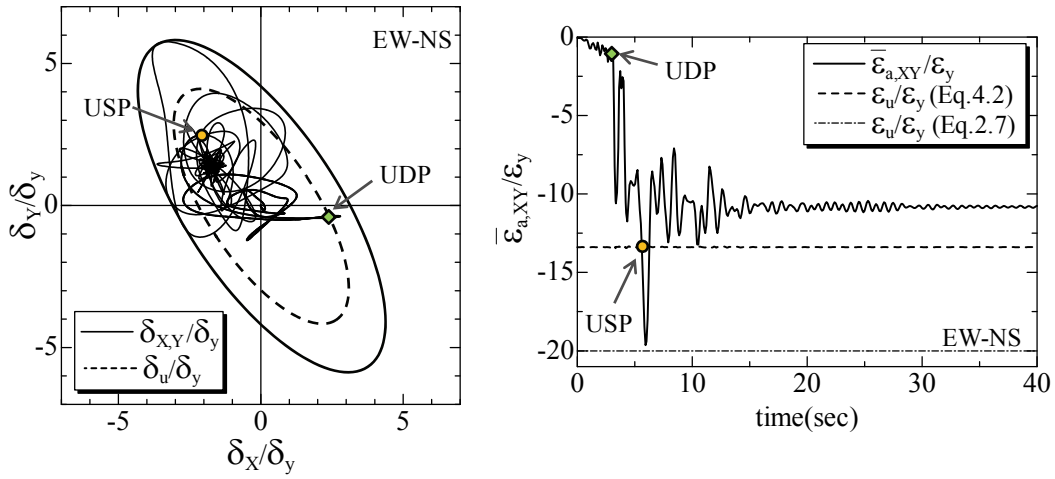

Fig. F.6 Bi-directional Earthquake EW-NS Response of P60-60

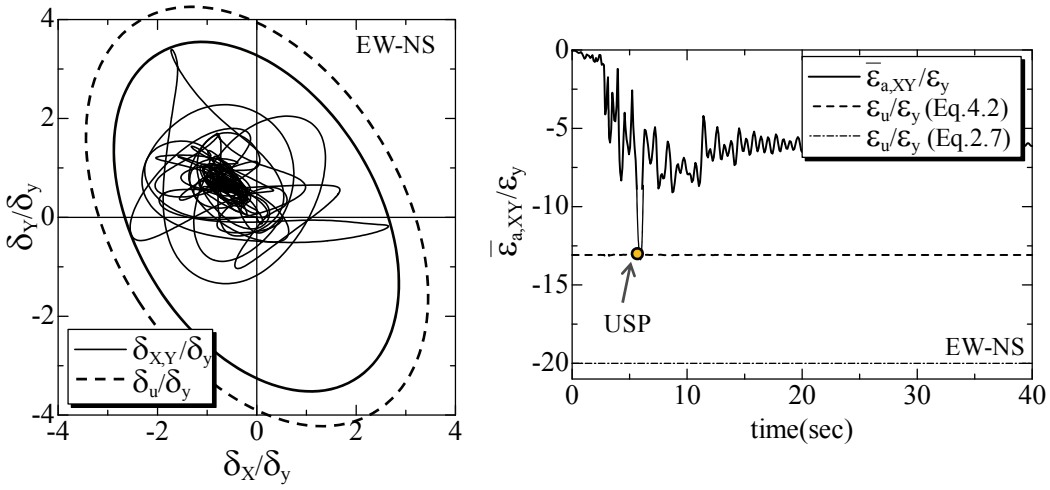

Fig. F.7 Bi-directional Earthquake EW-NS Response of P60-60 (Trail-1)

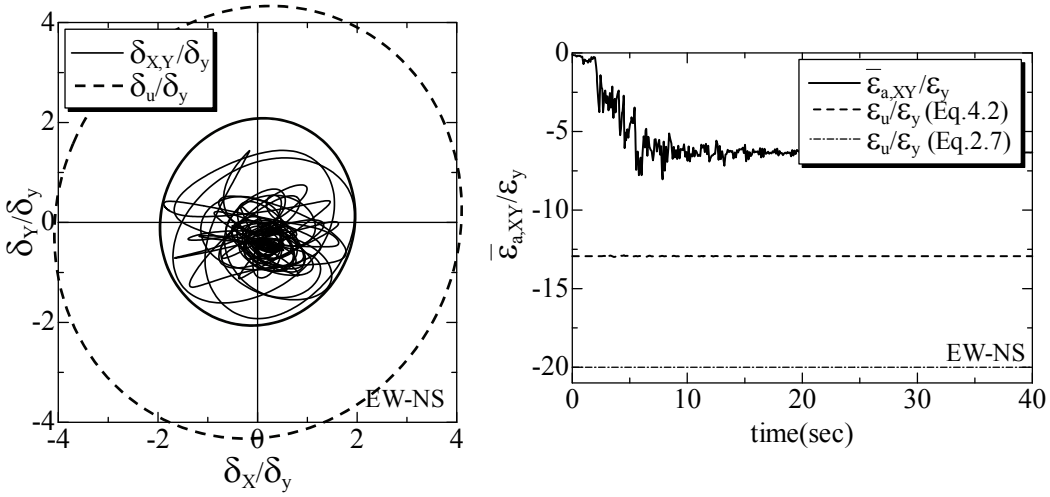

Fig. F.8 Bi-directional Earthquake EW-NS Response of P60-60 (Trail-2)

APPENDIX G

Verification for SPL 2 through Dynamic Analysis Method

G.1 Average Compressive Strain Responses for Pier 2 of Model 1

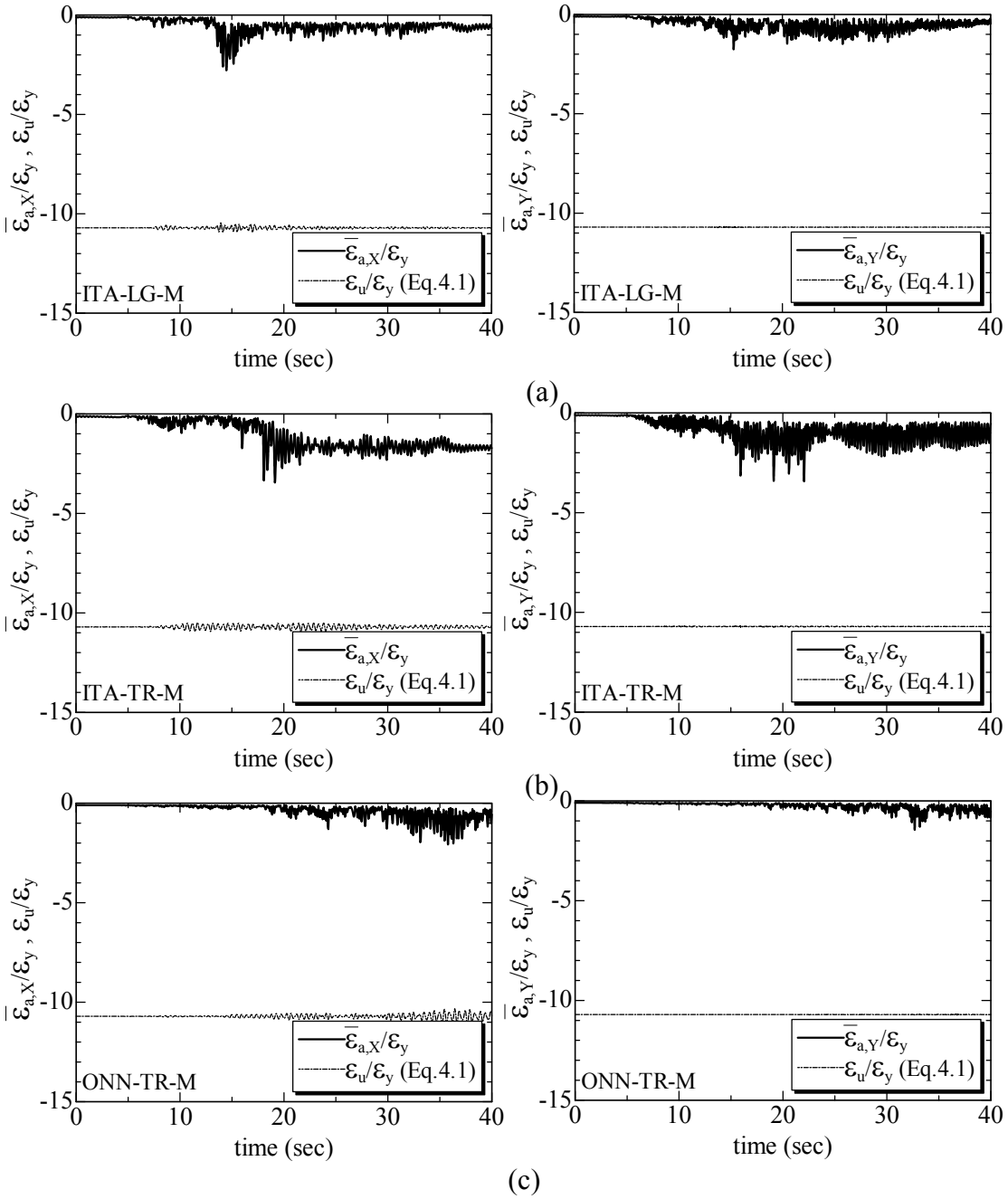

Fig. G.1 Strain Responses for Type I Earthquake Ground Motions (Model 1)

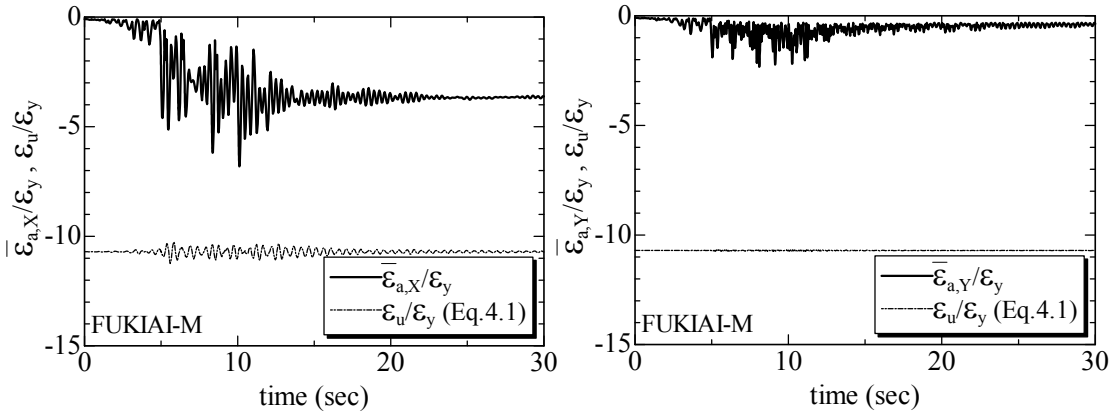

(a)

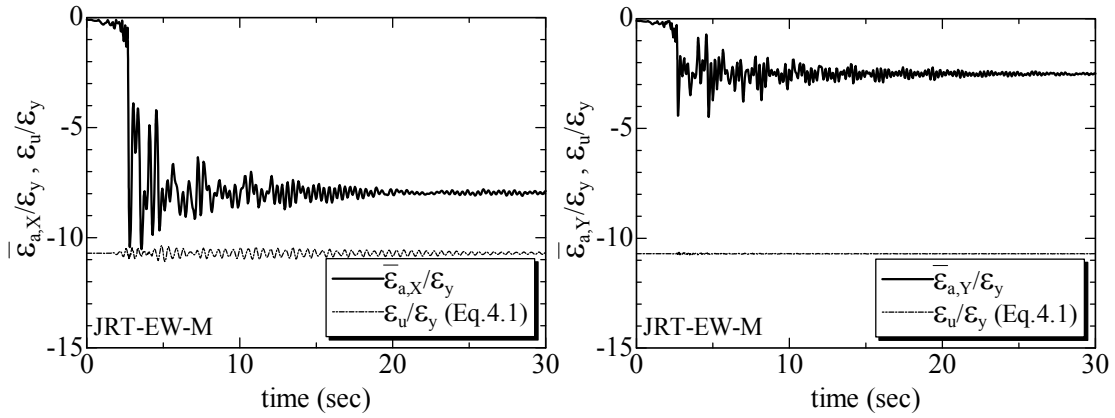

(b)

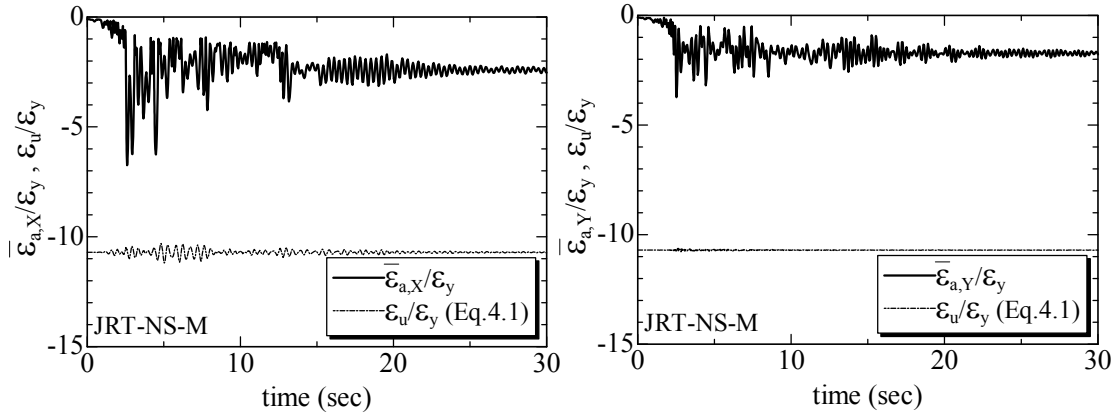

(c)

Fig. G.2 Strain Responses for Type II Earthquake Ground Motions (Model 1)

G.2 Average Compressive Strain Responses for Pier 2 of Model 2

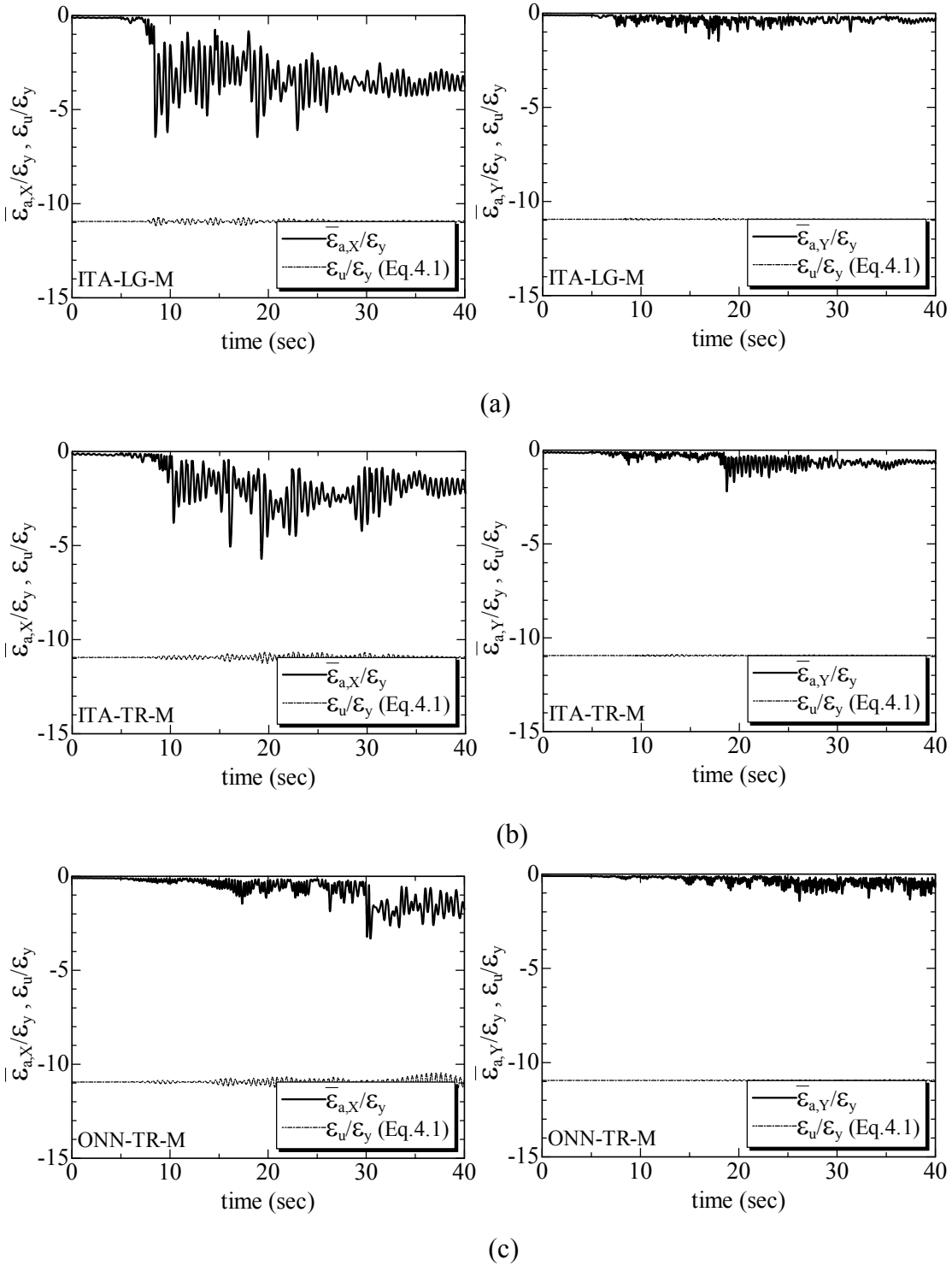

Fig. G.3 Strain Responses for Type I Earthquake Ground Motions (Model 2)

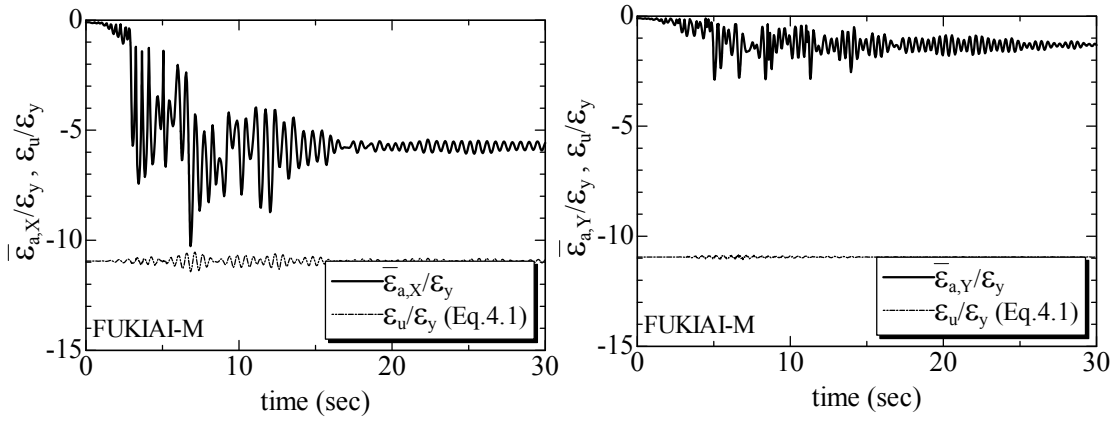

(a)

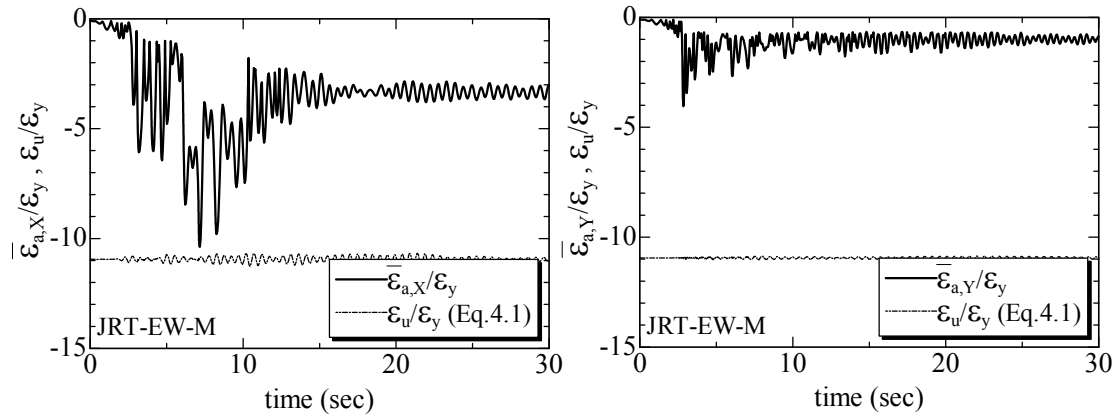

(b)

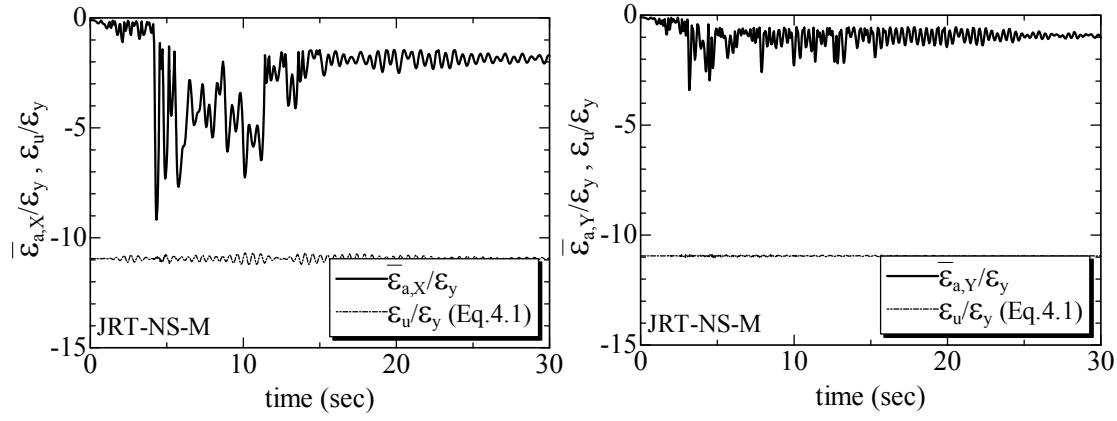

(c)

Fig. G.4 Strain Responses for Type II Earthquake Ground Motions (Model 2)

G.3 Average Compressive Strain Responses for Pier 2 of Model 3

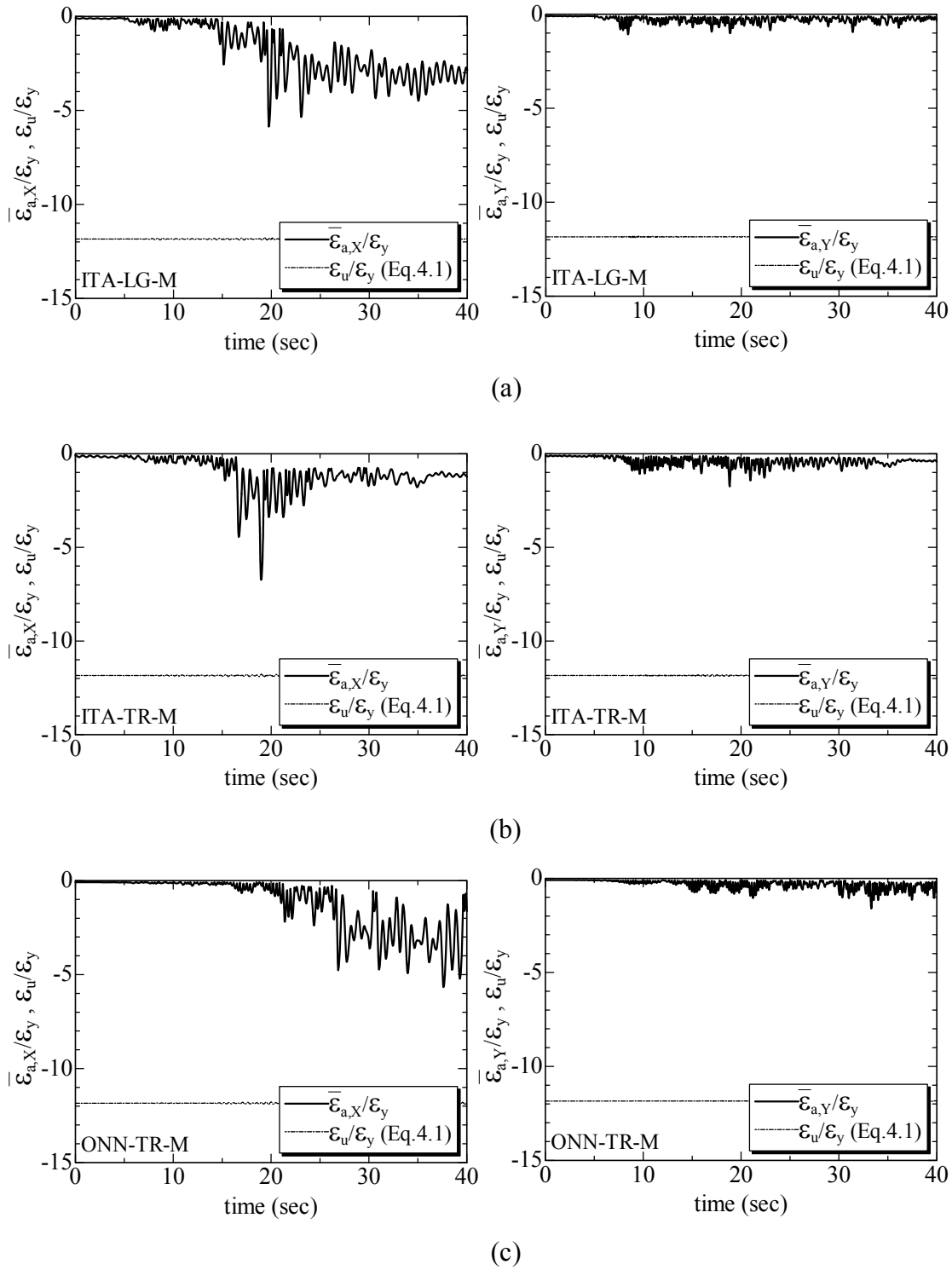

(a)

(b)

(c)

Fig. G.5 Strain Responses for Type I Earthquake Ground Motions (Model 3)

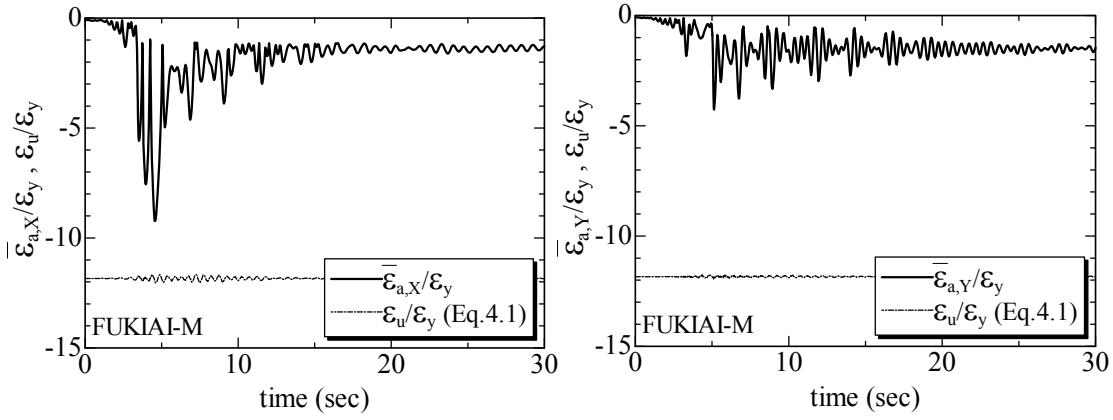

(a)

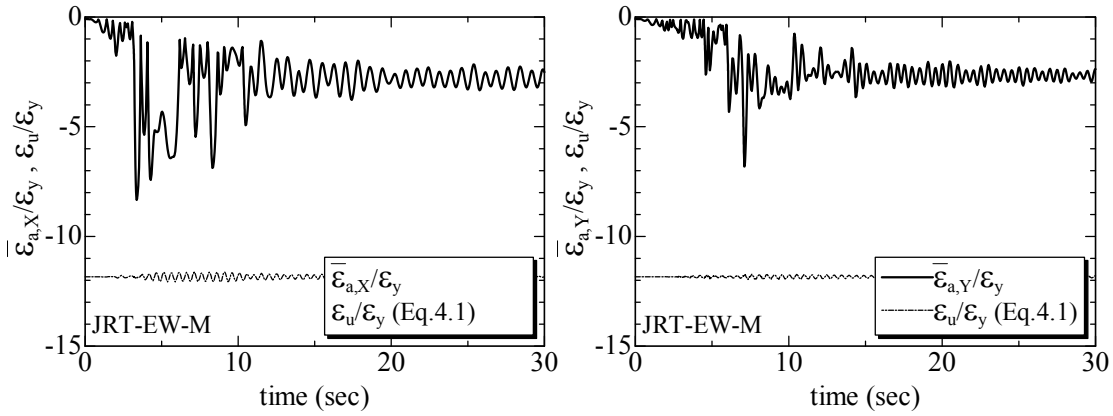

(b)

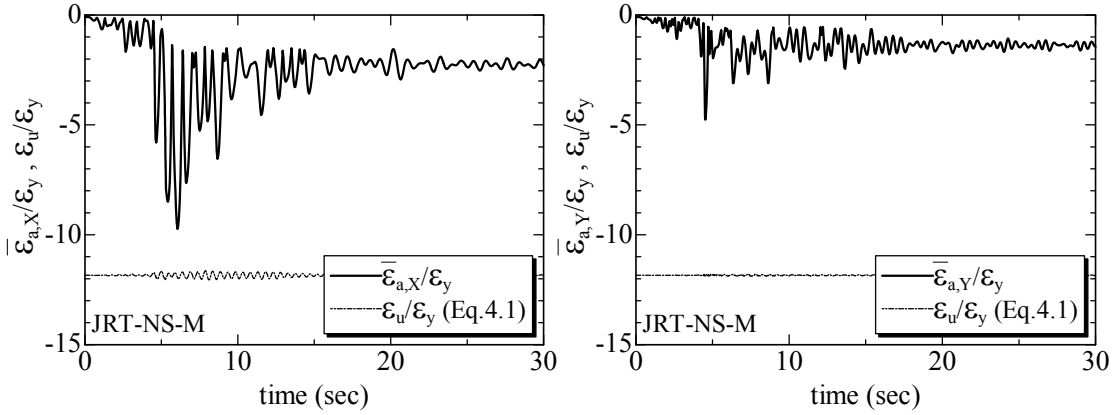

(c)

Fig. G.6 Strain Responses for Type II Earthquake Ground Motions (Model 3)

APPENDIX H

Input Earthquake Motions and Response Spectra

EW, NS and UD time-history records of five earthquakes are presented in **Fig. H.1**. Acceleration response spectra are also plotted for each component of earthquake separately. The observed fundamental natural periods of three designed bridge models are also indicated on each response spectrum.

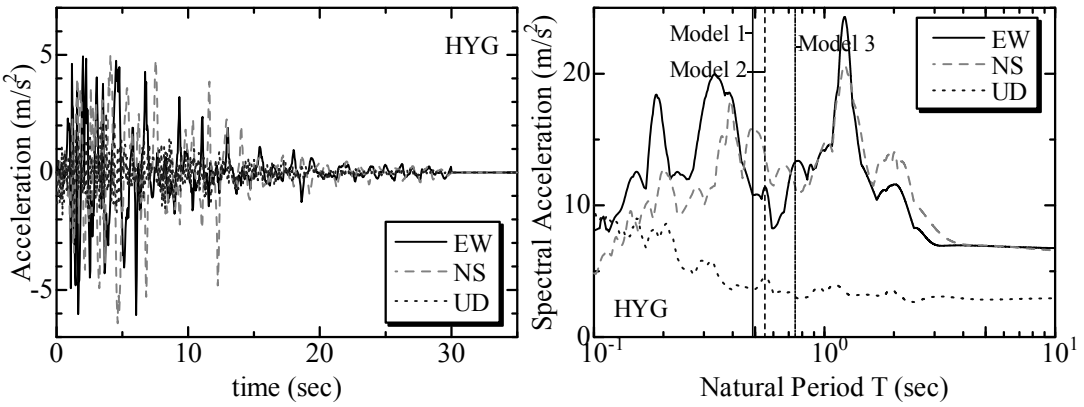

(a) The South Hyogo-ken Prefecture Earthquake in 1995

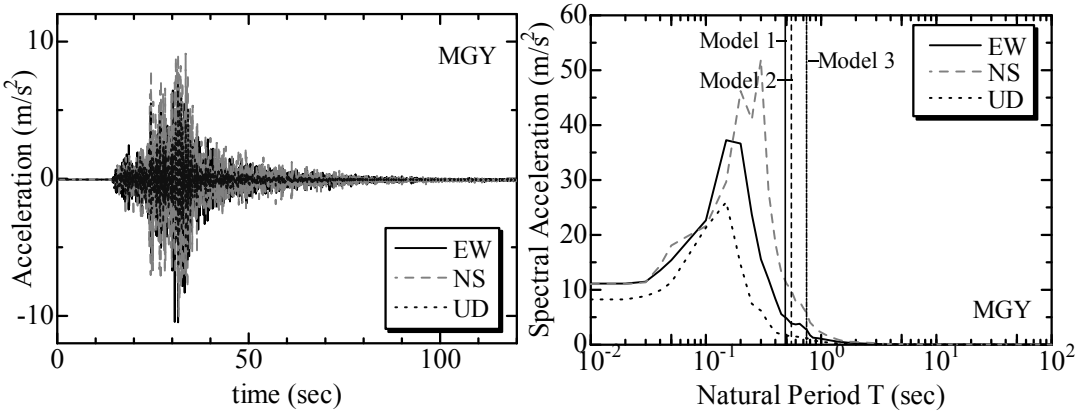

(b) The Miyagi Prefecture Hokubu-oki Earthquake in 2003

Fig. H.1 Time-history and Response Spectra of 5 Earthquake Motions

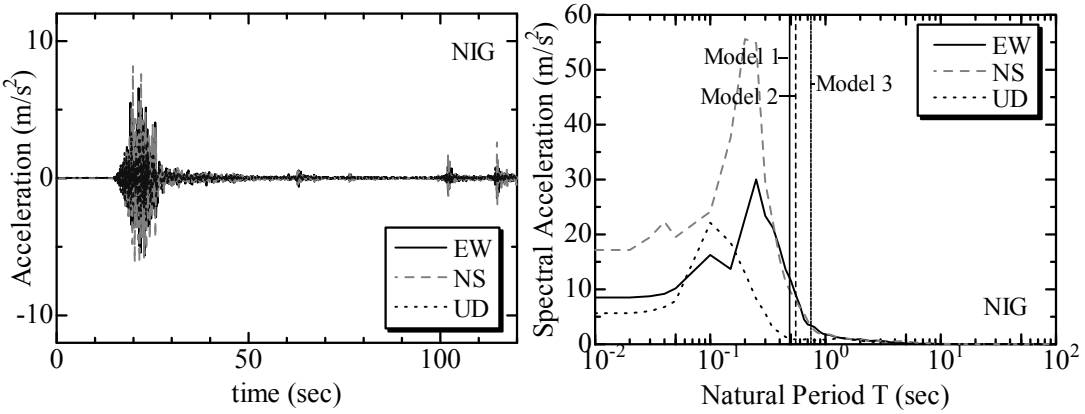

(c) The Mid Niigata Prefecture Earthquake in 2004

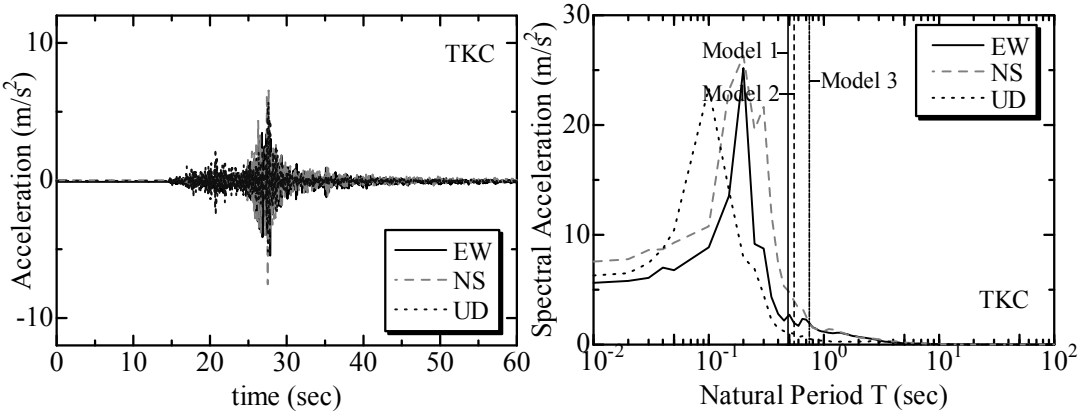

(d) The Hokkaido Tokachi-oki Earthquake 2004

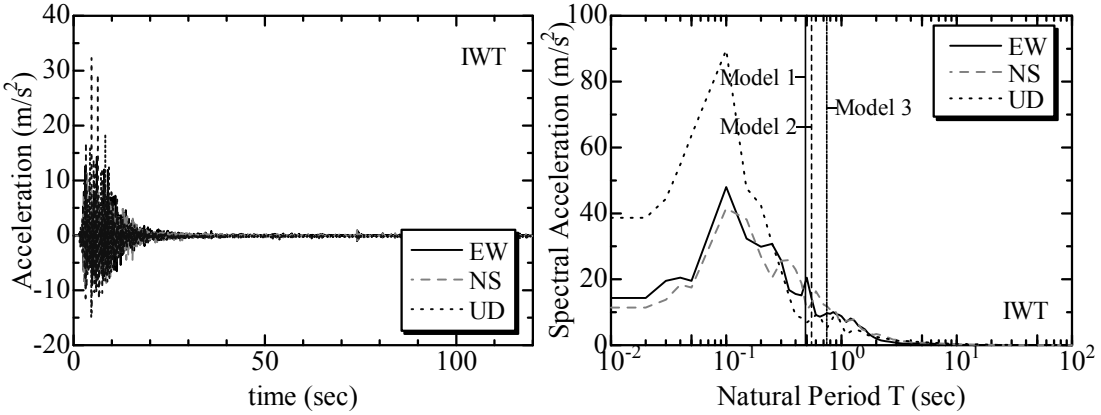

(e) The Iwate-Miyagi Nairiku Earthquake in 2008

Fig. H.1 Continued

APPENDIX I

Modal Frequencies and Effective Masses for Bridge Systems

The natural frequencies and periods in first 10 modes along with their effective masses are presented in following **Table I.1**, **I.2** and **I.3** for three bridge systems studied in Chapter 5.

Table I.1 Modal Analysis Values for Bridge Model 1

Mode No.	Frequencies (cyc/sec)	Period (sec)	Effective Masses (%)		
			X-comp.	Y-comp.	Z-comp.
(1)	(2)	(3)	(4)	(5)	(6)
1	2.05	0.49	0.51	3.53×10^{-6}	51.27
2	2.05	0.49	2.47×10^{-4}	3.98×10^{-6}	4.44×10^{-2}
3	2.85	0.35	24.64	1.06×10^{-6}	7.01
4	2.93	0.34	37.36.	6.85×10^{-2}	7.26
5	2.96	0.34	15.12	7.04×10^{-3}	4.67×10^{-4}
6	3.07	0.33	8.79	51.07	2.59×10^{-2}
7	3.14	0.32	4.29	7.59×10^{-3}	17.81
8	3.23	0.31	7.43	1.50×10^{-7}	16.57
9	3.58	0.28	1.38	39.75	1.02×10^{-4}
10	4.19	0.24	4.70	9.11	1.35×10^{-5}
		Total→	100	100	100

The Bridge Model 1 has shown first mode of vibration in vertical direction because of the short pier height. This is unusual case. However, for Bridge Model 2 and 3 the first mode is in longitudinal direction.

Table I.2 Modal Analysis Values for Bridge Model 2

Mode No	Frequencies (cyc/sec)	Period (sec)	Effective Masses (%)		
			X-comp.	Y-comp.	Z-comp.
(1)	(2)	(3)	(4)	(5)	(6)
1	1.82	0.55	57.94	7.43×10^{-4}	1.01
2	1.82	0.55	7.63	5.41×10^{-4}	0.13
3	1.82	0.55	21.07	2.13×10^{-2}	0.66
4	2.07	0.48	2.19	0.11	51.46
5	2.09	0.48	0.25	1.08	1.07×10^{-3}
6	2.09	0.48	9.51	40.89	0.11
7	2.58	0.39	0.55	57.02	7.08×10^{-6}
8	3.05	0.33	0.51	0.87	3.80×10^{-3}
9	3.10	0.32	0.11	2.84×10^{-4}	23.32
10	3.12	0.32	0.25	1.29×10^{-7}	23.29
		Total→	100	100	100

Table I.2 Modal Analysis Values for Bridge Model 2

Mode No	Frequencies (cyc/sec)	Period (sec)	Effective Masses (%)		
			X-comp.	Y-comp.	Z-comp.
(1)	(2)	(3)	(4)	(5)	(6)
1	1.34	0.75	71.90	1.06×10^{-3}	6.43×10^{-2}
2	1.35	0.74	9.76	8.39×10^{-3}	7.74×10^{-3}
3	1.36	0.74	6.93	2.14×10^{-2}	3.78×10^{-4}
4	1.61	0.62	10.31	39.82	1.73×10^{-4}
5	2.02	0.49	0.38	60.15	3.96×10^{-4}
6	2.05	0.49	7.82×10^{-2}	1.62×10^{-4}	53.03
7	2.07	0.48	1.15×10^{-4}	5.72×10^{-5}	3.75×10^{-5}
8	2.42	0.41	0.52	4.26×10^{-3}	8.07×10^{-6}
9	3.09	0.32	4.15×10^{-2}	6.07×10^{-5}	23.45
10	3.10	0.32	8.41×10^{-2}	1.43×10^{-8}	23.44
		Total→	100	100	100

APPENDIX J

Effect of Varying Axial Load on Cyclic Behavior of Circular Steel Bridge Piers

J.1 Introduction

The use of steel bridge pier is common practice in the urban area of developed countries like Japan because of their smaller section size and fast erection compared to reinforced concrete piers. However, most of the regions in Japan are alerted as seismically severe and also experienced strong ground motions in past few decades, which has been proved the importance of seismic design of the structures, like highway bridges, high rise buildings etc. Hence, learning the lessons from the previous earthquake effects on the bridges, researchers tried to evaluate the critical capacity of the bridge piers by applying the loading patterns more similar to earthquake motion pattern such as cyclic one directional considered by Gao et al. (1998) and cyclic bi-directional adopted by Goto et al. (2006), Kulkarni et al. (2009). In these types of past studies related to the steel piers, the axial load was assumed as constant during the numerical analysis, which fails to capture the effect of vertical component of the earthquake.

Fig. J.1 shows a typical bridge frame subjected to 3D earthquake motions and in the result generates the shear forces, bending moments and 3D deformations at the top of the piers. These types of few research studies related to the varying axial load effect on the reinforced concrete (RC) piers are available (Kim et al. (2006), Saadeghvaziri M. A. (1997), Lee et al. (2005)) which pointed out that simultaneously application of lateral loading and varying axial load on the

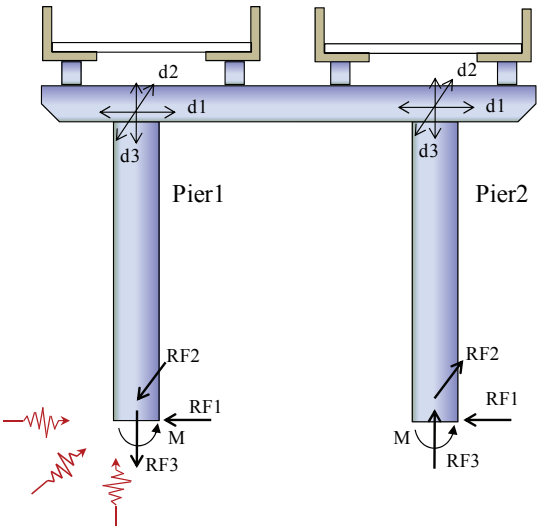

Fig. J.1 Frame Structure of Bridge Piers

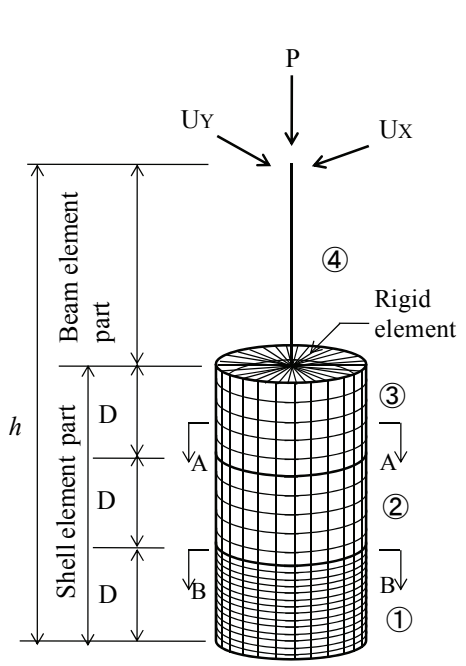

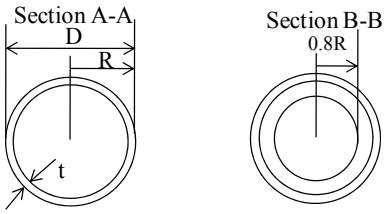

Table 1 Details of Analytical Model

Rt = 0.075	λ = 0.4	
h = 6454mm	D =1173mm	t =20mm
Shell element type= S4R		
Beam element type= PIPE31		
Part ①	Circumferential direction mesh=30 segments Lengthwise direction mesh=30 segments	
Part ②, Part ③	Circumferential direction mesh=30 segments Lengthwise direction mesh=5 segments	
Part ④	Lengthwise direction mesh=10 segments	

Table 2 Properties of Steel SM490

E (GPa)	σ_y (MPa)	ε_y (%)	E_{st} (GPa)	ε_y (%)	υ	σ_u (MPa)
200	315	0.157	6.67	1.10	0.3	490

Fig. J.2 FE Model of Bridge Pier and Material Properties of Steel

RC pier reduces its strength significantly. Therefore, it is required to confirm the three dimensional loading effect on the steel piers and which is an objective of the present work.

The piers designed based on the constant axial load, with a relatively low axial load ratio, might not satisfy the demand performance when the vertical ground motion exceeds the axial load. Hence in the present paper, a case study of a steel circular bridge pier subjected to the cyclic horizontal displacement loading and constant as well as varying axial load are discussed to understand the cyclic behavior of pier under critical loading condition.

J.2 Analytical Model and Loading Patterns

Analytical model

Fig J.2 indicates the finite element model developed through the ABAQUS (2007) program. The bottom part of 3 times diameter D of pier is made up of shell element and upper part is of beam element. At the interval of D the ring type diaphragms are placed and Sections B-B gives its details. Table 1 inserted in **Fig. J.2** shows the geometrical properties of FE model such as radius thickness ratio parameter R_t, slenderness ratio parameter $\bar{\lambda}$, dimensions, and element types and meshing pattern whereas, Table 2 gives the material properties of steel grade SM490.

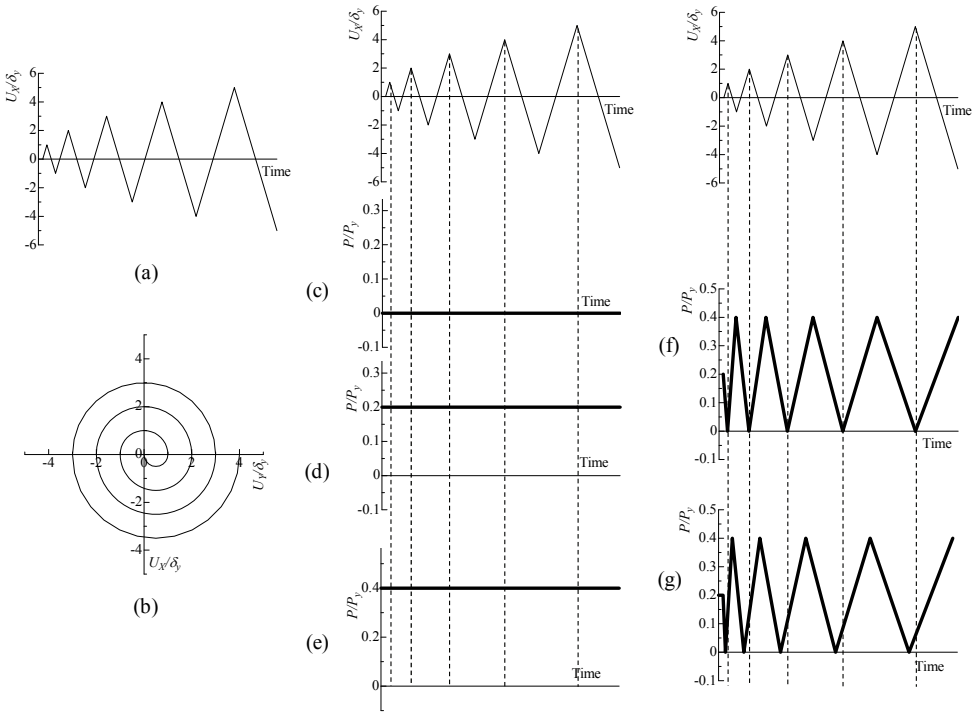

Fig. J.3 (a) Cyclic Uni-directional Displacement, (b) Cyclic Bi-directional Displacement, (c) No Axial Load (*P/Py*=0), (d) Constant Axial Load (*P/Py*=0.2), (e) Constant Axial Load (*P/Py*=0.4), (f) Proportional Varying Axial Load (*P/Py*=0~0.4), (g) Nonproportional Varying Axial Load (*P/Py*=0~0.4)

To achieve accuracy in the evaluation of strength and ductility, the two-surface model (M2SM) constitutive law is used which was developed at Nagoya University (Shen et al., 1995) and its accuracy has been checked against experimental results for bi-dire-ctional displacement loading on steel column by Kasai et al., (2004). Therefore, in the present work M2SM material constitutive law can be acceptable for analysis of steel pier with bi-directional displacements and varying axial load.

Loading patterns

Fig. J.3 (a), **(b)** indicate the cyclic horizontal displacements in cyclic uni- and bi-directions respectively, which are increased in multiple of yield deformation, δ_y per cycle. **Fig. J.3 (c)~(g)** show the no axial load, constant axial load, proportional and nonproportional varying axial load patterns. Proportional means both axial and lateral loads are applied simultaneously and both reach their extreme values at the same time (see **Fig. J.3 (f)**) whereas, nonproportional means variations are uncoupled (see **Fig. J.3 (g)**). The effect of these types of proportional and nonproportional axial loading on RC columns was explained by Saadeghvaziri M. A. (1997). Whereas in the present study for steel piers the variation of axial load ratio is assumed from 0 to 0.4

only on compression side, as it would be not possible to replicate all possible cyclic axial loading regimes during earthquake behavior.

J.3 Results and Discussion

The FE model shown in **Fig. J.2** was statically analyzed with the displacement and axial loading for the equal time period and results are prepared for strength versus ductility in two orthogonal directions (X, Y) and vertical downward deformation versus ductility in X direction which are shown in **Fig. J.4 (a)~(e)**.

It has been observed from the graphs that, for no axial load case (see **Fig. J.4 (a)**) the pier shows largest strength and ductility for both UNI and CIR displacement types with very less amount of vertical downward deformation. However, when the constant axial loads i.e. P/P_y = 0.2, 0.4 (see **Fig. J.4 (b)**, **(c)**) are applied to the pier, the strength reduces considerably than case of no axial loading and when comparing between the UNI and CIR lateral loading effect then it shows, cyclic bi-directional lateral loading considerably affect strength and ductility than uni-directional loading. Although P/P_y = 0.4 case shows greater strength than in case of P/P_y = 0.2, but it also shows sudden decrease in strength and which may cause early loss of strength than the P/P_y = 0.2 case.

Further, in the case of proportional varying axial load and uni-directional lateral loading (see **Fig. J.4 (d)**) the displacement reaches its maximum negative amplitude and at the same time axial load becomes maximum (P/P_y = 0.4) and vice versa, hence hysteretic loop indicates decrease in strength on negative side while slightly hardening on positive side. Whereas, in case of bi-directional lateral loading with proportional varying axial load, this phenomenon becomes complicated, however it is noticed that, strength distribution in X and Y direction is unequal on negative side which differs from constant axial loading cases (see **Fig. J.4 (b), (c)**). In the nonproportional axial load case, axial load varies in uncoupled manner with lateral displacement loading (see **Fig. J.3 (g)**), however in uni-directional displacement case (see **Fig. J.4 (e)**), when axial load P/P_y changes from 0 to 0.4, the displacement loading passes over positive side and vice versa, hence hysteretic loop indicates decrease in strength on positive side while slightly hardening on negative side. On the other hand, in bi-directional lateral loading the unequal distribution of strength in X and Y direction is observed on both positive and negative sides.

In all axial load cases except no axial load case, bi-directional lateral loading has shown large vertical deformation than uni-directional loading but there is no significant difference observed in their overall maximum deformations.

J.4 Conclusions

In the present case study, effect of varying axial load with uni- and bi-directional lateral loading are observed on circular steel pier, because three dimensional varying loads are analogous to actual earthquake components acting on the bridge piers. The observation shows that, assumed proportional and nonproportional varying axial loads have affected uni- and bi-directional cyclic behavior of steel pier. However, considering the overall performance of constant and varying axial load with lateral displacement loading, the divergence in strength and ductility is minor. Hence, it is required to investigate the alternative varying axial loading pattern which would be severe for the steel piers.

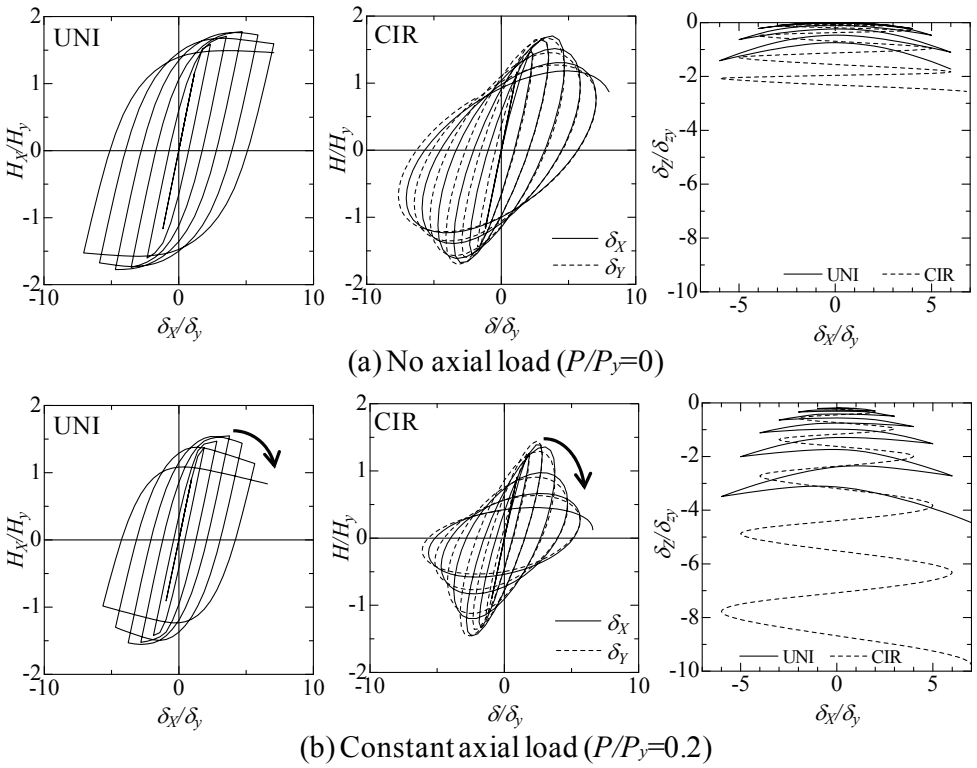

(a) No axial load (P/P_y=0)

(b) Constant axial load (P/P_y=0.2)

Fig. J.4 Hysteretic Behavior of Pier Under Various Axial Loadings

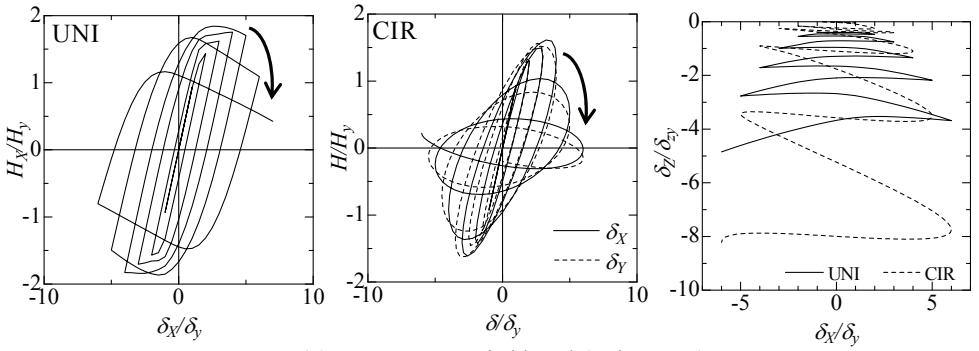

(c) Constant axial load (P/P_y=0.4)

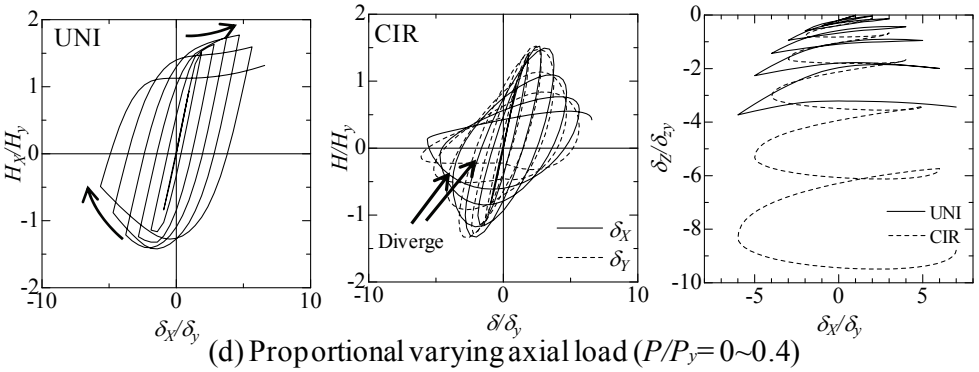

(d) Proportional varying axial load (P/P_y= 0~0.4)

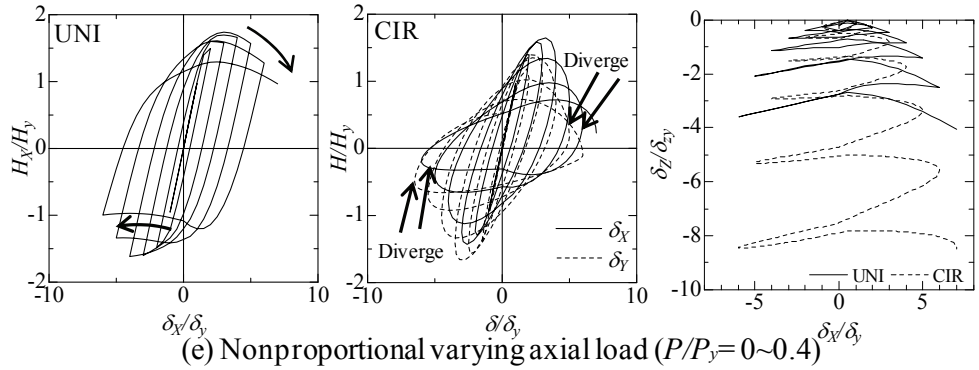

(e) Nonproportional varying axial load (P/P_y= 0~0.4)

Fig. J.4 Continued

PUBLICATION LIST

List of publications

1. **Kulkarni N.**, Kasai A. and Tsuboi H., (2009) Displacement based seismic verification method for thin-walled steel columns subjected to bi-directional cyclic loading; *Engineering Structures, 31(11), 2779-2786.*
2. **Kulkarni N.** and Kasai A., (2012) Effect of 3D Earthquake on Response of Circular Steel Bridge Piers and its Influence on Capacity Prediction; *Journal of Structural Engineering ,(Will be published in JUNE-JULY issue)*
3. **Kulkarni N**. and Kasai (2011) Seismic verification method for steel bridge piers with pipe section under two directional earthquake components; *Doboku Gakkai Ronbunshuu JSCE, (Under process)*

List of presentations

1. **Kulkarni N.** and Kasai A., (2008) Seismic Capacity of steel circular column subjected to bi-directional horizontal motions; *Proceedings of the 63rd Annual Conference of JSCE, CD-ROM.*
2. **Kulkarni N.** and Kasai A., (2009) Strain based seismic verification method for thin-walled steel circular columns subjected to bi-directional cyclic loading; *Proceedings of the Chubu branch of JSCE, CD-ROM.*
3. **Kulkarni N.** and Kasai A., (2009) Seismic verification method for thin-walled circular steel piers under bi-directional loading; *Proceedings of 2nd International conference on Computational Methods in Structural Dynamics and Earthquake Engineering, COMPDYN 2009, No. CD196.*
4. **Kulkarni N.** and Kasai A., (2009) Analytical study on seismic verification method of steel columns subjected to bi-directional loadings; *Proceedings of 10th International Conference on Structural Safety and Reliability, ICOSSAR2009.*
5. **Kulkarni N.** and Kasai A., (2009) Effect of varying axial load on cyclic behavior of circular steel bridge piers; *Proceedings of 11th International Summer Symposium, JSCE, 1-4.*
6. **Kulkarni N.** and Kasai A., (2009) Effect of bi-directional cyclic loading on seismic capacity and buckling behavior of thin-walled circular steel bridge piers; *Proceedings of 6th International Conference on Advances in Steel Structures, ICASS'09.*